

Morten Volland Finnekås

# Optimal Charge Planning in Hybrid Ferry Systems

June 2019





Norwegian University of  
Science and Technology

# Optimal Charge Planning in Hybrid Ferry Systems

**Morten Volland Finnekås**

Master of Science in Cybernetics and Robotics

Submission date: June 2019

Supervisor: Jon Are Suul, ITK

Co-supervisor: Lars Andreas Lien Wengersberg, Siemens

Norwegian University of Science and Technology  
Department of Engineering Cybernetics



# Problem Description

The maritime industry is currently undergoing several changes related to electrification of the fleet. Since the first all-electric car ferry, MF Ampere, was commissioned and put into operation in 2015, there has been several initiatives to renew a large part of the ferry fleet in Norway by introducing pure battery and hybrid concepts to reduce operational costs and decrease the environmental impact.

New-built hybrid ferries have specific characteristics both in terms of design, equipment, operational routes as well as requirements for emission and energy usage. One key problem to investigate is how to optimally plan the charging of such ferries. Optimal charging should take into account many factors, e.g. weather forecasts, battery lifetime, available grid power, electricity prices and power losses.

Large costs can be saved if an optimization routine is applied when calculating the requested charging energy per shore docking. This master thesis will contribute with an optimization framework aimed at optimal charge planning in hybrid ferry systems.

Sub-tasks to be solved are:

1. Identify key parameters necessary to plan charging of hybrid ferry systems.
2. Propose a cost function for the optimization problem.
3. Identify and compare possible optimization methods suitable for the problem.
4. Develop case study analyses for test and verification of the optimization framework using known ferry routes and datasets.
5. Investigate other potential savings for applying optimization algorithms on charging cycles.

# Abstract

The climate changes are arguably one of the biggest challenges for our generation. However, new technology is being developed as a result of this challenge, and is entering new solutions for us to achieve international and national targets for climate gas reductions. The hybrid ferry is such a solution, where new technology is implemented for making the transportation system more sustainable.

The hybrid ferry operates on low-emissions technology, by combining diesel generators with zero-emissions energy storage systems. As the battery is the most common type of energy storage used in hybrid ferries today, research on how to better utilize the battery can improve hybrid ferry efficiency.

This thesis focuses on the battery utilization in the hybrid ferry and the associated charging stations at shore. A methodology and an optimization framework for optimal charge planning in hybrid ferry systems, and an approach for quantifying the potential savings are the two main contributions.

Optimal charge planning is a collective term for the prediction of future external factors impacting the hybrid ferry system and for the calculation of optimal battery charge profiles based on a set of objectives. The external factors are defined to be the varying amount of passengers, wind conditions and ocean current conditions, which all contributes to the ferry energy consumption.

After considering possible factors impacting the battery charging, the objective to minimize the cost of electricity, battery power loss, battery aging and the penalizing cost of electricity is chosen for the optimization problem. As the set of objectives may

not include all the factors influencing battery charging, the solution is *an* optimal solution to the battery charging problem.

With the electricity price varying throughout the day, month and year, reduction in cost can be achieved by planning the transfer of energy accordingly to the price.

Battery power loss and aging are factors related to the battery usage and performance, and including these factors in the optimization is important for improving the efficiency and limiting battery degradation. Since the battery system cost takes a large share of the total ferry cost, large savings can be made by prolonging the battery life.

As the demand of power is increasing more rapid than the demand of energy for the end user in Norway, new network tariff models are currently examined for this new use of electricity. To study the impact of new tariff models, a term penalizing high power outtake during times with undersupply of power in the grid is included as an minimization objective for the optimal charging.

A numerical and an analytical method for solving the optimal control problem for ferry- and shore battery charging are proposed. As the analytical method, based on Pontryagin's minimum principle, gives better results with regards to performance and computation time, this method is further used in the hybrid ferry system simulations.

A hybrid ferry using optimal charge planning is more profitable than a hybrid ferry using the current standard method of charging, where the target is to substitute the energy consumed during the last trip. Simulations shows that for the modelled hybrid ferry system, under the influence of a grid penalty cost, large savings can be made by optimally calculate the distribution between grid power and charging station power. Prediction of future energy consumption is seen to give the largest savings related to battery power loss and aging in the modelled system.

Including an electricity planning factor when calculating the transfer of electricity to the batteries has a potential of reducing the total annual system cost for one modelled hybrid ferry system by approximately NOK 210,000,- compared to the current charging method. Around 72% of this can be assigned to savings in battery aging cost and 20% to the reduction in electricity cost.

Adding an additional optimization routine on top of the proposed optimization on the energy planning can improve the hybrid ferry operation even more. By looking

at the factors impacting the ferry on a longer term, and not just on the next crossing, can give more optimal scheduling of energy, and thus, improve system efficiency and savings. Future work, such as contribution to load leveling in the grid and ferry to grid storage capabilities, should further be studied as it may improve earnings for the ferry operator.

This thesis explores some of the potential of optimal charge planning in hybrid ferry systems. The proposed methods are likely to give savings for the ferry operator and profit for the system integrator. As a direct consequence of prolonging the battery life, the ferry system is also made more sustainable, which is an overall goal for all parts.

# Sammendrag

Klimaendringene er uten tvil en av de største utfordringene vår generasjon står ovenfor. Ny teknologi utvikles imidlertid som følge av denne utfordringen, og gjør sitt inntog i nye løsninger for at vi skal nå internasjonale og nasjonale mål for reduksjon i klimagassutslipp. Hybride ferger er en slik løsning, hvor ny teknologi er implementert for å gjøre systemet mer bærekraftig.

En hybrid ferge opererer på lavutslippsteknologi ved å kombinere dieselgeneratorer med nullutslipp-energilagringsystemer. Siden batteriet er den mest brukte typen for energilagring i hybride ferger i dag, kan forskning på hvordan man bedre utnytter batteriet forbedre effektiviteten i fergen.

Denne masteroppgaven fokuserer på batteriutnyttelsen i fergen og de tilhørende landbaserte ladestasjonene. En metodikk og et rammeverk for optimalisering av batterilading i fergesystemer, og en tilnærming for kvantifisering av mulige besparelser er de to viktigste bidragene fra denne oppgaven.

Planlegging av optimal lading er et samlebegrep for prediksjon av fremtidige eksterne faktorer som påvirker fergesystemet og for beregning av optimal batterilading basert på et sett med mål. De eksterne faktorene er i denne oppgaven definert til å være den varierende mengden med passasjerer, vindforhold og havstrømsforhold, som alle bidrar til energiforbruket i fergen.

Etter å ha vurdert de mulige faktorene som påvirker batteriladingen, er målet for optimaliseringen satt til å minimere kostnaden av strøm, kostnaden av effekttap i batteri, kostnaden av aldring i batteri og straffekostnaden ved å ta ut effekt av

strømnettet over en lading. Siden optimaliseringen ikke inkluderer alle faktorer som påvirker en batterilading, er løsningen på optimaliseringsproblemet en av flere mulige løsninger for optimal lading av batteri.

Ved at strømprisen varierer over en dag, over en måned og over et år, kan reduksjon i kostnaden oppnås ved å planlegge energioverføringen etter prisdynamikken.

Effekttap i batteri og aldring er faktorer knyttet til bruken og ytelsen av batteriet, og å inkludere disse i optimaliseringsproblemet er viktig for å forbedre effektiviteten og for å begrense batteriforringelsen. Siden kostnaden av batterisystemet er en stor del av kostnaden til hele fergesystemet kan det oppnås store besparelser ved å forlenge batterilevetiden.

Ettersom effektbehovet stadig øker mer en energibehovet for sluttbrukere i Norge, undersøkes for tiden nye nettariffer for denne nye typen bruk av strøm. For å studere virkningen av nye nettariffer inngår en faktor som straffer høyt uttak av effekt under perioder med underforsyning av elektrisitet i nettet som et minimeringsmål for optimal lading.

En numerisk og analytisk metode for å løse optimaliseringsproblemet er foreslått. Ettersom den analytiske metoden, basert på Pontryagin's minimeringsprinsipp, gir bedre resultater med hensyn til ytelse og beregningstid, blir denne metoden ytterligere brukt i simuleringene av fergesystemet.

Et fergesystem som tar i bruk planlegging av optimal lading er mer lønnsomt enn et fergesystem der dagens ladingsstrategi blir brukt, hvor målet er å erstatte energien som ble konsumert under den siste turen. Simuleringer viser at store besparelser kan oppnås ved å beregne den optimale fordelingen mellom effektuttak fra nettet og bruken av batteriet i ladestasjonen for et modellert fergesystem under påvirkning av en straffekostnad for effektuttak. Prediksjon av fremtidig energiforbruk er sett å gi de største besparelsene knyttet til effekttap i batteri og batterialdring for det modellerte systemet.

Inkluderingen av en planleggingsfaktor basert på strømkostnaden ved kalkulerings av energioverføring til batteriene har et potensial for å redusere den årlige systemkostnaden for et modellert fergesystem med rundt 210 000 kroner, sammenlignet med dagens strategi for energioverføring. Rundt 72% av besparelsen kan tilordnes reduk-

sjonen i kostnaden til batterialdring og 20% kan tilordnes reduksjon i strømkostnad.

Å legge til en ekstra optimaliseringsrutine på toppen av den foreslåtte optimaliseringen av energi, kan forbedre fergedriften ytterligere. Ved å se på faktorene som påvirker fergen på lengre sikt, og ikke bare ved neste overfart, kan mer optimal fordeling av energi oppnås, og dermed gi forbedring i systemets effektivitet og lønnsomhet. Fremtidig arbeid, som for eksempel bidrag til lastutjevning i nettet og muligheter innenfor “ferge-til-nett”-lagringsmuligheter, bør videre undersøkes, da dette kan gi mer inntekt for fergeoperatøren.

Denne masteroppgaven utforsker noe av potensialet for planlegging av optimal lading i hybride fergesystemer. De foreslåtte metodene vil trolig gi besparelser for fergeoperatøren og mer lønnsomhet for systemintegratoren. Som en direkte konsekvens av forlenget batterilevetid, blir fergesystemet også mer bærekraftig, noe som er et overordnet mål for alle parter.

# Preface

This master's thesis is the resulting work of the 5 year master's degree programme in Cybernetics and Robotics at the Norwegian University of Science and Technology (NTNU). The thesis is carried out during the spring semester of 2019 at the Department of Engineering Cybernetics.

The thesis problem is formulated by Siemens Offshore Marine Centre in Trondheim and involves research in the field of hybrid ferry systems and energy planning. When Siemens reached out and invited me to be a part of new research and development in sustainable technology, I was not late to accept. The given problem was well-suited for my main profile, background and interest.

The results are based on theoretical analysis of hybrid ferry systems operating in Norway, and modelling and simulation of such systems in Python. All software and models are self-made, if not stated else, with relevant data for the hybrid ferry system given by Siemens.

The thesis is a continuation of a specialization project conducted during the autumn of 2018, and since the project is not published and public available, some important background theory around hybrid ferry systems and battery technology are restated to provide a good reading experience.

A list of the material that is used as basis, but further developed from the specialization project is given below:

- History of marine electrical vessels (Chapter 2)
- Ferry power systems (Section 2.2.1)
- Ferry control system (Section 2.2.2)
- The lithium-ion battery (Section 3.1)
- Battery life (Section 3.2)

The work done throughout the semester has been in collaboration with my supervisor at NTNU, Prof. Jon Are Suul, and my co-supervisor at Siemens, MSc. Lars Andreas Lien Wennersberg. Acknowledgment must be given to the supervisors for their good help, relevant discussions and thoughts on the problem which has greatly improved my knowledge and ability to achieve the results in the report. I would also like to thank Siemens for allowing me to take the work in the direction I found most interesting.

By having good fellow students and friends, the last five years in Trondheim have been exciting. I wish to the end to thank my parents and my brother for giving me good moral support and for making the student life easier.

# Contents

<b>Problem Description</b>	<b>ii</b>
<b>Abstract</b>	<b>iv</b>
<b>Sammendrag</b>	<b>vii</b>
<b>Preface</b>	<b>x</b>
<b>Abbreviations</b>	<b>xxii</b>
<b>1 Introduction</b>	<b>5</b>
1.1 Motivation . . . . .	5
1.2 Relevant literature . . . . .	9
1.2.1 Electric vehicles . . . . .	9
1.2.2 Battery degradation . . . . .	10
1.3 Thesis goal . . . . .	12
1.4 Tools . . . . .	13
1.5 Contributions . . . . .	15
1.6 Outline . . . . .	16

<b>I</b>	<b>Background Theory</b>	<b>19</b>
2	<b>Hybrid Ferries</b>	<b>21</b>
2.1	Hybrid ferry operation . . . . .	23
2.2	Hybrid ferry system . . . . .	26
2.2.1	Ferry power system . . . . .	27
2.2.2	Ferry control system . . . . .	33
2.3	The charging station . . . . .	35
3	<b>Battery Energy Storage System</b>	<b>37</b>
3.1	The lithium-ion battery . . . . .	37
3.2	Battery life . . . . .	39
3.2.1	Battery aging . . . . .	39
4	<b>The Norwegian Electricity System</b>	<b>43</b>
4.1	Electricity grid structure . . . . .	44
4.1.1	Power supply to hybrid ferry system . . . . .	45
4.2	Electricity tariffs . . . . .	46
5	<b>Optimization Methods</b>	<b>51</b>
5.1	Numerical methods . . . . .	52
5.1.1	Dynamic programming . . . . .	53
5.2	Analytical methods . . . . .	56
5.2.1	Pontryagin's minimum principle . . . . .	56
<b>II</b>	<b>Methods &amp; Modelling</b>	<b>59</b>
6	<b>Hybrid Ferry Modelling</b>	<b>61</b>
6.1	Modelling of operation . . . . .	61
6.1.1	Working days operation . . . . .	62
6.1.2	Weekend operation . . . . .	62
6.1.3	Energy consumption . . . . .	63

6.1.4	Implementation of operation in model . . . . .	64
6.2	Modelling of ferry system . . . . .	65
6.2.1	Implementation of ferry system in model . . . . .	67
<b>7</b>	<b>Charging Station Modelling</b>	<b>69</b>
7.1	Implementation of charging station in model . . . . .	70
<b>8</b>	<b>Battery Modelling</b>	<b>73</b>
8.1	Electrical circuit model . . . . .	75
8.2	Power loss model . . . . .	77
8.3	Battery aging model . . . . .	79
<b>9</b>	<b>Modelling of Electricity System</b>	<b>85</b>
9.1	Grid supply modelling . . . . .	85
9.1.1	Modelling of grid capacity . . . . .	86
9.2	Transmission line modelling . . . . .	89
9.3	Electricity cost modelling . . . . .	90
<b>10</b>	<b>Modelling of External Factors</b>	<b>93</b>
10.1	Car and passenger load modelling . . . . .	93
10.2	Modelling of environmental forces . . . . .	97
10.2.1	Wind modelling . . . . .	97
10.2.2	Ocean current modelling . . . . .	103
<b>III</b>	<b>Optimal Charge Planning</b>	<b>109</b>
<b>11</b>	<b>Problem Formulation</b>	<b>111</b>
11.1	Cost function . . . . .	113
11.1.1	Shore charging cost function . . . . .	115
11.1.2	Ferry charging cost function . . . . .	115
11.1.3	Nightlay charging cost function . . . . .	117
11.2	Optimal control problem . . . . .	118

<b>12 Comparison of Optimization Methods</b>	<b>123</b>
12.1 Dynamic programming . . . . .	127
12.1.1 Optimal charging using dynamic programming . . . . .	129
12.2 Pontryagin’s minimum principle . . . . .	133
12.2.1 Optimal charging using minimum principle . . . . .	135
12.3 Numerical versus analytical method . . . . .	140
<b>13 Prediction of Future Energy Consumption</b>	<b>141</b>
13.1 Planning by power losses . . . . .	141
13.2 Planning by the route schedule . . . . .	142
13.3 Planning by external factors . . . . .	142
13.3.1 Passenger planning . . . . .	143
13.3.2 Wind and ocean current planning . . . . .	144
13.4 Planning by cost of electricity . . . . .	146
<b>IV Simulation</b>	<b>149</b>
<b>14 Scenario I: Energy Planning</b>	<b>151</b>
14.1 Scenario description . . . . .	151
14.1.1 Operational profile . . . . .	152
14.1.2 External factors . . . . .	154
14.2 Scenario simulation . . . . .	156
14.2.1 Standard method charging . . . . .	156
14.2.2 Optimal charge planning method . . . . .	158
14.3 Scenario results and discussion . . . . .	164
<b>15 Scenario II: Energy Planning by Cost of Electricity</b>	<b>169</b>
15.1 Scenario description . . . . .	169
15.2 Scenario simulation . . . . .	170
15.2.1 Standard- and optimal method charging from Scenario I . . . . .	170
15.2.2 Ferry data . . . . .	172

15.2.3 Charging station data . . . . .	173
15.3 Scenario results and discussion . . . . .	176
<b>V Conclusions &amp; Future Work</b>	<b>181</b>
16 Conclusions	183
17 Future Work	187
<b>Appendix</b>	<b>191</b>
A Application File Structure	191
B LiFePO <sub>4</sub> Cell Datasheet	193
C Ferry Route Schedule	197
D Weather Data	199
E Ocean Current Data	201
<b>References</b>	<b>203</b>

# List of Tables

2.1	Time in different operational modes with associated average speed [knots] and motor power [% of maximum continuous rating (MCR) of engine] . . . . .	26
3.1	Explanation of battery terms . . . . .	39
6.1	Energy consumption under reference conditions . . . . .	63
6.2	Reference conditions . . . . .	64
6.3	Ferry construction parameters[60] . . . . .	66
6.4	Ferry system specifications and component efficiencies . . . . .	66
7.1	South- and north charging station specifications and component efficiencies . . . . .	70
8.1	LiFeOP <sub>4</sub> cell specifications . . . . .	75
8.2	Nominal battery parameters . . . . .	80
9.1	Grid capacity . . . . .	86
10.1	Number of crossings each hour . . . . .	95
12.1	Results and costs associated with nightlay charging using DPM . . .	130
12.2	Results and costs associated with normal charging using DPM method	132

12.3	Results and costs comparison between DPM and standard method under normal charging . . . . .	132
12.4	Results and costs associated with nightlay charging using PMP method	135
12.5	Results and costs associated with normal charging using PMP method	139
12.6	Results and costs comparison between PMP and standard method under normal charging . . . . .	140
13.1	Electricity prices during working day operational hours . . . . .	146
13.2	Electricity prices during weekend operational hours . . . . .	147
14.1	Results and costs associated with standard method charging . . . . .	157
14.2	Results and costs associated with optimal charge planning . . . . .	164
14.3	Comparison of system costs . . . . .	165
14.4	Comparison of battery degradation in Scenario I . . . . .	165
14.5	Annual savings . . . . .	166
15.1	Results and costs associated with the standard- and optimal charging method from SI . . . . .	170
15.2	Results and costs associated with optimal charge planning in scenario II	176
15.3	Comparison of system costs in Scenario II . . . . .	177
15.4	Electricity cost comparison in Scenario II . . . . .	178
15.5	Comparison of battery degradation in Scenario II . . . . .	179
15.6	Annual savings using energy planning by cost of electricity . . . . .	179

# List of Figures

1.1	Web-based application built by using Dash. Based on [1] . . . . .	14
2.1	The Elektra by Siemens & Halske. Photo from [2]. . . . .	22
2.2	Overview of hybrid ferry operation . . . . .	24
2.3	Generic operational profile of hybrid ferry . . . . .	25
2.4	A modern hybrid ferry system. Photo from [2]. . . . .	27
2.5	Structure of an Integrated Power System (IPS) . . . . .	28
2.6	Hybrid AC-DC distribution system. From [3] . . . . .	29
2.7	DC distribution system. From [3] . . . . .	31
2.8	Topology of a hybrid ferry control system hierarchy . . . . .	33
2.9	Topology of a charging station . . . . .	36
3.1	Charging and discharging in a lithium-ion battery. Based on [4] . . . .	38
3.2	Development of SEI. Figure from [5]. . . . .	40
4.1	The Norwegian electricity grid structure. Illustration from [6] . . . . .	44
4.2	Electricity price dynamic. Prices from [7] . . . . .	47
5.1	Arc costs of charging . . . . .	54
5.2	Optimal charging trajectory . . . . .	55
6.1	Ferry dimensions. Illustration from [8] . . . . .	65
6.2	Modelling of hybrid ferry . . . . .	68

7.1	Modelling of charging station . . . . .	71
8.1	Modelling of battery . . . . .	74
8.2	Battery electrical circuit model . . . . .	75
8.3	Effect of SoC on battery parameters . . . . .	77
8.4	Battery power loss approximation . . . . .	78
8.5	Predicted capacity loss for nominal profile . . . . .	81
8.6	Severity factor map . . . . .	83
9.1	Modelling of grid supply . . . . .	86
9.2	Grid net exchange for Nordic region . . . . .	87
9.3	Modelling of transmission line . . . . .	89
9.4	Electricity price dynamics. Prices from [7] . . . . .	90
10.1	Day variation of PBEs on ferry . . . . .	94
10.2	Wind force acting on ferry . . . . .	99
10.3	Wind power on ferry in surge direction . . . . .	101
10.4	Wind power on ferry in sway direction . . . . .	102
10.5	Current force acting on ferry . . . . .	104
10.6	Current coefficient approximation values using $c_{c,x} = 0.45$ , $c_{c,y} = 0.65$ for ferry crossing in north direction. . . . .	105
12.1	Electricity price variation during a working day from 02 to 06 . . . . .	124
12.2	Nightlay charging using standard method . . . . .	125
12.3	Normal charging using standard method . . . . .	126
12.4	Nightlay charging using the dynamic programming method . . . . .	130
12.5	Normal charging with DPM . . . . .	131
12.6	Nightlay charging with PMP charging method . . . . .	136
12.7	Effect of initial co-state value on target SoC. . . . .	137
12.8	Normal charging with PMP charging method . . . . .	138
12.9	Shore battery recharging using PMP . . . . .	139
13.1	PCU prediction by the south charging station controller . . . . .	143

13.2	Wind prediction by the charging station controllers . . . . .	145
13.3	Ocean current prediction by the charging station controllers . . . . .	145
14.1	Working day operational profile . . . . .	152
14.2	Weekend day operational profile . . . . .	153
14.3	External factors during working day . . . . .	154
14.4	External factors during weekend day . . . . .	155
14.5	Battery SoC dynamic in ferry and charging stations . . . . .	157
14.6	Ferry characteristics during working day . . . . .	159
14.7	Ferry characteristics during weekend day . . . . .	160
14.8	South charging station characteristics . . . . .	162
14.9	North charging station characteristics . . . . .	162
14.10	Charging station dynamics of battery SoH and accumulated el. cost . . . . .	163
15.1	Battery SoC dynamic in ferry and charging stations using optimal method from SI . . . . .	171
15.2	Ferry dynamics during working day in scenario II . . . . .	172
15.3	Ferry characteristics during weekend day in scenario II . . . . .	173
15.4	South charging station characteristics in scenario II . . . . .	174
15.5	North charging station characteristics in scenario II . . . . .	175
15.6	Charging station dynamics of battery SoH and accumulated el. cost in scenario II . . . . .	175
A.1	Application file structure . . . . .	191
C.1	Ferry route schedule used in modelling . . . . .	198

# Abbreviations

<b>AC</b>	Alternating Current
<b>DC</b>	Direct Current
<b>DoD</b>	Depth of Discharge
<b>DP</b>	Dynamic Programming
<b>ECMS</b>	Equivalent Consumption Minimization Strategy
<b>EMS</b>	Energy Management System
<b>ESS</b>	Energy Storage System
<b>HEV</b>	Hybrid-Electric Vehicle
<b>IAS</b>	Integrated Automation System
<b>ICT</b>	Information and Communications Technology
<b>IPS</b>	Integrated Power System
<b>NOK</b>	Norwegian krone (Currency of Norway)
<b>PMP</b>	Pontryagin's Minimum Principle
<b>PMS</b>	Power Management System
<b>RCS</b>	Remote Control System
<b>SoC</b>	State of Charge
<b>VSC</b>	Voltage Source Converter
<b>VSD</b>	Variable Speed Drive



# **Optimal Charge Planning in Hybrid Ferry Systems**



"Electrification and energy storage plays an essential role in a low-emissions future.

In 2015, the Storting decided that all new ferries serving municipal or regional ferry connections should be low- or zero emission vessels. Today, as a rule, all new public tenders for car ferries require zero or low emission technology.

This has triggered considerable creativity and technological development."

---

*Prime Minister Erna Solberg*[9]



# Chapter 1

## Introduction

This introductory chapter will present the motivation behind the thesis and provide context for the problems to be solved. Both social and technical aspects with optimal charge planning of hybrid ferry systems will be enlightened. Relevant literature on the area of charge planning is presented, together with the contributions on the topic from this thesis. At last, the outline gives the reader an overview of the structure of the thesis and a description of each of the upcoming parts.

### 1.1 Motivation

Challenging the climate changes is probably the most important work for the current and future generations. Through the Paris Agreement, the international community has agreed to keep the global warming well below 2 degrees and strive to limit the temperature increase to 1.5 degrees. To reach this goal, an immense effort must be taken in all sectors contributing to pollution and greenhouse gas emissions.

In 2010, the transport sector was responsible for 14% of the direct global greenhouse gas emissions and approximately 23% of total energy-related  $CO_2$  emissions. The transport sector is the fastest growing contributor to climate emissions and therefore sustainable mitigation policies should be implemented to stop this rate of increase[10, 11].

In Norway, the transport sector accounts for 30% of the national greenhouse gas emissions and the country has a goal to decrease the emissions by 35-40 % by 2030[12, 13]. To reach both national and global climate goals for pollution and greenhouse gas emissions, several initiatives have been taken the recent years to implement sustainable and clean alternatives for modern transportation systems.

Norway is a unique country in terms of electrifying the transport sector. With over 98% of the energy production coming from renewable energy sources, Norway has the highest share of electricity produced from renewable sources in Europe, and the lowest emissions from the power sector[14, 15]. The country has the world's highest share of electric vehicles per capita with a market share of 34 % and has an ambitious goal that all new bought cars should have zero-emissions technology by 2025[16, 17, 18]. In addition, the country is in the frontline for an emissions modernization of another transportation system: the ferry.

By the end of 2021, one-third of the ferries that operates on domestic ferry routes will have batteries installed, operating either as all-electric or as hybrid ferries. The National Public Road Administration (NPRA) considers that in 2030, two-thirds of the domestic car ferry routes will be possible to operate with ferries powered by electricity, which has a potential of annual reduction of approximately 400.000 tonnes  $CO_2$ [19].

A report by the Maritime Battery Forum states that for an all-electric ferry, the environmental payback period for greenhouse gas emissions contributing to Global Warming Potential (GWP) and  $NO_x$  emissions are 1.4 months and 0.3 months, respectively, when the Norwegian mix of energy sources are used[20].

Most of the hybrid ferries in operation today combine diesel generators and a battery energy storage system for meeting the energy demand in the ferry. As the ferry operates on a relatively short and determined route, the energy storage system onboard can be recharged when the ferry docks at the harbour for loading and unloading passengers.

As the route schedule must be strictly followed, the ferry charging time is limited, and often very short. A consequence of this is that a large amount of energy is needed to be transferred to the ferry in a short amount of time, which has a big impact on the landbased grid supply. To handle this, a charging station with a battery energy

storage system is used as a buffer between the grid supply and the ferry, and works by transferring power in parallel with the grid supply to decrease the grid load.

Two different charging strategies are used in the current hybrid ferry charging process:

1. The operator determines the power amplitude and typically selects the highest possible power such that the ferry has the highest energy margin at all times.
2. The charging system determines the power amplitude that charges the battery back to nominal state of charge, i.e., each charging aims to replace the energy consumed during the last crossing.

As a consequence, only the ferry operation is taken into account when deciding the charging power. However, many factors have a direct or indirect impact on the charging and energy consumption of a ferry. By utilizing statistical data and models for the battery and the ferry, both economical and operational considerations can be accounted for when planning the charging of a hybrid ferry system.

One factor to consider is the cost of electricity, which varies throughout the day, week and year. On a general term, the electricity price is highest in the morning and evening, and during the winter months. By planning higher energy transfer when the electricity price is low, and lower energy transfer when the price is high, the tender can possibly reduce the overall cost of electricity.

As the investment cost of the battery energy storage system is a large part of the total hybrid ferry cost, increasing the expected battery life will have a large impact on the overall profitability of the system. Therefore, by finding the key factors contributing to battery aging and reducing the degradation, the profitability, and in addition the sustainability, of the system can be increased.

Power losses in the electric components reduces the efficiency grade of the ferry system. In addition, the power that is dissipated has no contribution, and is needed to be repurchased to be utilized. Thus, by trying to minimize the power losses during a charging process, both the efficiency and the profitability can be increased.

Keeping the balance between production and consumption can be challenging for the grid system operator when electric transportation systems, with high power

demand, suddenly connects to the grid. Adding a penalizing cost on the power outtake during times undersupply in the grid is a measure the grid operator can do to not overload the grid and for avoiding future investments. With new network tariff models coming up, taking these factors into consideration, the ferry tender may benefit from changing the charging strategy.

Ferry energy consumption is also influenced by factors such as the amount of passengers and weather- and ocean conditions. These factors can, however, be predicted by statistical data and weather prognosis, and be used in the energy planning for more efficient battery utilization. Prediction of the external factors can also improve the operational safety and reliability, by having better knowledge of the forthcoming energy usage.

By considering the factors stated above, this thesis addresses some of the potential in energy planning and optimal charging in hybrid ferry systems.

## 1.2 Relevant literature

As most literature regarding charging and energy management of batteries in vehicles are considering hybrid- or electric cars, this transportation system is also used as the platform for further study. Current literature on hybrid ferries are, on the other hand, mostly concerned with optimal scheduling of energy between the storage system and the diesel generators.

The number of articles concerning battery aging and degradation mechanisms are very high and the relevant literature on the topic is difficult to navigate. Articles regarding lithium-ion batteries used in electric vehicles are mostly examined, with their models for battery degradation and data on battery aging.

Typical key words used for search are:

- Battery degradation
- Battery life optimization
- Optimal energy management
- Optimal charging of electric vehicles

Number of citations for the different papers have been used as a measure of quality and to find reliable references during the literature study.

### 1.2.1 Electric vehicles

In [21] by L. Tang et al. an optimal control-based energy management strategy for hybrid-electric vehicles (HEVs) including battery life optimization is presented. The paper uses a solution based on Pontryagin's minimum principle to minimize the fuel consumption while maintaining the battery state of charge within reasonable bounds by using knowledge of the forthcoming driving cycle. The study shows that it is possible to extend battery life without adversely affecting vehicle performance.

In [22] by L. Serrao et al. an analytical derivation of the Equivalent Consumption Minimization Strategy (ECMS) for energy management of hybrid vehicles is presented. This strategy allows for real-time computation of the optimal energy distribution between the diesel engine and energy storage system, and thus, the requirement of a-priori knowledge of the driving cycle is not needed.

A different approach on electric vehicle charge optimization including effects of battery degradation is presented in [23]. Here, the degradation model consist of state of charge-related degradation, depth of discharge-related degradation and temperature-related degradation, where both energy capacity fade and power fade are estimated. The optimization algorithm minimizes the total cost, which is the sum of the cost of electrical energy and the cost of battery degradation.

A comparative analysis of energy management strategies for HEVs is given in [24] by L. Serrao et al. The paper presents a formalization of the energy management problem in HEVs and the three different strategies for solving the optimization problem: dynamic programming (DP), Pontryagin's minimum principle (PMP) and ECMS.

### 1.2.2 Battery degradation

A review on lithium-ion battery aging mechanisms and estimations for vehicle applications is given in [5] by A. Barré et. al. The papers states that battery degradation takes place at all times, but with different proportions as usage and external conditions interact to provoke degradations. The battery aging is further divided in calendar aging and cycle aging. The more recurrent factors involved with calendar aging are temperature, storage SoC and time. For cycle aging temperature, variation of SoC and cycle number are some of the factors that contributes.

The main aging mechanisms in lithium-ion batteries are presented in [25] by M. Broussely. It concludes with the most critical part of the cell being the negative electrode/electrolyte interface, where the growth of solid electrolyte interface, loss corresponding to lithium corrosion and degradation of active surface area takes place.

In [26] by V. Marano et al. a damage accumulation model for the battery aging under hybrid vehicular operation is described. The model builds on the concept that damage is accumulated with every charge and discharge of the battery, modulated by

a severity factor.

A generic empirical model to describe the main degradation mechanisms in a lithium-ion battery was initially proposed in [27]. This model is further improved in [28] and [21] to predict degradation in HEV batteries. In [26] by V. Marano, different models for battery life estimation are proposed, where the weighted Ah-throughput model is used to determine the damage on the battery life related to a given driving cycle.

The formulation of the optimization problem and the battery aging model used later in the report are highly influenced by the work done in [22, 21].

### 1.3 Thesis goal

This thesis aims to apply the concepts of energy planning and optimal charging of batteries in a hybrid ferry system. Energy planning is defined as the ability to accurately predict future energy need and consumption within a predefined time to ensure safe, uninterrupted and optimal operation. Optimal charging is achieved when a control trajectory of charging powers minimizes the total cost of a set of objectives.

In this thesis, the amount of passengers on the ferry and the wind- and ocean current conditions are the external factors considered when planning the energy transfer. Hence, sufficient modelling of the impact of the different external factors is a requirement for accurate prediction.

The objectives considered by the optimal charging problem are: 1) minimize the electricity cost, 2) minimize the battery power loss, 3) minimize the battery aging cost and 4) minimize the grid penalty cost. As the objectives are at times competing, the control algorithm is required to take tradeoffs between the objectives.

The hybrid ferry system is defined as the ferry with its associated charging stations. Thus, when calculating the charging profile with regards to energy planning and optimal charging, the charging routine is applied to both the ferry- and charging station batteries.

To reach the overall thesis goal, specific objectives to be solved are listed as follows:

- Obtain sufficient knowledge of hybrid ferry system and operation.
- Establish a modelling framework for the hybrid ferry system and operation.
- Define an optimal control problem minimizing the set of objectives.
- Identify and compare suitable optimization methods.
- Perform case studies utilizing the optimization routine on a hybrid ferry system with external factors and electricity price variation acting on the system.

## 1.4 Tools

A large part of the work has consisted in modelling and simulation of hybrid ferry systems. The outcome of this is an application that can be used to simulate a hybrid ferry system with a corresponding operational profile. The properties of the hybrid ferry and the charging stations can be changed accordingly to simulate different behavior. The structure of this application is illustrated in Appendix A.

The most relevant tools used to achieve the thesis goal are described below:

### Siemens' Battery Profile Tool

For realistic modelling of the hybrid ferry system, Siemens has contributed with selected operational profiles for different hybrid ferry projects in Norway. The profiles are generated by Siemens' Battery Profile Tool, which calculates battery states based on route-, battery- and ferry specifications.

### Python

Python is the programming language used for modelling the system and for data analysis. Mostly, Python classes are used to model the different objects in the system, with a top-down approach. Meaning that the ferry class consists of several sub-classes such as a battery class and a controller class.

## Dash by Plotly

Dash is a Python framework for building analytical web applications[29]. The tool is used to display the results from the simulations in a web based interface application. The application is based on a financial application, with open source code given in [1].

A facsimile from the web page after a simulation is shown in Figure 1.1. The results are grouped in 6 bars at the top, which are representing the data in respectively the ferry, the south charging station, the north charging station, the electricity cost, the external factors and the battery.



Figure 1.1: Web-based application built by using Dash. Based on [1]

## 1.5 Contributions

The main contributions of this thesis are:

1. A methodology and an optimization framework for optimal charge planning in hybrid ferry systems.
2. An approach for quantifying the potential savings in a hybrid ferry system.

Following this, an outlining of the most important factors impacting the charging process, and how they can be transformed into a cost are presented. A key part in this is how the battery degradation can be expressed as a performance parameter, giving a quantified saving in overall cost when optimizing the battery usage.

The use of optimal charge planning in a hybrid ferry system to calculate charging profiles for the ferry- and shore batteries and how to quantify the charging performance factors have, to the author's best knowledge, not been studied before.

## 1.6 Outline

The thesis is composed of 5 parts. The main content of each part and its including chapters are briefly described below:

### **Part I: Background Theory**

Part I provides the background material required to understand the work presented in parts II and III. Theory on the history of electric ferries, together with material on hybrid ferry systems and operation are given in chapter 2. A description of the lithium-ion battery, with the key factors for battery aging, is presented in chapter 3. A summary of measures to limit the battery degradation is also given. Chapter 4 gives an overview of the electricity system needed for providing a stable and secure supply of energy to the hybrid ferry system. The cost of drawing energy from the grid is also discussed. As a background for the formulation of the optimization problem in Part III, material on the optimization methods used is given in chapter 5.

### **Part II: Methods and Modelling**

This part focuses on the modelling and the implementation of the hybrid ferry system and external factors impacting the ferry. The modelling of the ferry system and operation are presented in chapter 6. The model, with its parameters and characteristics, is used as the basis for the simulations in Part IV. Chapter 7 provides the specifications and modelling of the charging station. The charging station is regarded as the most important module in the overall system, with the controller calculating new charging profiles for the batteries.

Battery dynamics, power losses and aging are modelled in chapter 8. The battery modelling is important as it is a vital part of the optimal control problem formulation. The connection between the hybrid ferry system and the grid supply is presented in chapter 9. In addition, the cost of drawing power from the grid, and how this is

implemented in the model, are discussed. Implementation and impact of external factors are elaborated in chapter 10. The external factors impacting the ferry are defined to be the amount of passengers, wind conditions and ocean current conditions.

### **Part III: Optimal Charge Planning**

This part focuses on optimal charge planning in hybrid ferry systems and formulates the optimization problem and the prediction of future energy consumption. The optimal control problem for charging is formulated in chapter 11. The problem includes a cost function with a set of objectives which is subject for minimization. The optimal control problem is in chapter 12 solved using dynamic programming and the Pontryagin's minimum principle. Results using the two optimization methods are presented and compared for further use. Energy planning and how it is applied to the system are discussed in chapter 13.

### **Part IV: Simulation**

Two scenarios for hybrid ferry operation are simulated in this part. In chapter 14, energy planning, together with optimal battery charging, are applied to the modelled hybrid ferry system. The operational profile, external factors and system states are presented, and then compared with the current charging method used today. Another method for energy planning, which accounts for the varying electricity price, is presented in chapter 15. The new method shows the potential for further optimizing the scheduling of energy on a longer time horizon.

### **Part V: Conclusions and Future Work**

The thesis is then summarized in Part V, with conclusions and recommendations on future work.



## **Part I**

# **Background Theory**



## Chapter 2

# Hybrid Ferries

People and villages are connected to the outside society and national roads are connected together through the use of ferries. Today there are about 270 ferries that includes as an important and necessary part of the Norwegian transportation infrastructure[30].

As Norway has a clear goal to reduce greenhouse gas emissions, a larger share of the ferry fleet is now being replaced by hybrid ferry solutions. This switch to a more greener transportation is made possible by new technology and more efficient energy storage systems. The following brief description of the electric marine history is based on paper [31] by E. Skjong et al. The paper highlights the different stages in the evolution of the marine vessel's development and the impact of electricity. Most of the material in the chapter is also a further development of the work done in the specialization project, given in [32], on the same topic.

The first recorded effort to apply electric power on a marine vessel occurred in the late 1830s after Moritz Hermann Jacobi of Germany invented a simple battery-powered DC motor which was installed experimentally on small boats. In 1880s, the first commercially available shipboard electrical system was built, with the onboard DC system in SS Columbia, and in 1885, the first successful electrical powered vessel, The Elektra, build by Siemens & Halske was developed<sup>1</sup>. A photo of The Elektra is given in Figure 2.1.



Figure 2.1: The Elektra by Siemens & Halske. Photo from [2].

An arms race with new technological breakthroughs in electric propulsion and diesel-electric power systems followed in the World Wars I and II, where the development and use of the AC motor and the transformer were central.

The advances in semiconductor technology after World War II revolutionized the field of electronics, and modern electric ships takes extensively use of power electronics to control and convert the electrical energy. The use of power electronics to maximize fuel efficiency became a trend in the 1980s[31].

In late 2012, the world first hybrid car ferry MV Hallaig was launched. The ferry, built at Fergusons shipyard with support of more than £20 millions from the Scottish

---

<sup>1</sup>The Elektra was intended to operate as a kind of water taxi and solve the transport problems in Berlin back in 1886. The vessel could carry 25 passengers at a speed of 14 kilometer per hour[33].

government, is powered by a hybrid combination of lithium-ion batteries and a small diesel engine. MV Hallaig marked the start for a more environmental friendly ferry configuration, which is the norm in new build ferry contracts today[34].

The recent development in more efficient batteries and energy storage systems has made it possible to build marine vessels operated by only renewable energy sources. In January 2015, the world's first fully electric passenger and car ferry, MF Ampere, was commissioned. The ferry has an installed battery capacity of 1040 kWh, two electric motors of 450 kW and is capable of transporting 360 passengers and 120 cars between Oppedal and Lavik in Sognefjorden[31].

Based on report [30] from DNV GL, a hybrid ferry operated on purely battery power is profitable against other conventional ferry types where the transit time for crossing is approximately 30 minutes. This calculation is based on a ferry with a car capacity of 120, a crossing speed of 12 knots and the requirement that the ferry should manage to be fast charged within 5 minutes at quay.

## 2.1 Hybrid ferry operation

The 270 ferries in Norway operates in excess of 160 individual connections, where traffic volumes, crossing distances, number of crossings and general conditions varies considerably. While some crossings are simple round trips, others are more complicated with several harbours and with route schedules that changes a lot between days of the week and during one day[30].

The biggest operational difference between a conventional ferry and a hybrid ferry is that the hybrid ferry normally needs to be charged when docked at quay to have sufficient energy onboard for the crossing. To be charged, the ferry docks to a charging station at shore when it unloads and loads passengers.

An illustration of the hybrid ferry system is given in Figure 2.2. The ferry crosses between two harbours and connects to a charging tower at each harbour to charge the battery. The charging station determines the distribution between the grid power and the power from the batteries implemented in the station, and then deliver this collective power to the charging tower. When the ferry has finished the route schedule

for the day, it travels to a nearby nightlay harbour where it is slowly recharged. For the rest of the thesis, the charging tower is assumed as a part of the charging station.

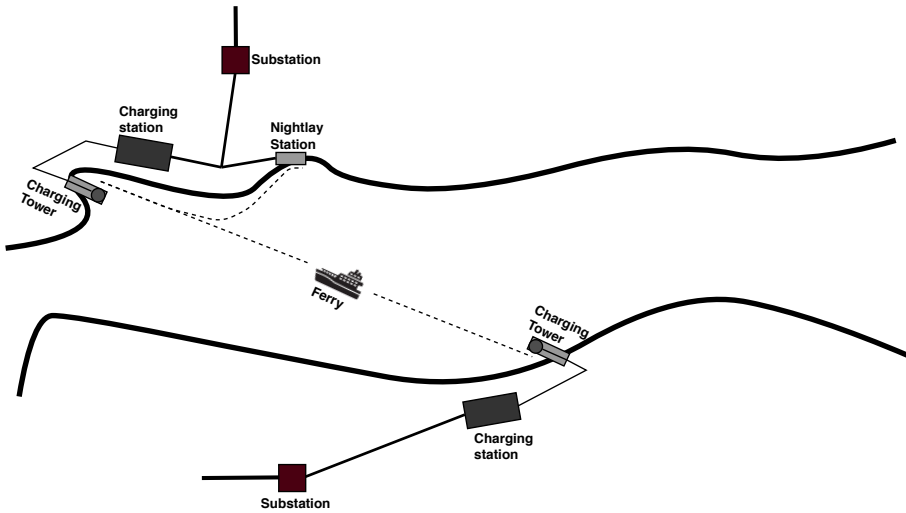


Figure 2.2: Overview of hybrid ferry operation

A generic profile for a hybrid ferry crossing is presented in Figure 2.3 and given numerically in Table 2.1. The profile is based on data from MF Ampere detailed in report [30] by DNV GL. As seen, the profile consist of six different modes: maneuvering from quay, acceleration to transit speed, transit, deceleration to maneuvering speed, maneuvering to quay and docked. For a normal trip, the crossing time is 25 minutes and the docking time is 5 minutes<sup>2</sup>.

The ferry has the highest power demand when maneuvering from/to quay and in acceleration mode. In transit-mode, the ferry keeps a constant speed and motor power, and when docked, the ferry uses the thrusters for a stable mooring. A different approach for the mooring is to use a vacuum based mooring system that draws the vessel against the quay, and thus enables reduced thruster utilization. Note that external

<sup>2</sup>The actual charging time for MF Ampere is approx. 10 minutes, but 5 minutes is used as a reference for the case studies in [30]

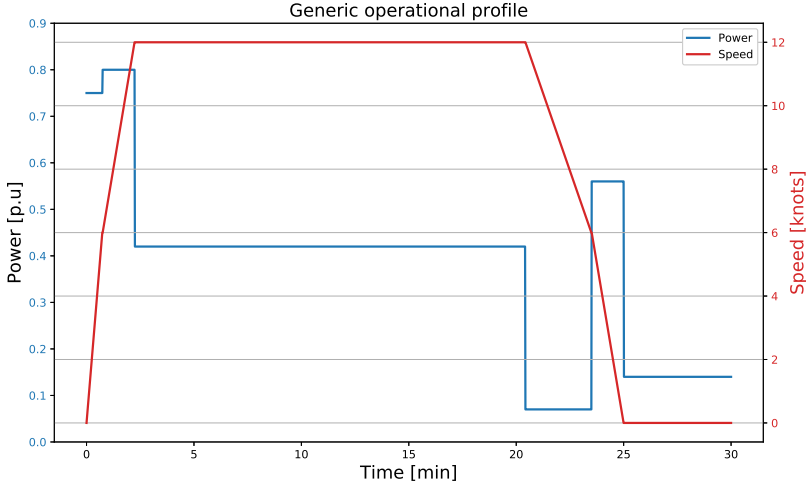


Figure 2.3: Generic operational profile of hybrid ferry

factors such as weather and ocean conditions are not considered in this profile.

Given the generic profile, the ferry is charged to a desired or necessary state of charge level within the docking time - meaning a high power is needed to ensure enough energy transferred from the charging station to the ferry battery. As an example, with an energy consumption of 190 kWh per crossing and a charging time of 5 minutes, the required constant power to refill the same amount of energy used during the latest crossing is given by

$$P_{chrg} = \frac{E_{consumption}}{T_{chrg}} = \frac{190 \text{ kWh}}{\frac{5}{60} \text{ h}} = 2.28 \text{ MW}. \quad (2.1)$$

To avoid a too high impact on the land based grid, the charging station is equipped with a battery system to work as a buffer and to reduce the grid power demand.

Table 2.1: Time in different operational modes with associated average speed [knots] and motor power [% of maximum continuous rating (MCR) of engine]

	Maneuvering from quay	Acceleration	Transit	Deceleration	Maneuvering to quay	Docked
Time in mode [min]	0.75	1.5	18.17	3.08	1.5	5
Average speed in mode [knots]	2	6	12	6	2.5	0
Motor power in mode [%]	75	80	42	7	56	14

## 2.2 Hybrid ferry system

A hybrid ferry combines multiple power sources, where a combination of diesel with electric battery power is the most common, to meet the power demand in the vessel's propulsion drive system and auxiliary loads. The main advantages of a hybrid ferry are the reduction in greenhouse gas emissions, reduced noise levels and the flexibility of being able to have a secondary energy source whenever required. The prominent disadvantages are the weight and installation cost of the battery system.

A modern hybrid ferry is illustrated in Figure 2.4. The ferry has a fully redundant power system, with a forward and aft (rear) power station that can be operated independently. The power stations have both a battery system and diesel generators, providing a more reliable and secure operation.

The system is also highly influenced by information and communication technology and uses this to control the ferry and the charging process more effectively. The ferry is communicating its states with the charging stations at shore and can remotely command the charging plug to prepare for charging before arriving to optimize the charging period.

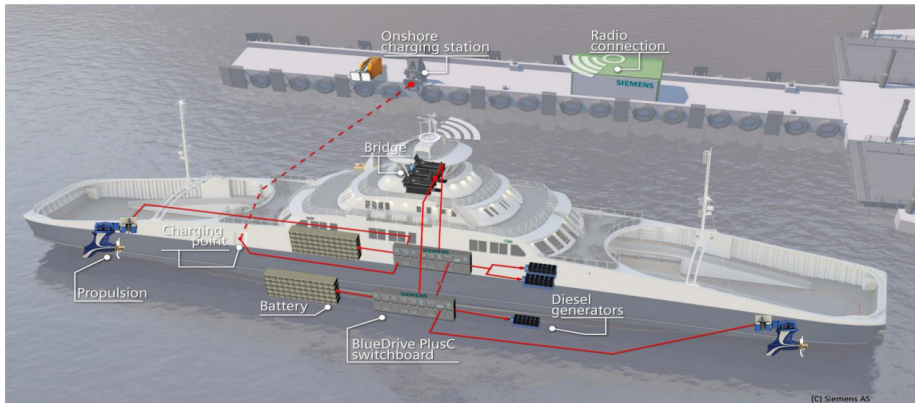


Figure 2.4: A modern hybrid ferry system. Photo from [2].

### 2.2.1 Ferry power system

The power system in a hybrid ferry has much in common with a land based distribution system, where energy sources are combined and power is distributed from an electrical substation to small and large loads. However, ferry power systems can have different configurations dependent on shipboard architecture and technology.

Common for all the configurations is that they are structured as an Integrated Power System (IPS). In an IPS, as shown in Figure 2.5, all the required power, for the vessel's propulsion and service loads, is generated and distributed by the same main energy sources. The IPS shares all power from the energy sources on an integrated power grid, which distributes the power to all individual consumer systems located throughout the grid in an utility fashion. The property of power sharing is the main advantage of IPS and improves power flexibility and availability[31].

An important component in the ferry power system is the voltage source converter (VSC), which is able to convert the electric power from one form to another (AC/DC, AC/AC, DC/AC, DC/DC). The VSC can be programmed to produce voltage and current waveforms, different power factors, and obtain a desired frequency from a range of different input waveforms. The VSC are used in motor drives, active power filters and inverter systems[31]. The shipboard power system is normally divided into two types:

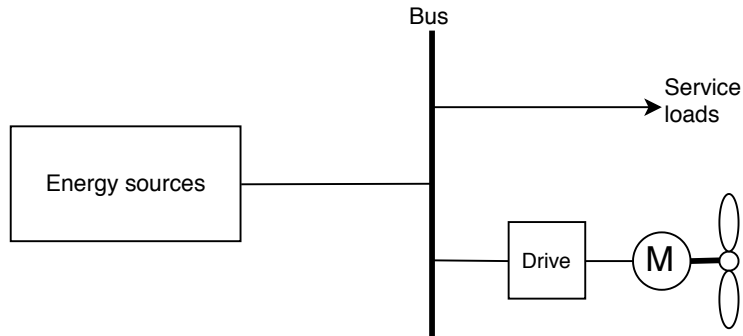


Figure 2.5: Structure of an Integrated Power System (IPS)

An AC- or a DC distribution power system.

### 2.2.1.1 AC distribution

An illustration of one type of an AC distribution power system is given in Figure 2.6. Here, the propulsion drive system is connected to the same AC electrical bus as the diesel generators. With today's requirement for flexibility, a DC bus is added to the power system such that loads can be interfaced to both the AC or DC bus. The DC bus is connected to the AC bus through a VSC and a transformer, and hence, some associated power loss must be considered when transferring power between the two voltage forms. The system can be compared to a land-based Smart Grid system, where both electrical producers, consumers and storage systems are connected together. The energy storage system (ESS) is connected to a constant voltage DC bus through a VSC which controls the power flow to and from the ESS. The ESS can both deliver energy and store the excess energy in the system.

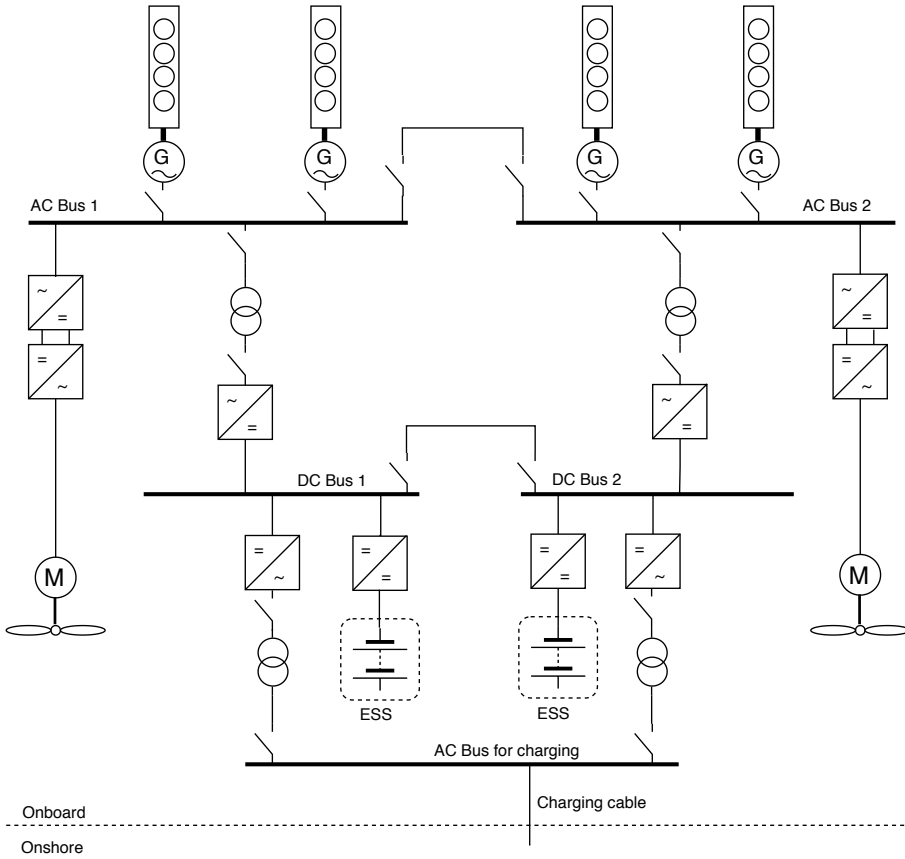


Figure 2.6: Hybrid AC-DC distribution system. From [3]

Some of the advantages of an AC distribution power system are given in the list below and based on paper [35] by V. Staudt et al:

- Simple Switches - electrical arcs clear at zero-crossing of the current.
- Easy and reliable adaption of the voltage level by transformers.
- Impedance in the cables, together with generator- and transformer impedance, limits the short circuit currents.

If the batteries are used as the main source of energy in the system, it can, on the other hand, be more suitable to connect the propulsion system directly to the DC bus. By doing this, the power from the batteries no longer have to flow through the VSC and the transformer to the drive system, which then increases the efficiency grade. A power system like this is usually called a DC distribution system, and is described in the following section.

#### **2.2.1.2 DC distribution**

When the propulsions drive system is connected to a DC bus, the shipboard power system has a DC distribution. One example of a DC distribution system is given in Figure 2.7. Here, the propulsion systems, the ESSs and the diesel generators are all connected directly to the DC bus through VSCs. In this configuration, an inverter and a transformer is connecting the DC bus to the AC bus, where the charging cable and the other AC utilities are connected. Another configuration could be to use individual generators connected to the DC bus through diode rectifiers, which then makes only one transformer necessary between the shore grid supply and the VSC connecting the battery to the DC bus.

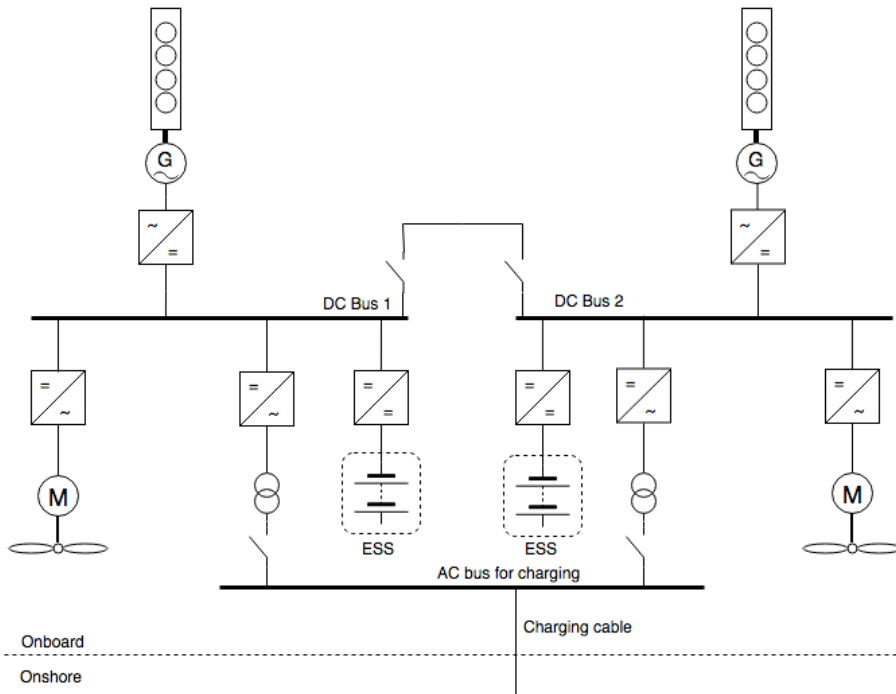


Figure 2.7: DC distribution system. From [3]

The main benefits of a DC distribution power system with respect to an AC distribution are given in the list below and based on papers [35, 31]:

- Higher energy transport capabilities due to no reactive currents.
- Two conductors are needed instead of three at AC.
- Phase matching is not needed, resulting in a faster generation response time.
- Since frequency control is not a concern at the DC bus connecting the diesel generators, the prime movers can be operated at optimized speed, and thus increasing fuel efficiency.

By removing the VSC from the ESS and letting the DC bus voltage float<sup>3</sup>, even fewer power electronic components are needed. This would require the VSC connecting the diesel generator to control the DC side voltage to the varying voltage amplitude at the DC bus. In addition, with the configuration given in the figure, there would be no opportunity to charge the two batteries independently when removing the VSC.

The DC distribution can be seen as less complex than the AC distribution power system presented in Figure 2.6. Fewer power electronic components are needed for a fully functional DC system, and the implementation of ESS is simpler. Since the drive system for the motor propulsion is connected directly to the DC bus, there is no need for a “front-end”-converter for the VSD.

---

<sup>3</sup>The battery terminal voltage is dependent on the SoC, as further described in Section 3.1

### 2.2.2 Ferry control system

Ferry maneuvering, power and energy management, alarms and instrumentation are important control mechanisms implemented in a modern hybrid ferry, and it all relies on a good functioning control system. The control system described in this section consist of three parts, with the energy management system (EMS) being the unit in which all other parts are connected to. One part is considering the charging station at shore, another part is considering the power and energy management onboard the ferry and the last part is considering the maneuvering and control of the ferry system

An illustration of the topology of the ferry's control system is given in Figure 2.8, and a brief description of important blocks in the figure and their objectives are given as follows:

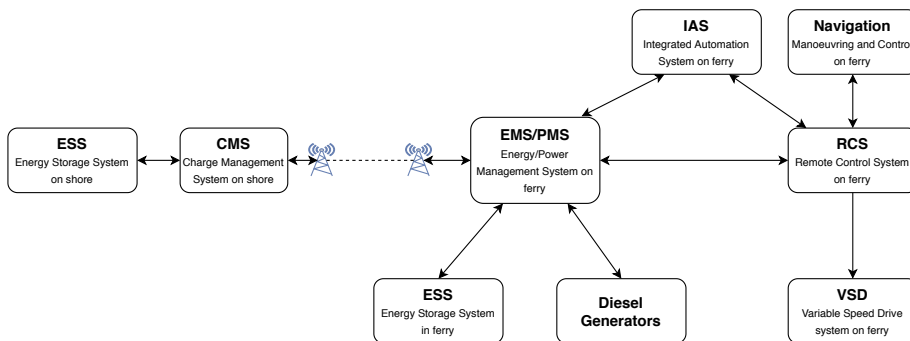


Figure 2.8: Topology of a hybrid ferry control system hierarchy

- **Energy / Power Management System (EMS/PMS)**

The overall objective of the energy and power management system (EMS/PMS) is to supply the load demand, thus ensuring that all online consumers, and especially consumers that are critical for a given operation, experience a stable and reliable supply of power[31].

- **Charge Management System (CMS)**

A CMS implemented in both the ferry EMS and the charging station is handling the communication between the ferry and the charging station. The communication is wireless and can be built up by different types of protocols, such as radio waves and 4G mobile internet. Before the charging process of the ferry begins, the CMS in the ferry EMS sends a request for a desired power to be transferred. The CMS in the charging station then finds the available power level from the grid and battery and sets the transferred power output to the ferry.

- **Remote Control System (RCS)**

The RCS is controlling the propulsion drive system and interfaces with the navigation system. Both the RCS and the navigation system are typically placed on the ferry bridge. When the RCS receives a maneuvering command, it communicates with the EMS to provide the necessary power and with the variable speed drive system (VSD) to actuate the commanded action.

- **Integrated Automation System (IAS)**

All systems are connected to an IAS. The IAS is monitoring all process values of interest and alarms the operators when an abnormal situation occur.

## 2.3 The charging station

The main function for the charging station is to deliver the necessary power to the ferry such that safe and efficient operation can be achieved. As the charging stations normally works as a buffer to decrease the grid power outtake, ESSs of varying dimensions are usually installed. The topology of a charging station, with its main components, is shown in Figure 2.9. As seen, the charging station is divided in 2 houses: one transformer and converter house (house 1) and one battery house (house 2). A thermal management system is normally installed in each house for controlling the temperature, which is crucial for a secure and optimal operation of the ESS and the power electronic components.

When the ferry is charging, the charging station operates as a generator in parallel with the grid supply to deliver the necessary power to charge the ferry. The CMS in the ferry EMS sends a request of power to the charging station's CMS, which then determines the distribution of power between the grid supply and the battery. Normally, the highest available power from the grid is selected by the CMS, which results in the battery delivering the additional power needed. The power to the ferry is dynamically changed by the CMS which adjusts the voltage level on the charging plug to obtain the desired power.

There are different types of solutions for the connection between the ferry and the charging station. The charging station in Figure 2.9 has two connection systems; a plug-in system and pantograph system. Other types of systems are wireless charging through induction, such as the Wärtsilä wireless charging system[36], and robot automated charging systems, such as the ABB Robotic solution[37].

During the time the ferry is in transit, the charging station battery is recharged back to nominal state of charge. This charging power is also controlled by the charging station's CMS, which adjusts the battery terminal voltage level to the corresponding desired input power.

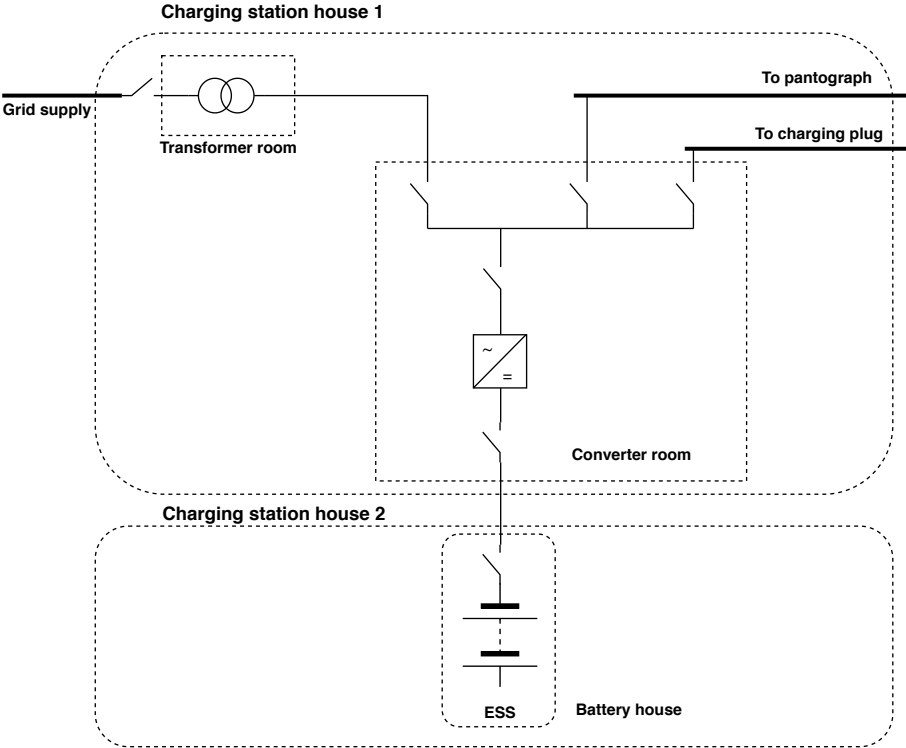


Figure 2.9: Topology of a charging station

## Chapter 3

# Battery Energy Storage System

Ferry operation can be more reliable, secure and sustainable by implementing energy storage as second energy source. The energy storage, dependent on the capacity, can supply all the power demand in the ferry, work as a supplement for the diesel generator, act as a peak shaving component or as an emergency energy source. There are different types of energy storage systems available, such as hydrogen fuel cells and flywheels, but the battery, which is the type of energy storage used in most hybrid ferries today, is further described in this chapter. The following sections gives a brief summary of the battery technology section elaborated in the specialization project[32].

### 3.1 The lithium-ion battery

The lithium-ion battery is today the preferred battery technology type used in consumer electronics and vehicle applications. This is due to its many benefits, such as high energy density, high power density, long life and environmental friendliness[38].

Common for all battery types is that they are built up by an anode that receives electrons, a cathode which emits electrons and an electrolyte that transports ions between them. A battery must also have a separator to avoid a short circuit between the cathode and the anode, and the separator is typically a porous film which can pass through ions[4].

The movement of ions in a lithium-ion battery is illustrated in Figure 3.1. During charging, external current forces lithium ions to move from the cathode to the anode. During discharge, ions naturally move from the anode to the cathode, creating a useful current. Hence, lithium ions have the lowest energy when they are in the positive electrode (cathode) and the highest energy when they are in the negative electrode (anode)[39].

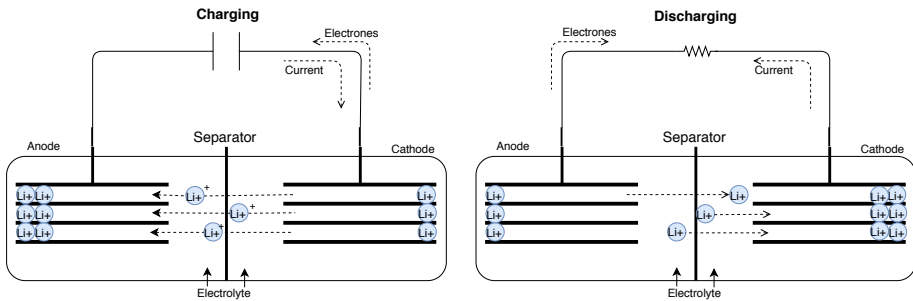


Figure 3.1: Charging and discharging in a lithium-ion battery. Based on [4]

A fast charging lithium-ion battery should have a larger anode than cathode. This is because as the volume in the anode material fills up with lithium atoms, it becomes harder for the latter atoms to find space, and a larger anode than cathode will therefore make it easier to find space. The rate of charge and discharge is also determined by the porosity of both the anode and the cathode. High porosity makes the lithium migration easier and provides high current, but at the same time, the charging capacity decreases[4].

A list of terms used to describe the battery characteristics are given in Table 3.1.

Table 3.1: Explanation of battery terms

Characteristic	Explanation
Depth of Discharge (DoD)	Indicates how deeply the battery is discharged.
State of Charge (SoC)	Indicates how much capacity remaining in the battery. The inverse of DoD.
Self-Discharge Rate	A measure of how quickly a cell will lose its energy without any connection between the electrodes due to unwanted chemical reactions within the cell[40].
C-rate	Describes how fast the battery will be fully charged or discharged. 1C is equivalent to nominal battery capacity divided by 1 hour.
State of Health (SoH)	Describes how much the battery capacity is reduced.

## 3.2 Battery life

For reliable and secure use of batteries as energy storage, knowledge about the expected lifetime is crucial. Battery life is a measure of battery performance and longevity, which can be quantified in several ways: for a rechargeable battery, the typical measurements are the number of charge cycles and the estimate in ampere-hours until the end of useful life. When the battery lifetime is reached, the active anode material is exhausted and there will no longer be a current flowing between the anode and cathode[41, 42].

A typical end-of-life criterion for the battery is when the capacity has decreased by 20% from the initial capacity. At this point, the available power output has also faded down to a level which is not sufficient for operation in high power applications.

### 3.2.1 Battery aging

Estimating the remaining battery life is a hard and complex task. Each lithium-ion chemistry behave differently and both internal and external factors contribute to battery aging. However, there are some mechanisms that are pointed out to influence the battery aging on a general term.

Battery aging limits the performance and occurs throughout the whole battery life, whether the battery is used or not, which is a major drawback in applications using this type of energy storage. Furthermore, aging takes place in every condition, but in different proportions as usage and external factors interact to provoke aging, which in turn makes the aging difficult to quantify[5]. Aging effects occurring at the positive

and negative electrode should further be discussed separately:

### Aging effects on negative electrode (anode)

Changes at the electrode/electrolyte-interface due to reactions of the anode with the electrolyte is considered by many to be the major source for aging of the anode. Graphitic carbon is the most used anode material in lithium-ion batteries and aging effects at the graphite anode leads to a modification of the electrode properties with time and use[43].

During the reaction between the anode and the electrolyte, a Solid Electrolyte Interphase (SEI) is developed. This interface is naturally created during the beginning of cycling, and has the job to protect the charged anode from corruptions and the electrolyte from reductions. The SEI is therefore important for providing good efficiency in the battery. However, when the battery operates outside of the electrochemical stability range of the electrolyte, the SEI develops, which induces loss of lithium ions and decomposition of the electrolyte. With time, the SEI expands into the electrolyte, which results in a decrease of accessible active surface area of the electrode, increasing the electrode's impedance[5, 43]. The different stages of SEI development are illustrated in Figure 3.2.

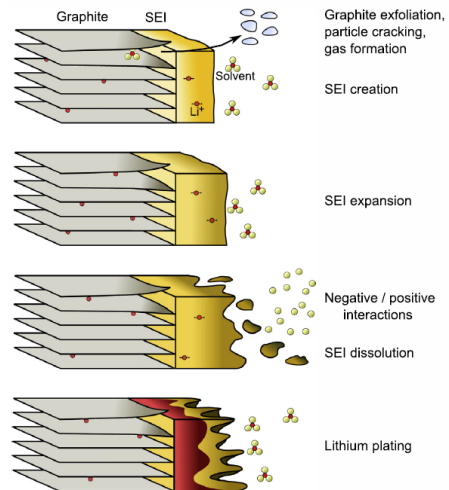


Figure 3.2: Development of SEI. Figure from [5].

Operating the battery on a high SoC accelerates these phenomena since the potential difference between the electrode interface and electrolyte is important. High temperatures, overcharge, short circuit and too low temperatures are other factors that accelerates the anode aging[5].

### **Aging effects on positive electrode (cathode)**

Wear of active material, electrolyte degradation, electrolyte oxidation and formation of SEI at the positive electrode are factors that contribute to aging at the cathode. As for the anode, the aging at the cathode highly depends on the SoC and the temperature[5].

Further, two types of aging situations can be distinguished and are often considered as additive: calendar aging and cycle aging[25].

#### **3.2.1.1 Calendar aging**

Calendar aging is the irreversible proportion of lost capacity during storage and is quantified by the self discharge rate. SEI expansion and loss of available lithium-ions due to side reactions at the graphite negative electrode has been reported as the main source of calendar aging. Hence, the main considerations to take when storing energy is the storage temperature and SoC[5].

#### **3.2.1.2 Cycle aging**

Cycle aging is a direct consequence of battery utilization and happens when charging and discharging the battery. Factors contributing to cycle aging are the variation of state of charge during a cycle,  $\Delta SoC$ , the charging/discharging voltage and all the factors that were present for calendar aging. Results shows that a high  $\Delta SoC$  and a high charging voltage contributes to battery power loss and acceleration of the aging phenomenons. [5].

At high current rates, the internal resistance will increase and result in a larger change in battery voltage and a increase in temperature. Results shows that increasing the current rate accelerates the battery aging mechanisms[44]. Thus, keeping control of temperature, operating the battery inside appropriate state of charge levels and lowering the charging voltage and current rate will effectively prolong the battery lifetime.



## Chapter 4

# The Norwegian Electricity System

The Norwegian electricity system is a collective name for all the components that are needed for transferring electricity from a producer, through a transmission network and to a end consumer in Norway. The system is built up as a integrated joint operation model consisting of production companies, producing the electricity, distribution companies, delivering the electricity, regulatory and legal requirements from the authorities and market solutions for trading electricity. All the building blocks contributes to a stable, acceptable and secure delivery of electricity, with the right quality and price.

As Norway has the highest share of electricity produced from renewable energy sources in Europe, and the lowest emissions from the power sector, the country is in a special position in the transition to a sustainable electrified society. At the beginning of 2018, the installed capacity of the Norwegian power supply system was 33 755 MW, and the normal annual production was 141 TWh[15].

## 4.1 Electricity grid structure

The Norwegian electricity grid is made up of three main networks: the transmission network, the regional distribution network and the local distribution network. In Figure 4.1, an illustration of the electricity grid is presented, with the different networks and voltage levels.

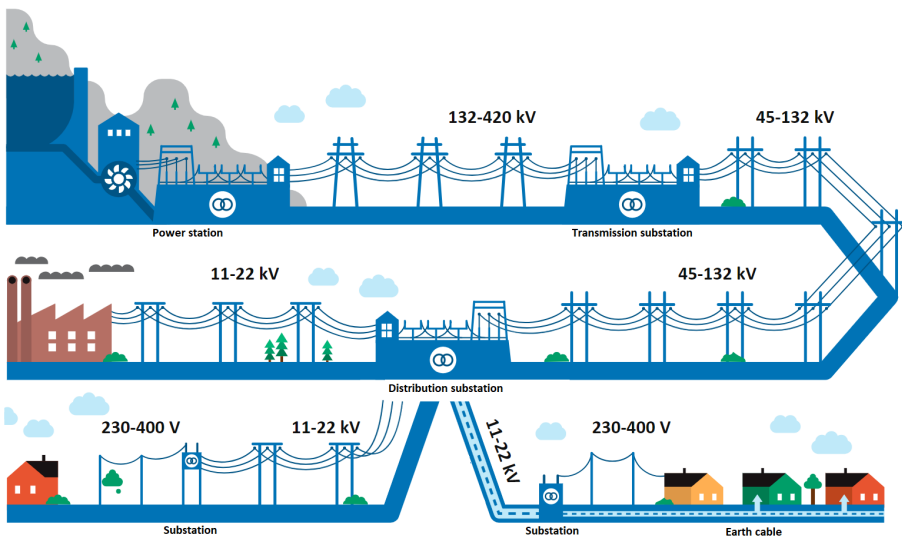


Figure 4.1: The Norwegian electricity grid structure. Illustration from [6]

### The transmission grid

The transmission grid is the central grid and motorway system for the electricity supply, linking producers with consumers in different parts of the country. The capacity of the central grid is high, and it normally carries a voltage of 300 kV to 420 kV, but in certain parts of the country there are also lines carrying 132 kV. The total length of the central grid is about 11 000 km[45].

Statnett SF is the largest owner of the transmission network in Norway, with 90%

ownership of the grid. The rest is owned by 20 other grid companies. Statnett SF is the only Transmission System Operator (TSO) and is responsible for maintaining the instantaneous balance of the electricity system and ensuring that the quality of supply is satisfactory[46, 47].

### **The regional distribution grid**

The regional distribution grid links the high voltage transmission grid to the low voltage local distribution grid. In addition, it may also include small-scale power plants and major consumers such as power-intensive manufacturing. The grid carries a voltage between 45 kV up to 132 kV, and the total length is approximately 19 000 km[45].

### **The local distribution grid**

The local distribution grid normally supply power to end users such as households, services and industry. The distribution grid has a normal voltage of up to 22 kV, but this voltage is reduced to 230 V for delivery to ordinary consumers. The length of the distribution grid carrying over 1 kV constitutes just under 100 000 km[45].

There are 146 grid companies that own and operate regional distribution and/or local distribution networks. Some also own minor parts of the transmission network[46].

#### **4.1.1 Power supply to hybrid ferry system**

For the hybrid ferry to be able to operate on batteries, there is a requirement for a stable and available power supply. The power from the electricity system is used to charge the ferry- and shore batteries, and with regards to the different systems, the power drawn from the grid when charging the ferry typically lies in the region from 2 MW to 8.5 MW. The need for high capacity in the grid decreases when installing bigger batteries in the charging station.

The charging station is normally connected to the regional distribution grid due to the high demand of power. In the transformer room, seen in Figure 2.9, the voltage can be transformed down from 22 kV to 11 kV, which is the preferred voltage level for

power transmission to the ferry system. High voltage is chosen to minimize the power loss in the transmission lines, transformers, switchboards and converter components.

Reactive effect compensation is often a requirement for utilities drawing high power from the grid. The batteries in the charging can be used for this compensation by sending reactive effect back towards the public grid.

## 4.2 Electricity tariffs

Factors that goes into determining the total electricity tariff charge for the end user are the price of electricity production, network tariffs and government taxes. In Norway, the distribution of the tariff charge is as follows: ~ 39% of the invoiced cost goes to public taxes, ~ 32% to the electricity provider and ~ 29% to the grid company[48].

### Electricity Production Cost

The electricity provider is paid for the cost of electricity production, for trading electricity and for marketing and customer service. Public taxes added on the cost to the electricity provider are value added tax (VAT) at 25% and electric certificates, which is a support system for the electricity provider for producing from renewable energy sources[48].

### The Electricity Market

While grid operations are strictly regulated, electricity production and trading are market-based. In market-based trading, the power exchange sets daily prices that gives a planned balance between overall generation and consumption for every hour of the next day. Thus, the market and all its players contributes to a reliable and efficient operation of the electricity system[45].

The Nord Pool Spot power exchange is used as the trading platform for the Nordic countries. The production companies sell their production of electricity to the exchange and the electricity retailers buy this electricity for then to resell to their own customers.

Ordinary private customers can not buy their own electricity directly through Nord Pool Spot.

The market price is a result of supply and demand, and changes both within 24-hours periods and through seasons and years. The price depends on factors such as temperature, variations in precipitation and the transmission conditions both between areas and countries within the Nordic region and the rest of Europe[45]. Figure 4.2 shows the dynamic electricity price for the Molde region as an average over the working days from 8th of April to 29th of April 2019. As seen, the price is highest during the morning and evening, when the energy usage among the end users are also at its highest.

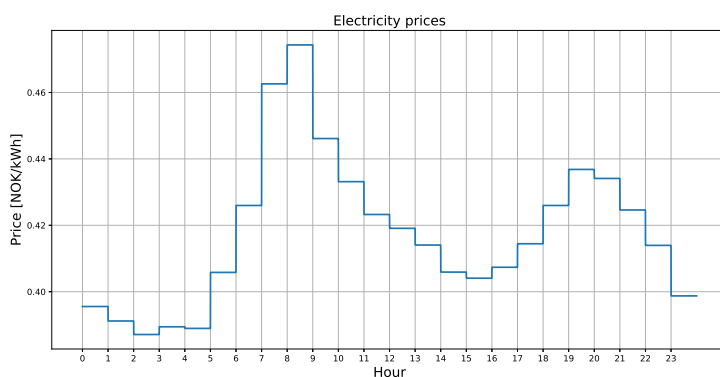


Figure 4.2: Electricity price dynamic. Prices from [7]

### Network tariffs

As grid operations are considered to be a natural monopoly, there are no opportunities for competition within grid distribution as there are in the rest of the power market. The Norwegian Water Resources and Energy Directorate (NVE) is regulating the local grid companies through revenue caps and network tariff rules. All consumers and producers connected to the electricity grid pay tariffs to their local grid company for electricity transmission[45].

The tariff is used to meet the cost of providing a stable and secure electricity supply. It is also intended to cover the costs that the grid company has in connection with the construction, operation and maintenance of power lines, cables and substations[49]. The current model used and the total network tariff charge is given by

$$\begin{aligned} \text{Tariff charge} = & \text{Fixed component [NOK/year]} \\ & + \text{Power component [NOK/kW/year]} \\ & + \text{Energy component [NOK/kWh]}. \end{aligned} \tag{4.1}$$

Here, the fixed component covers the customer-specific costs and the energy component the marginal network losses of consuming one more kWh. The power component is an additional cost for high consumer costumers and is included to account for the customers high influence on the network capacity. On average, the fixed component constitutes 30% of the network tariff[50].

### **Future network tariffs**

With new technology, new ways of using electricity and a different consumption pattern than earlier, the current network tariff model is subject for a change. Today's electricity customers are demanding more power (kW) than energy (kWh) and with the use of Smart Meters, more efficient and correct settlement of consumption can be obtained[51, 52].

NVE has prepared three different proposals on future network tariffs in the distribution network. The actual models are outlined in [51] and presented in short form below:

**Tariffs based on measured capacity usage**

In this tariff model, the cost distribution will be based on how much grid capacity the customer has used in the hour during the settlement period where the highest power demand has taken place. The charge is given by

$$\begin{aligned} \text{Tariff charge}_{\text{measured}} = & \text{Fixed component [NOK/year]} \\ & + \text{Energy component [NOK/kWh]} \\ & + \text{Capacity component [NOK/kWh/h]}. \end{aligned} \quad (4.2)$$

**Tariffs based on subscribed capacity**

Subscribed capacity means that customers subscribe to a certain amount of network capacity at a given price per kW. If the end user consumes beyond this subscribed capacity, a significantly higher price could be charged through the overspending component. The charge is given by

$$\begin{aligned} \text{Tariff charge}_{\text{subscribed}} = & \text{Fixed component [NOK/year]} \\ & + \text{Subscription component [NOK/kWh/h]} \\ & + \text{Energy component [NOK/kWh/h]} \\ & + \text{Overspending component [NOK/kWh/h]}. \end{aligned} \quad (4.3)$$

**"Time of use" - tariffs**

In this tariff, the grid company determines in which time of day and period of year an additional kW is more expensive. Using capacity during the times when the grid is heavily loaded will cost the customer more. The customer will be given price signals and incentives to lower their capacity use during these times. The charge is given by

$$\begin{aligned} \text{Tariff charge}_{\text{timeofuse}} = & \text{Fixed component [NOK/year]} \\ & + \text{Energy component}(t) \text{ [NOK/kWh/h]}, \end{aligned} \quad (4.4)$$

where the energy component is a function of the time  $t$ .



## Chapter 5

# Optimization Methods

Optimization is an important tool in decision science and in the analysis of physical systems. In optimization, the goal is to find values of the system variables that optimize an objective. This objective could be profit, time, potential energy, or any quantity or combination of quantities that can be represented by a single number[53]. The following mathematical formulation is based on the definition of an optimal control problem for hybrid vehicles in [24] by L. Serrao.

A general dynamic system with state equation

$$\dot{x} = f(x, u, t), \quad (5.1)$$

can be defined for an optimal control problem.  $x \in \mathcal{R}^n$  indicates the vector of state variables,  $u \in \mathcal{R}^m$  is the vector of the control inputs, and  $t$  denotes the time.

The optimal control problem in the time interval  $t \in [t_0, t_f]$  corresponds to the choice of the law  $u(t) : [t_0, t_f] \rightarrow \mathcal{R}^m$  that leads to the minimization of the cost function

$$J(x(t_0), u(t), x(t_f)) = \phi(x(t_0), x(t_f)) + \int_{t_0}^{t_f} L(x(t), u(t), t)dt, \quad (5.2)$$

where  $L(x(t), u(t), t) \in \mathcal{R}$  is the instantaneous cost function and  $\phi(x(t_f), t_f) \in \mathcal{R}$

represents the terminal cost and is a function of the system state at the final time. The dynamic system is subject to the state constraints

$$G(x(t), t) \leq 0, \quad \forall t \in [t_0, t_f], \quad (5.3)$$

and the control action constraints

$$u(t) \in \mathcal{U}(t), \quad \forall t \in [t_0, t_f], \quad (5.4)$$

where  $\mathcal{U}(t)$  indicates the set of admissible control values at time  $t$ . Over the next sections, background theory on two different methods for solving the optimal control problem is presented.

## 5.1 Numerical methods

As system dynamics can be highly non-linear, it may be impossible to solve an optimization problem using calculus. In such a case, it is necessary to attempt to approximate the problem satisfactorily by numerical methods. By using numerical methods, the best available values optimizing the objective function, given a defined domain (or input), are selected.

Dynamic programming and numerical search methods are principles that can be used to solve numerical optimization problems. In these methods, the entire system dynamic is taken into consideration and the global optimization is calculated. Hence, a-priori knowledge of the dynamics is needed and the solution must be calculated offline[54].

Model predictive control and stochastic dynamic programming are numerical methods used for local optimization. These techniques considers a short-term optimization horizon extending into the future, during which the system dynamic is predicted. A-priori knowledge of the system dynamics is therefore not needed and the methods can be used for online optimization[54].

The dynamic programming principle is further pointed out as the numerical method used in the optimal control problem for battery charging.

### 5.1.1 Dynamic programming

As described by T. Cormen in [55], dynamic programming solves problems by combining the solutions to subproblems. It is typically applied to optimization problems where there are several possible solutions. Each solution has a value, and the goal is to find a solution with the optimal (minimum or maximum) value. Such a solution is called *an* optimal solution to the problem, as opposed to *the* optimal solution, since there may be several solutions that achieve the optimal value.

Dynamic programming is based on Bellman's principle of optimality:

*An optimal policy has the property that no matter what the previous decision (i.e. controls) have been, the remaining decisions must constitute an optimal policy with regard to the state resulting from those previous decisions[56].*

Based on an analogy in [57], suppose that the fastest route from München to Berlin passes through Nürnberg and Leipzig. The principle of optimality translates to the obvious fact that the Nürnberg to Berlin portion of the route is also the fastest route for a trip that starts from München and ends in Berlin. The same also holds for the portion from Leipzig to Berlin.

In the sense of a hybrid ferry system, the principle could be applied to a battery charging process. The objective could be to charge the battery from 20% SoC to 60% SoC with a set of minimization objectives.

An illustration of this optimization problem is given in Figure 5.1, where the given charging time is divided in  $N$  steps and node A and node V marks the initial SoC and target SoC, respectively. The other nodes (B - U) are possible states the battery can have during the charging process, and the arrows indicates possible transitions from one node to another.

Each arrow has an attributed weight which gives the cost of moving between the nodes. As seen, going from node A to B has a cost of 0.8, moving from A to C has a cost of 1.2, and moving from A to D has a cost of 1.5. For clarity, the other weights are not added to the figure.

Utilizing the dynamic programming principle, the solution to the optimization problem is the trajectory from node A to V that has the lowest cost of all possible trajectories. One possible optimal trajectory is illustrated in Figure 5.2 by the thick

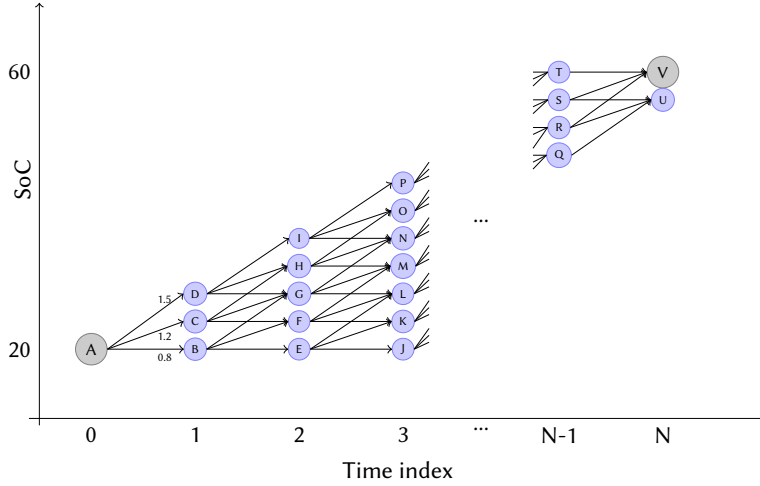


Figure 5.1: Arc costs of charging

arrows. The optimal solution can be solved by using algorithms with the objective to find the shortest path through the graph. Since the graph can be defined as a directed acyclic positive weighted graph, algorithms such as Bellman-Ford and Dijkstra's Shortest Path First-algorithm can be used to find the optimal solution. The two algorithms are further described by T. Cormen in [55].

After the optimal solution is found, the charging control actions from the solution can be applied to the battery. Accuracy of the optimal solution is dependent on the resolution of the state of charge, the control actions and the step size. Hence, the optimal control problem can fast be very computational heavy. Dynamic programming is, however, the only optimal control technique capable of providing the optimal solution to problems of any complexity level and can easily be applied to non-linear systems. The method is non-causal, thus, it requires information of the system dynamics over the entire optimization horizon[24].

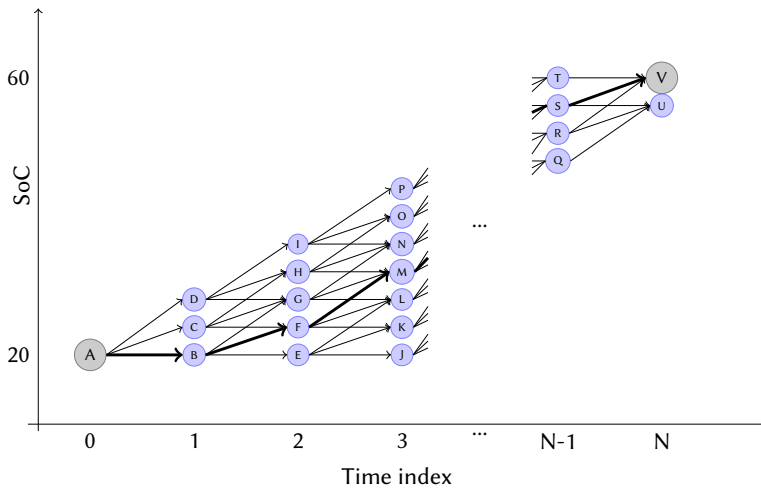


Figure 5.2: Optimal charging trajectory

## 5.2 Analytical methods

Analytical optimization methods consider the entire system dynamic and uses an analytical problem formulation to find the solution in a closed, analytical form, or in a form that makes the solution faster to solve compared to using numerical methods. The Pontryagin's minimum principle (PMP) and the Hamilton-Jacobi-Bellman equation (HJB) are the most significant analytical methods[24].

The Pontryagin's minimum principle is further pointed out as the analytical method used in the optimal control problem for battery charging.

### 5.2.1 Pontryagin's minimum principle

Pontryagin's minimum principle<sup>1</sup> (PMP) provides a set of necessary optimality conditions<sup>2</sup> that the solution must satisfy. Every solution that satisfies the necessary conditions are called an extremal solution, and if the optimal solution exists, then it is also extremal[24].

---

<sup>1</sup>Some regards this principle, and the work by L.S. Pontryagin and his students, as the start of optimal control theory[58]

<sup>2</sup>*Necessary* conditions are conditions that must be satisfied by any solution point under certain assumptions. *Sufficient* conditions are those that, if satisfied at certain point  $x^*$ , guarantee that  $x^*$  is in fact a solution[53].

The following mathematical formulation follows the same structure as given in [54] by L. Serrao. The Pontryagin's minimum principle states that if the control law  $u^*(t)$  is optimal for the control problem defined in the introduction of this chapter, the following conditions are satisfied:

1.  $u^*(t)$  minimizes at each instant the Hamiltonian of the optimal control problem:

$$H(x(t), u(t), t, \lambda(t)) \geq H(x(t), u^*(t), t, \lambda(t)), \quad \forall u \neq u^* \quad (5.5)$$

where the Hamiltonian is defined as

$$H(x(t), u(t), t, \lambda(t)) = \lambda^T(t) \cdot f(x(t), u(t)) + L(x(t), u(t), t) \quad (5.6)$$

with  $f(x(t), u(t))$  being the system dynamic equation,  $L(x(t), u(t))$  being the instantaneous cost, and  $\lambda(t)$  being a vector of auxiliary variables called co-states of the system.  $\lambda$  has the same dimension as the state vector.

2. The co-state variable satisfies the following dynamic equation:

$$\dot{\lambda}(t) = -\frac{\partial H(x(t), u(t), t, \lambda(t))}{\partial x}. \quad (5.7)$$

In practical applications, the minimum principle can be used to find solution candidates by computing and minimizing the Hamiltonian function at each instant, which generates, by construction, extremal controls. If the Hamiltonian is a convex function of the control, then there is only one extremal solution, which is therefore optimal[54].



## **Part II**

# **Methods & Modelling**



## Chapter 6

# Hybrid Ferry Modelling

Both the operation and the ferry system are considered when modelling the hybrid ferry. The ferry system involves the ferry construction and the internal controller, battery and generator components. A route schedule including one working day and a weekend day schedule is used as the basis for the modelling of operation. The model presented here is further used in the simulations in Part IV.

### 6.1 Modelling of operation

The modelled operation is based on the route schedule between Aukra and Hollingsholmen, detailed in Appendix C. This ferry service is operated by Fjord1, and the updated route schedule can be found at their website[59].

The ferry currently operating Aukra - Hollingsholmen is MF Eira, which is a diesel engine ferry. However, the ferry service is currently being examined for a change towards hybrid ferry operation.

In general, the operation consist of one ferry crossing between two charging stations. When the ferry docks at the harbour, it connects to the charging station and charges the battery with the pre-determined power from the charging station battery and the grid. The ferry follows a pre-defined route schedule and after finishing the schedule it travels to a nightlay station where it is charged by grid power over

night. The ferry is modelled to cross between the two charging stations in a directly north-south direction.

Normally, the ferry uses 11 minutes for one crossing with a following charging time of 3 minutes. When docking, the ferry uses 30 seconds to connect to the charging station and when undocking, the ferry uses 30 seconds to disconnect from the charging station. The total time from leaving one quay to leaving the next is then 15 minutes.

The operation is further divided into working days- and weekend operation. This is because factors such as the route schedule, amount of passengers and the electricity price varies a lot between a working day and a weekend day.

### **6.1.1 Working days operation**

Throughout a working day, the ferry has 66 crossings between south- and north harbour, where 59 of them are normal crossings with a duration of 11 minutes. In addition, a crossing with a duration of 10 minutes, from the nightlay station to the south charging station at the beginning of the day, is included in the route schedule. The operation begins at 04:45, when the ferry leaves the nightlay station. Deviations from normal operation are given in the list below:

- Crossings 05:00, 11:00, 23:00 and 23:30 takes 12 minutes and has a following extended charging time of 17 minutes.
- Crossings 05:30, 20:45 and 22:00 takes 12 minutes and has a following extended charging time of 32 minutes.

### **6.1.2 Weekend operation**

The schedule on Saturday, the day with the lowest amount of passengers, is chosen as the weekend operation. Over a weekend operation, the ferry crosses between the two charging stations 58 times, where 47 of them are normal crossings. In addition, the nightlay charging between the working day and the weekend, and the nightlay charging at the end of the weekend day are added to the operation. This means

that crossings from 00:00 to nightlay charging Sunday night are also included in the weekend operation.

Deviations from normal operation and important notes are given in the list below:

- Time in nightlay between working day and weekend is 4 hours and 50 minutes, from 01:10 to 06:00.
- Time in last nightlay is 4 hours and 5 minutes, from 01:55 to 06:00.
- Crossings 11:00, 23:00 and 23:30 takes 12 minutes and has a following extended charging time of 17 minutes.
- Crossings 06:30, 07:30, 15:45, 18:15, 19:45, 20:45 and 22:00 takes 12 minutes and has a following extended charging time of 32 minutes.
- Crossing 00:15 Sunday night takes 12 minutes and has a following extended charging time of 47 minutes.

### 6.1.3 Energy consumption

The energy consumption, calculated by Siemens' battery Profile Tool, under normal operation is given in Table 6.1. As seen, the crossing with the highest energy consumption, is the normal crossing with the shortest transit time. When the transit time is 12 minutes, the ferry reduces the consumption with 29.5 % by lowering the transit speed, and hence decreasing the propulsion power. The 10 minute crossing is assigned the transit time between the south station and the nightlay station.

Table 6.1: Energy consumption under reference conditions

Transit time	Energy consumption
10 min	174 kWh
11 min	190 kWh
12 min	134 kWh

The reference values for the external factors impacting the ferry under normal operation are given in Table 6.2. As seen, the ferry does not experience any wind and ocean current effects during transit. The external factors, how they variate and their impact on the ferry system, are further described in Chapter 10.

Table 6.2: Reference conditions

Factor	Value	Unit
Passenger car units	25	PCU
Wind speed	0	m/s
Wind direction	0	°
Ocean current	0	m/s
Current direction	0	°

#### 6.1.4 Implementation of operation in model

Since the Battery Profile Tool generates the ferry profile in an excel sheet, the operation is also first constructed in Excel. The states are updated with new values ever 30 seconds, meaning that for the whole operation period of 49 hours and 15 minutes, there are 5910 data points for the operation. For each point the parameters for the date and time, mode, leg, propulsion power and hotel power are updated with new values accordingly to the operational profile.

When the model is initialized in Python, the excel sheet for the operational profile is imported and each parameter is structured in a Pandas DataFrame for quick access.

## 6.2 Modelling of ferry system

Modelling of the ferry system includes the ferry construction and components needed for operation. The length measurements of the construction are illustrated in Figure 6.1.  $p/p$  is the length between perpendiculars,  $w/l$  is the length at waterline,  $o/a$  is the overall length,  $b$  is the beam length,  $f$  is the freeboard length and  $d$  is the draft length. The ferry construction parameters are based on MF Eira, and listed in Table 6.3.

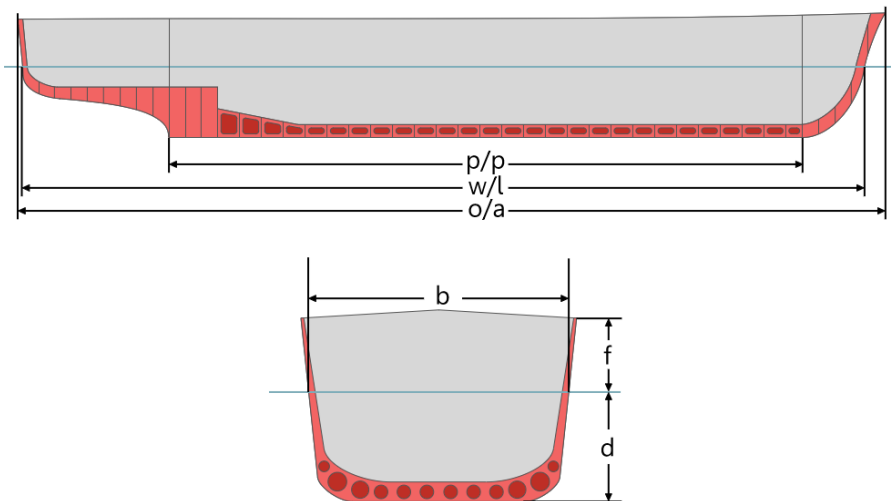


Figure 6.1: Ferry dimensions. Illustration from [8]

The ferry specifications are listed in Table 6.4. The battery energy storage capacity is dimensioned after the requirement for the ferry to be able to operate 100 % on battery power over one operation day with good margin. Ideally, the battery should be operated between 20% - 60% SoC to not accelerate battery degradation. The ferry battery should also be able to give the propulsion thrusters full rated power and to receive a high enough current to recharge sufficient energy when docked. The rated power from the generator is included for giving an overview of the ferry system.

Table 6.3: Ferry construction parameters[60]

Parameter	Value	Unit
Ferry waterline length, $w/l$	84	meters
Ferry beam length, $b$	16	meters
Ferry draft length, $d$	4	meters
Ferry freeboard length, $f$	5	meters

Table 6.4: Ferry system specifications and component efficiencies

Specification	Value	Unit
Passenger capacity	87	PCU
Battery energy storage capacity	1800	Ah
Number of cells	205,920	Cells
Battery cost	10,296,000	NOK
Battery power rating	5148	kW
Battery voltage (nominal)	943.8	V
Battery C-rating	5400	A
Thruster rated power	2x1200	kW
Generator rated power	4x800	kW
Ferry switchboard	99	%
Transformer	98	%
Converter	99	%
Battery charging (2C)	96	%
Battery discharging (0.5C)	98	%
Gen set	95	%

As the electrical components in the ferry does not have 100% efficiency, there is a loss of power when transferring energy through the system. The efficiency grade for each of the included electrical components are give in Table 6.4. When the ferry is charging, the power on the ferry side flows through a ferry switchboard, a transformer, a converter and into the battery system, and energy is dissipated in all the components. Hence, this loss of energy needs to be compensated for when calculating the charging power.

A higher loss of battery power is associated with charging the ferry battery than discharging the battery during a crossing. The battery efficiency values are approximated by measurements made on hybrid ferry batteries under operation. A further discussion on battery power loss is given in Section 8.2.

### 6.2.1 Implementation of ferry system in model

The ferry components are defined as the battery, the gen set and the controller. The controller is controlling the battery- and gen set power to meet the ferry power demand and is keeping control of the battery's SoC and SoH and the ferry's passenger volume and weight.

Under transit, power from the battery and the gen set are joined to meet the load demand. As the gen set can deliver more power than the total load demand, excess power can be used to charge the battery. However, in this model, the gen set does not generate any power to the ferry propulsion system or battery. This is done to simplify the model, and for only to focus on the power flow between the batteries at shore and the ferry. By including the effect of the gen set power, energy management during transit should also be implemented in the ferry controller.

The ferry components are modelled with the approach of Python classes, where the ferry class is built up by three sub-classes: a controller, a battery and a gen set. The battery class is further built up by a cell class. An illustration of the ferry system, with its classes, is given in Figure 6.2.

When the ferry is charging, the power flows through the input line from the charging station to the battery. The ferry controller is updated with the battery states and communicates with the charging station controller, which sets the charging power.

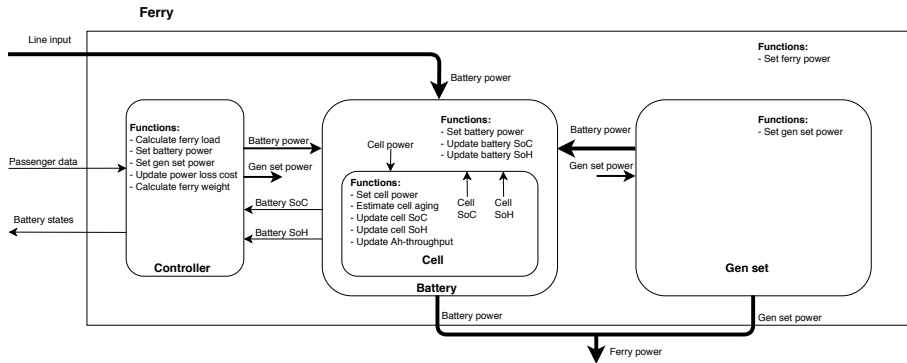


Figure 6.2: Modelling of hybrid ferry

Under transit, the controller calculates the ferry load based on the propulsion power, hotel load and external factors, and sets the battery power accordingly to meet this load. The controller also updates, and keeps track of, the battery power loss for later use as a performance parameter.

## Chapter 7

# Charging Station Modelling

The specifications for the south- and north charging station are listed in Table 7.1. The stations are identical, with the same capacity in the energy storage and efficiency in the electrical components. The shore battery has less capacity compared to the ferry battery, but is well dimensioned to operate as a buffer between the grid and the ferry.

When using grid power to charge the ferry battery, only the transformer room switchboard contributes to the power loss before reaching the ferry system. Hence, the power loss due to stepping down the voltage level before the charging station is not included. When charging the shore battery, the switchboard, transformer, converter and battery all contributes to a loss of power. The same also occurs when using the shore battery to charge the ferry. This is important to keep in mind when determining the distribution of power between the grid and shore battery, since more power loss are assigned the battery. If the controller calculates a charging profile with a higher battery power than the power rating, the power is saturated down to the allowed amplitude.

A higher loss of battery power is associated with discharging the shore battery than charging. The battery efficiency values are approximated by measurements made on the batteries under operation. A further discussion on battery power loss is given in Section 8.2.

Table 7.1: South- and north charging station specifications and component efficiencies

Specification	Value	Unit
Battery energy storage capacity	1200	Ah
Number of cells	137,280	Cells
Battery cost	6,864,000	NOK
Battery power rating	3432	kW
Battery voltage (nominal)	943.8	V
Battery C-rating	3600	A
Transformer room switchboard	99	%
Transformer	98	%
Converter	99	%
Battery charging (1C)	97	%
Battery discharging (3C)	94	%

## 7.1 Implementation of charging station in model

For optimal charge planning in the hybrid ferry system, the charging station module plays an important role. It controls the transfer of energy to the charging station's battery and to the ferry. The module is built up by two components: the battery and the controller.

The controller is the heart of the overall system and where the most logic is implemented. The controller calculates new optimal charging profiles for the batteries by taking in the external factors and using optimization algorithms for finding the best charging dynamic. The charging station module is implemented as a Python class, with two subclasses: a controller and a battery. An illustration of the charging station module, with its classes, is given in Figure 7.1.

During the process of connecting the ferry to the charging station, the controller starts calculating the new charging profile for the ferry. It first start by estimating the energy consumption for the next crossing by taking the crossing time, amount of passengers, the wind conditions and the ocean current conditions over the next

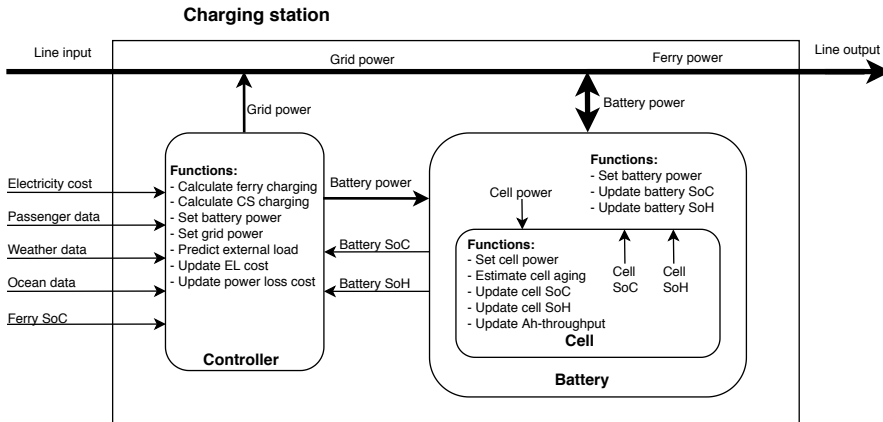


Figure 7.1: Modelling of charging station

crossing into account. Compensation of power loss under transmission and in the electrical components of the charging station and the ferry are also included.

When the energy consumption is estimated, the controller determines the target SoC of the ferry battery. This is determined by the initial SoC before the charging process and the estimated energy consumption. The optimal charging dynamic is then calculated with the objective to minimize the electricity cost, battery power loss, battery aging and the grid penalty cost.

During the process of disconnecting the ferry from the charging station, the controller starts calculating the new charging profile for the shore battery. The strategy when charging the shore battery is to replace the energy transferred to the ferry during the last discharge. Thus, the objective is to recharge back to nominal SoC, which typically is 60%. The charging dynamic is then calculated with respect to minimization of the same objectives as when charging the ferry.

When the optimal charging profile is calculated, the controller sets the grid- and battery power accordingly to the optimal values. The controller communicates with the ferry controller to be able to keep track of the SoC and SoH in the ferry battery. Calculation of the optimal charging profile is further elaborated in detail in Part III, and the estimation of external factors are described in Chapter 10.



## Chapter 8

# Battery Modelling

To apply battery in applications and for development in battery technology, an accurate modelling of the battery dynamics is crucial. Vehicle range prediction is only possible through the application of advanced battery modelling and estimation techniques to determine current state and predict remaining endurance. In addition, battery modelling is essential for safe charging and discharging, optimal utilization of batteries, fast charging and other applications[61].

In the modelled hybrid ferry system, both of the charging stations and the ferry have a battery module implemented. The battery is implemented as a Python class with a cell sub-class. The cell class is representing all the cells that the battery is built up by, and the number of cells are set accordingly to meet the power and capacity specifications for the ferry- and shore batteries, as given in Tables 6.4 and 7.1. It is further assumed that all cells are working equally, with the same properties, such that SoC, SoH and Ah-throughput can be calculated proportionally to the cell characteristics.

The battery module that is implemented in the ferry- and shore batteries are illustrated in Figure 8.1. The battery is controlling the cell power, and the cell are providing the cell SoC and SoH back to the battery. The cell dynamic is based on an electrical circuit model and the cell performance is based on an empirical aging model, as discussed in Sections 8.1 and 8.3, respectively.

The two terms *battery* and *cell* are used interchangeably and can easily be a factor

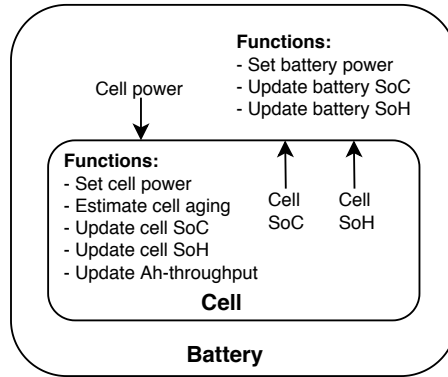


Figure 8.1: Modelling of battery

of confusion. However, when discussing models for battery dynamic and aging, the equations work on cell level. The combined performance of all the cells that makes up the battery system is then used for setting the battery dynamic and aging.

The major categories of battery models are mathematical models, electrochemical models and electrical equivalent circuit models. The more accurate the battery model is, the more reliable results are obtained using simulation softwares. However, increasing the accuracy of the model increases the complexity and also the computations time[61, 62].

Mathematical models are divided into analytical- or stochastic models. In an analytical model, differential equations are used to describe battery properties and dynamics. Stochastic models work on the principle of the discrete-time Markov chain, where future states can be predicted based on the present state without knowing its full history[61].

The electrochemical models are based on chemical reactions occurring inside the battery cell. As a result, they are the most accurate models, since they simulate the cell at microscopic scale[62]. However, they are complex and the computation is expensive. The battery model presented in the following sections, with the formulation for power loss and aging, is further used in the simulations in Part IV.

## 8.1 Electrical circuit model

An electrical circuit battery model, as given in Figure 8.2, is used to obtain the dynamics in the ferry- and shore batteries. The type of battery that is modelled is a  $\text{LiFePO}_4$  cell from A123 system[63], with the specifications given in Table 8.1. The battery type is chosen on basis of good data in other literature ([21, 28]) on battery degradation performance. The battery type are used in many HEVs applications, but it should be noticed that this is not the type used in Siemens' battery systems.

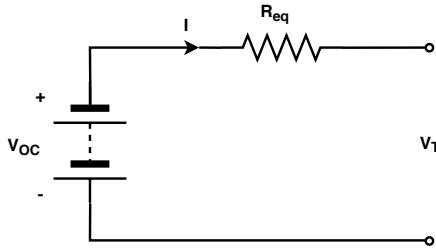


Figure 8.2: Battery electrical circuit model

Table 8.1:  $\text{LiFeOP}_4$  cell specifications

Specification	Value	Unit
Cell capacity	2.5	Ah
Cell voltage (nominal)	3.3	V
Rated power	25	W
Internal resistance, $R_{eq}$	12	m

In the circuit, the terminal voltage is calculated as

$$V_T = V_{OC} - R_{eq}I, \quad (8.1)$$

where  $V_{OC}$  is the open-circuit voltage,  $R_{eq}$  is the equivalent internal resistance and  $I$  is the current flowing at the battery terminal. The terminal voltage can also be

expressed as  $V_T = \frac{P_{batt}}{I}$ , where  $P_{batt}$  is the power in or out of the battery. This can further be used to obtain the battery current with respect to the power as

$$I = \frac{V_{OC} - \sqrt{V_{OC}^2 - 4R_{eq}P_{batt}}}{2 \cdot R_{eq}}. \quad (8.2)$$

By definition, the variation of SoC is proportional to the current at the terminals, such that

$$S\dot{O}C = -\frac{1}{Q_{nom}} \cdot I, \quad (8.3)$$

where  $Q_{nom}$  is the nominal charge capacity of the battery. Hence, inserting Equation (8.2) in Equation (8.3), the variation of SoC with respect to battery current and power can be expressed as

$$S\dot{O}C = -\frac{1}{Q_{nom}} \cdot \frac{V_{OC} - \sqrt{V_{OC}^2 - 4R_{eq} \cdot P_{batt}}}{2 \cdot R_{eq}}. \quad (8.4)$$

Both the open-circuit voltage,  $V_{OC}$ , and the equivalent internal resistance,  $R_{eq}$ , depends on the battery SoC. The effect of SoC on the two battery parameters are given in Figure 8.3. As discussed in Section 3.1, the voltage is varying with respect to the energy stored in the battery due to moving ions, making the potential difference between the electrodes higher or lower. This causes the effect of SoC on  $V_{OC}$  as seen in the figure.

The voltage curve for the LiFePO<sub>4</sub> cell, given in Figure 8.3a, is relatively flat, and approximately 80 % of the stored energy lies inside this flat region. When using voltage to determine the SoC in a practical application, this flat profile can make the estimate inaccurate. However, in this model, the estimate between the voltage and the SoC is assumed to be 1:1.

The internal resistance is sensible to factors such as temperature, SoC, current rate and the electrochemical structure, and the variation can be complex to model. For simplicity, the effect of SoC on the internal resistance is here modelled to be constant, which gives the flat curve as seen in Figure 8.3b.

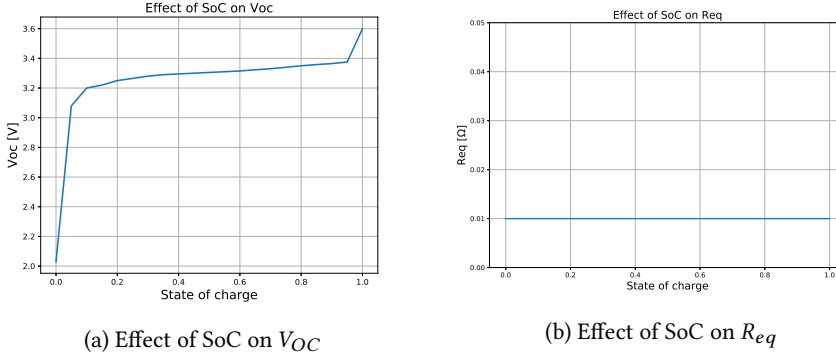


Figure 8.3: Effect of SoC on battery parameters

## 8.2 Power loss model

The battery is experiencing power loss due to the internal resistance, making some of the power dissipate to heat. A general calculation of power loss is given by

$$P_{loss} = I^2 R_{eq}, \quad (8.5)$$

which is formulated directly from the equivalent circuit in Figure 8.2. This calculation of power loss is a fairly good approximation of the loss in a battery cell, but does not include all the loss factors impacting the whole battery energy storage system.

Power electronics for security and controllability, and variation of internal resistance due to heat generation are some of the other factors that contributes to power loss in a battery system. In Figure 8.4 the measured power loss under different C-rates are shown as red dots. The measured data is collected from ferry- and shore batteries under realistic operation.

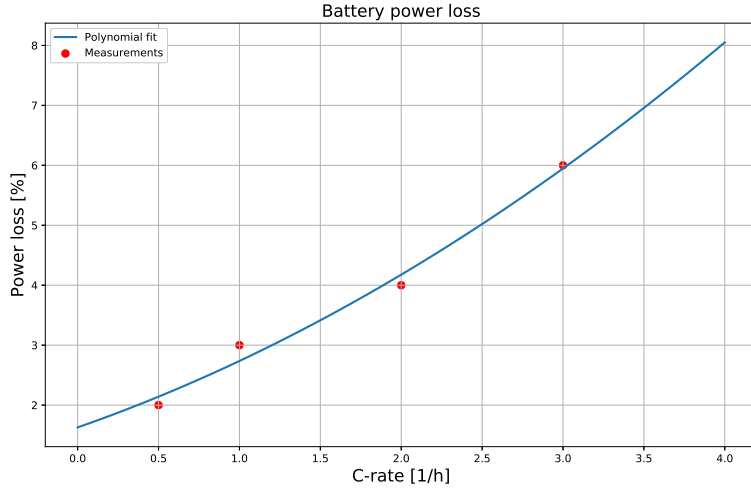


Figure 8.4: Battery power loss approximation

Using a polynomial fit of second degree, an approximation curve for the measured data points is calculated, and given as the blue line in Figure 8.4. The curve has the equation

$$P_{loss,\%}(I_c) = 0.0017 \cdot I_c^2 + 0.0094 \cdot I_c + 0.0163, \quad (8.6)$$

with a coefficient of determination

$$R^2 = 0.986. \quad (8.7)$$

This curve is further used in the model to determine the battery efficiency, which is given as

$$\eta_{loss,\%}(I_c) = 1 - P_{loss,\%}(I_c), \quad (8.8)$$

and in the cost function for the optimal control problem to calculate the cost of

power loss.

The approximation curve for battery power loss are used both during charge and discharge, which is a simplification. Based on data from Siemens, the associated efficiency of charging the battery is higher than discharging the battery, and the given curve in Figure 8.4 is more equal the efficiency of charging the battery. This is important to keep in mind when discussing cost of power loss, since the event of charging the ferry with the shore battery could contribute to a larger cost at the charging station side.

### 8.3 Battery aging model

Aging models for lithium-ion batteries can be classified into two categories: physical–chemical models and empirical models. Physical–chemical models are usually developed to study or describe a single aging mechanism inside a cell and are helpful in understanding aging under different battery modes and performance aspects. The models are complex and often require long computation time[21].

Various empirical and semi-empirical models have been proposed to meet the shortcomings of the physical-chemical models. These models are developed by considering simplified physical relations in the battery by fitting the parameters of the model with experimental data obtained from aging tests, resulting in a set of equations that describe the main degradation mechanisms[21].

The following empirical battery aging model is based on a generic model initially proposed in [27] and further developed for electric vehicle applications in [21, 28, 64]. The model captures the capacity loss of the battery with dependence on the SoC, temperature ( $\theta$ ), and C-rate ( $I_c$ ), and is expressed as

$$Q_{loss,\%}(p, Ah) = \sigma_{func}(p) \cdot Ah^z, \quad (8.9)$$

where  $p$  is the vector of severity factors,  $p = (I_c, \theta, SoC)$  and  $z$  is the power law exponent that represents Ah throughput dependence.  $\sigma_{func}(p)$  is a nonlinear function of severity factors, called the severity factor function, that is given by

$$\sigma_{func}(p) = (\alpha \cdot SoC + \beta) \cdot \exp\left(\frac{-E_a + \kappa \cdot I_c}{R_g \cdot (273.15 + \theta)}\right), \quad (8.10)$$

where  $\alpha, \beta$  define SoC dependence,  $\kappa$  models the  $I_c$  dependence,  $R_g$  is the universal gas constant and  $E_a$  is the activation energy constant. The C-rate,  $I_c$ , is calculated as

$$I_c = \frac{|I|}{Q_{batt}}. \quad (8.11)$$

With the battery aging parameters listed in Table 8.2, the capacity loss of the battery cell with respect to the Ah-throughput is given in Figure 8.5.

Table 8.2: Nominal battery parameters

Parameter	Value	Unit
Nominal SoC, $\bar{SoC}$	35	%
Nominal c-rate, $\bar{I}_c$	2.5	1/h
Nominal temperature, $\bar{T}$	25	°C
Ah-throughput dependence, $z$	0.57	-
SoC dependence, $\alpha$	2795.6	-
SoC dependence, $\beta$	6716.7	-
C-rate dependence, $\eta$	152.5	-
Universal gas constant, $R_g$	8.314	$J \cdot K^{-1} \cdot mol^{-1}$
Activation energy, $E_a$	31500	$J \cdot mol^{-1}$

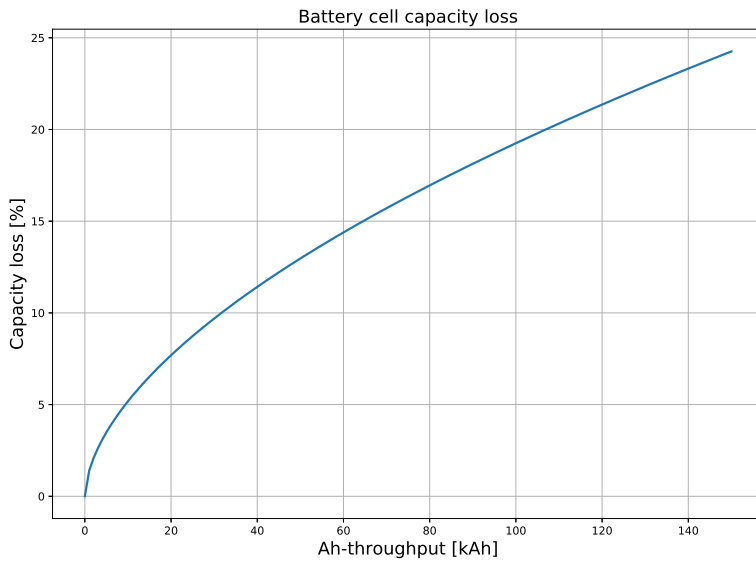


Figure 8.5: Predicted capacity loss for nominal profile

The nominal battery life function,  $\Gamma$ , expressed in terms of Ah-throughput, can be calculated as

$$\Gamma = \int_0^{EoL} |I_{nom}(t)| dt, \quad (8.12)$$

where  $I_{nom}$  is the nominal current. With the end of life criterion defined to be 20 % loss of capacity, Equation (8.9) with nominal battery parameter values can be written as

$$20 = \sigma_{f_{unc,nom}} \cdot \Gamma^z, \quad (8.13)$$

which then can be used to calculate the predicted nominal battery life as

$$\Gamma = \left[ \frac{20}{\sigma_{f_{unc,nom}}} \right]^{\frac{1}{z}}. \quad (8.14)$$

To calculate the battery aging under specific operating conditions, the relative battery life, given in terms of Ah-throughput, is given by

$$\gamma(I_c, \theta, SoC) = \left[ \frac{20}{\sigma_{f_{unc}}(I_c, \theta, SoC)} \right]^{\frac{1}{z}}, \quad (8.15)$$

where the relative values for the SoC, temperature and C-rate are used instead of the nominal. The relative aging effects of any other operating condition can then be reflected by the severity factor

$$\sigma(I_c, \theta, SoC) = \frac{\Gamma}{\gamma(I_c, \theta, SoC)}. \quad (8.16)$$

When the severity factor is greater than 1, an operating condition with a more severe load than the nominal is applied and the expected battery life is reduced. On the other hand will a condition less severe than the nominal set the severity factor below 1 and the battery life will increase.

A map illustrating the severity factor in Equation (8.16) for a fixed temperature at 25° C, SoC values ranging from 20 % to 80 % and C-rate values ranging from 0 to 3.5 C

is given in Figure 8.6. By operating the battery in the blue area, the expected battery life will increase, and by operating in the red area, the life will decrease.

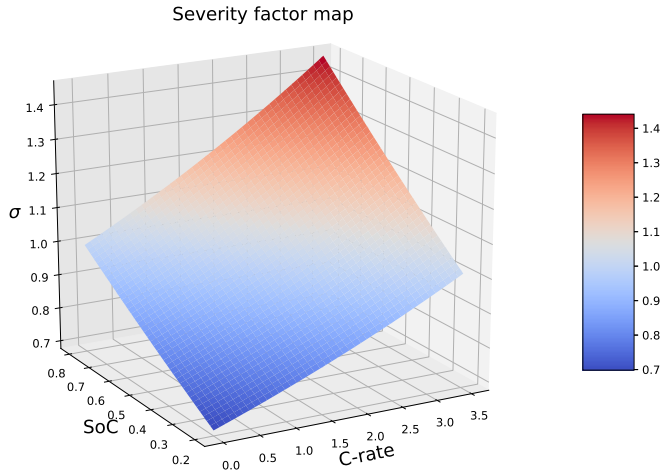


Figure 8.6: Severity factor map

The severity factor is finally used to give the effective aging due to operation of the battery at various loads. The effective Ah-throughput is given by

$$Ah_{eff}(T) = \int_0^T \sigma(I_c(t), \theta(t), SoC(t)) \cdot |I(t)| dt, \quad (8.17)$$

and expresses the effective use of the battery with respect to the nominal battery life defined by  $\Gamma$ . The SoH dynamic can further be calculated as

$$SoH(t) = 1 - \frac{Ah_{eff}(t)}{\Gamma}. \quad (8.18)$$

When  $Ah_{eff} = \Gamma$ , the battery has reached the end of life criterion, with a capacity loss equal to 20%. The operational objective should then be to delay this as long as possible.

As the battery degrades, the effect of SoC on the open-circuit voltage will deviate from the curve in Figure 8.3a. This is however not included in this model, as the simulation period is relatively short and the effect of degradation is negligible during this period.

## Chapter 9

# Modelling of Electricity System

### 9.1 Grid supply modelling

The grid supply is an important part of the overall system, as it supplies electricity to the ferry- and shore batteries. Drawing electricity from the grid is, however, something the system operator needs to pay for, and this cost is a large part of the overall cost of operating the hybrid ferry system.

The grid is modelled as a Python class, where one instance variable sets the grid capacity and the other sets the grid supply power. A third variable is representing the transmission line output to the charging station. The grid class is illustrated in Figure 9.1.

The capacity from the grid supply is defined to be constant over the whole simulation period. This may deviate the modelled system from a realistic system, where the available power can vary throughout the day. Although this variation of capacity is relatively small, it can have an impact on operation, since the grid capacity is often low when there is a high request of power from the ferry, as will be discussed further in this section.

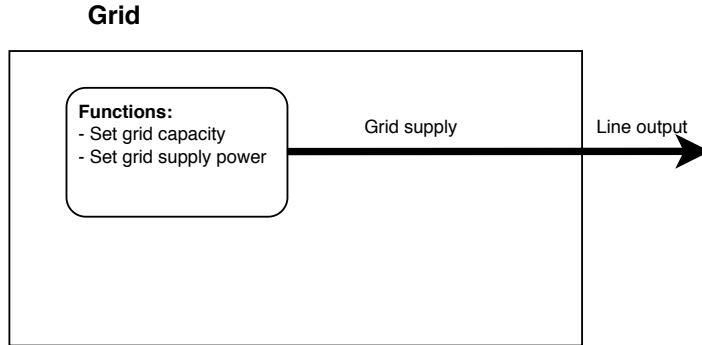


Figure 9.1: Modelling of grid supply

### 9.1.1 Modelling of grid capacity

The grid capacity for each connection is given in Table 9.1. The south- and north harbour is assumed to be connected to a regional distribution grid supply. As seen, the capacity at south- and north harbour is equal, while the capacity in the grid at the nightlay station is reduced. A nightlay station is normally connected to the local distribution grid, which provides a lower capacity than the regional distribution grid. Reactive power and compensation are not included in this model and the grid is assumed to only supply real power.

Table 9.1: Grid capacity

Grid	Value	Unit
Nightlay	1000	kW
South	3042	kW
North	3042	kW

The grid net exchange is varying and has an impact on the cost of drawing power from the grid. The difference between the produced electricity and consumed electricity in the grid gives the net exchange, and the value gives an indication about how much

undersupply or oversupply of electricity there is at a given time. The net exchange for the Nordic region as an average between 22nd of April and 12th of May 2019 is shown in Figure 9.2, and is collected from the open data available at Statnett's web page[65]. The net exchange is further divided into working day and weekend as the characteristic is clearly different.

As seen in the figure, there is an undersupply of power over the working day between 06:15 - 11:30 and 17:45 - 21:00. For the rest of the day, and throughout the whole weekend, there are more production than consumption of electricity.

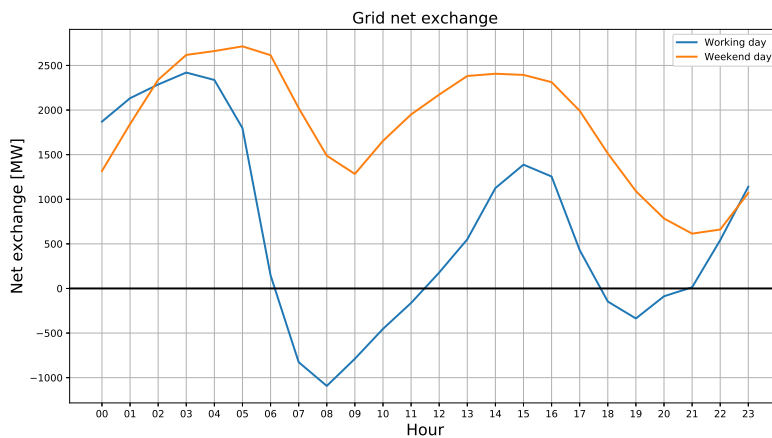


Figure 9.2: Grid net exchange for Nordic region

From the perspective of the TSO, there is a goal to obtain a stable balance in the grid, where the production of electricity match the consumption. As the end users today are demanding more power outtake from the grid, there is also a goal to limit the future investment needs in the grid. Therefore, new tariff models, as discussed in Section 4.2, are including terms to penalize the end user for drawing too much power at times with high grid demand. This penalizing cost is further studied by constructing a fictive cost of drawing power from the grid when two conditions are satisfied:

1. The power outtake from the grid is equal or above 1000 kW. Hence,  $P_{grid} \geq 1000$  kW.
2. There is an undersupply of power in the grid. Hence,  $P_{net}(t) < 0$ .

If these two conditions are satisfied, the ferry operator is charged with an additional cost given as

$$\xi_{load}(t, P_{grid}) = -60 \cdot \frac{P_{net}(t)}{1000 \text{ MW}} \cdot (P_{grid} - P_{pen}), \quad [\text{NOK/kWh/h}] \quad (9.1)$$

where  $P_{net}$  is the instantaneous net exchange in MW and  $P_{pen}$  is the penalty power level, defined as 1000 kW. Thus, the cost is dependent on the amount of undersupply and the grid power above 1000 kW. The penalty cost can be linked to the tariff model based on subscribed capacity, where the function in Equation (9.1) works as the overspending component, or the time of use tariff model, where the function works as the energy component with respect to time.

As an example, drawing 3000 kW for 1 minute between 08:00 - 08:01 the working day will cost NOK 18.2,- in addition to the cost of electricity. The cost is set at that level so that the savings achieved by reducing the grid power will be higher than the costs associated with more battery utilization.

## 9.2 Transmission line modelling

The transmission lines are connecting the public grid to the charging station, and the charging station to the ferry. The transmission line is modelled as a Python class consisting of an instance variable containing the sender object and an instance variable containing the receiver object. The sender object is setting the input power on the line and the input power on the receiver object is calculated by the transmission line class. An illustration of the line class is given in Figure 9.3.

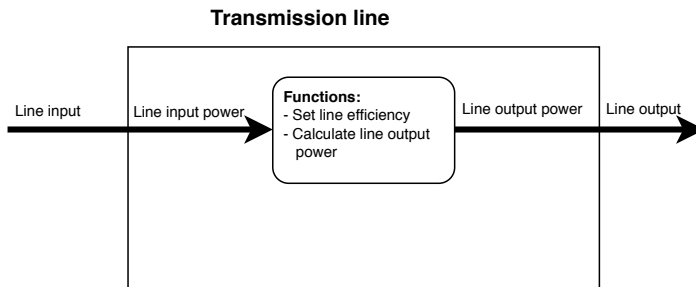


Figure 9.3: Modelling of transmission line

In this model, the transmission lines are assumed to have superconductivity, such that the efficiency is 100% and zero power is dissipated during transmission. This means that the input power from the sender object is the power that the receiver object receives.

### 9.3 Electricity cost modelling

The total cost of electricity is the sum of the varying electricity market price and the network tariff cost.

#### Electricity market price

The modelled market electricity prices are given in Figure 9.4. The prices are collected from Nord Pool's market data for Elspot day-ahead prices as an average in the Molde region between 8th - 29th of April 2019[7]. As there is a significant difference between working days and weekend, the two periods are separated.

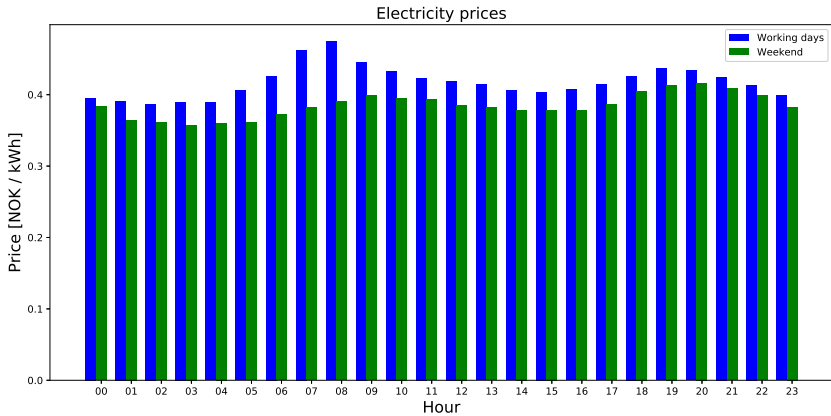


Figure 9.4: Electricity price dynamics. Prices from [7]

When simulating the system, the instantaneous cost of electricity per hour is obtained by multiplying the time varying electricity price with the instantaneous grid power,  $P_{grid}$  in kW. Hence,

$$\xi_{el}(t, P_{grid}) = \text{Electricity price}(t) \cdot P_{grid}. \quad (9.2)$$

**Network tariff cost**

The tariff model used is the current network tariff model, given as

$$\begin{aligned}
 \text{Network tariff} &= \text{Fixed component [NOK/year]} \\
 &+ \text{Power component [NOK/kW/year]} \\
 &+ \text{Energy component [NOK/kWh]},
 \end{aligned} \tag{9.3}$$

where the fixed component is defined to be NOK 18,000,- per year, the power component defined to be NOK 612,- per kW per year, and the energy component defined to be NOK 0.028,- per kWh. The prices are based on actual network tariff prices for high consumer costumers from the distributor Skagerak Nett[66]. As discussed, the modelled system is not settled for reactive power.

The total network tariff cost per hour is then calculated as

$$\begin{aligned}
 \xi_{network}(P_{grid}) &= \text{Fixed component [NOK/h]} \\
 &+ \text{Power component [NOK/kW/h]} \cdot P_{grid} \\
 &+ \text{Energy component [NOK/kWh]} \cdot P_{grid}.
 \end{aligned} \tag{9.4}$$

Hence, the total cost of electricity per hour is given as

$$\xi(t, P_{grid}) = \xi_{el}(t, P_{grid}) + \xi_{network}(P_{grid}). \tag{9.5}$$



## Chapter 10

# Modelling of External Factors

The modelled external factors impacting the ferry are:

- Cars and passengers
- Wind conditions
- Ocean current conditions

The external factors brings some degree of uncertainty to the simulations, and hence, contributes to a more realistic modelling of the system.

### 10.1 Car and passenger load modelling

As the ferry is becoming heavier or lighter with respect to the amount of passengers and cars onboard, the volume of water that the ferry needs to push away to move, is either becoming more or less. This results in an increase or decrease of power from the propulsion drive system to obtain the desired speed.

Data from the Hollingsholmen - Aukra service is used to modell the amount of passenger car units (PCU) for the crossings. The data consist of the amount of PCUs in the period between week 4 and 6 in 2018, and is collected from “Ferjedatabanken”[67], operated by the Norwegian Public Roads Administration.

The average day variation is given in Figure 10.1. Because of significant difference between working days and the weekend, the two periods are separated. On working days, the average number of PCUs is 1637 per day, and on the weekend, including both Saturday and Sunday, the average number per day is 696. The average number of PCUs crossing between Hollingsholmen and Aukra was 1399 per day in 2018[67].

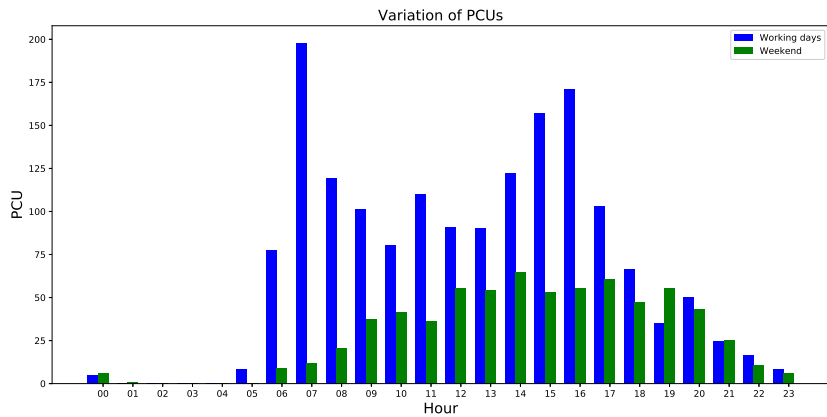


Figure 10.1: Day variation of PBEs on ferry

Over a working day, the amount of PCUs on the ferry is highest during the morning, between 6 - 8, and over the period between 14 - 17. On a weekend day, the amount of PCUs are lower, with a peak between 14 - 15. By comparing the day variation of PCUs during the working days with the electricity prices in Figure 4.2, there is a clear similarity.

As the resolution from “Ferjedatabanken” is only on hourly basis, the number of crossings each hour is used to divide the accumulated hourly amount of PCUs into amount of PCUs per crossing. Table 10.1 gives the number of crossings for each hour over the working day and the weekend. Using the average number of PCUs per crossing in an hour may deviate the modelled system from a realistic system since there is no guarantee that the PCUs will arrive at the ferry evenly over an hour.

Table 10.1: Number of crossings each hour

Hour	00	01	02	03	04	05	06	07	08	09	10	11	12	13	14	15	16	17	18	19	20	21	22	23
Working days	2	0	0	0	0	2	3	4	4	4	4	3	4	4	4	4	4	4	4	4	4	2	2	2
Weekend	4	0	0	0	0	0	2	2	3	4	4	3	4	4	4	4	2	4	2	4	2	2	2	2

When the charging station controller calculates a new charging profile for the ferry, it also predicts the number of PCUs and the additional energy consumption that needs to be compensated for. The additional energy consumption, which can be both positive or negative is calculated by

$$E_{PCU,\%} = \frac{PCU_{predicted} - PCU_{mean}}{PCU_{mean}} \cdot \alpha_{PCU} \cdot 0.01, \quad (10.1)$$

where  $PCU_{predicted}$  is the predicted number of PCUs for the crossing, based on the statistical data in Figure 10.1.  $PCU_{mean}$  is the average number of PCUs per crossing throughout a working day and defined to be 25.  $\alpha_{PCU}$  is an energy factor determining the effect of cars and passengers on the ferry and defined to be 5. As an example, with an estimated number of 50 PCUs for one crossing, the additional energy consumption for the ferry is given by

$$E_{PCU,\%} = \frac{50 - 25}{25} \cdot 5 \cdot 0.01 = 5\%, \quad (10.2)$$

meaning an additional 5 % is added to the total load of the ferry. On the other hand, if there was no PCUs onboard, there would be a decrease of 5 % to the total load.

Given the ferry energy consumption and conditions in Tables 6.1 and 6.2, the energy consumption will increase with 6.7 kWh for a crossing lasting 12 minutes in normal

weather with 50 PCUs. For a crossing time of 11 minutes, the energy consumption will increase with 9.5 kWh.

When the ferry disconnects from the charging station, a random value, based on the statistical data in Figure 10.1, representing the actual number of PCUs onboard the ferry is calculated. The random number is calculated by a normal Gaussian distribution with mean value given by the statistical data for the number of PCUs at the given time and a standard deviation of 3 PCUs. This is done to model some deviation between the estimated and actual value of PCUs in a realistic system.

## 10.2 Modelling of environmental forces

The weather conditions have an important impact on the ferry. Waves, sea currents, headwind and tailwind are factors that will change the ferry's energy consumption and thus, must be considered when the goal is realistic modelling of a hybrid ferry.

When designing control systems for marine applications, it is common to assume the principle of superposition when modelling wind and wave disturbances[68]. Therefore, the two effects are calculated independently and added together to find the total contribution on the ferry.

The modelling of wind and ocean current is mainly based on the models in [68] by T. Fossen, and the formulations outlined in the next sections follows the same structure as given in the reference.

### 10.2.1 Wind modelling

Wind is defined as the movement of air relative to the surface of the Earth[68]. A force from the wind is acting on the ferry when wind hits the construction. This force can be described by the pressure from the wind per unit area, given as

$$\mathbf{F}_w = q_a \cdot A. \quad (10.3)$$

As power is equal to the force times the speed, the wind power can be calculated as

$$P_w = \mathbf{F}_w \cdot \mathbf{V}_w, \quad (10.4)$$

where  $\mathbf{V}_w$  is the average wind vector acting on the ferry.

Since the ferry is modelled to cross the fjord in a north - south direction, a wind direction from north would effect the ferry as a headwind when the ferry is in transit to the north harbour, and as a tailwind when the ferry is in transit to the south harbour. The vice versa is happening if the wind is coming from the south, or if the ferry is in transit to the south harbour.

### 10.2.1.1 Wind forces on ferry

The modelled wind forces acting on the ferry is illustrated in Figure 10.2.  $V_w$  and  $\gamma_w$  denotes the wind speed and the angle of attack relative to the bow, respectively. As the body frame,  $\{b\}$ , and the north-east-down frame,  $\{n\}$ , relative to the Earth's reference ellipsoid is defined here to have the same orientation, the wind direction and angle of attack is equal. Further, it is assumed no boundary layer conditions on the wind speed.

$A_{Fw}$  represents the frontal projected wind area of the ferry and  $A_{Lw}$  represents the lateral projected wind area.  $u_w$  is the wind force acting on the frontal projected area and  $v_w$  is the wind force acting on the lateral projected area.

The dynamic pressure of the apparent wind is

$$q_w = \frac{1}{2} \rho_a V_w^2, \quad (10.5)$$

where  $\rho_a$  is the air density defined here to be  $1.225 \text{ kg/m}^3$ .

Given the calculation in Equation (10.3), the wind force vector can be formulated as

$$\mathbf{F}_w = \frac{1}{2} \rho_a V_w^2 \begin{bmatrix} C_{w,x}(\gamma_w) A_{Fw} \\ C_{w,y}(\gamma_w) A_{Lw} \end{bmatrix}, \quad (10.6)$$

where  $C_{w,x}$ ,  $C_{w,y}$  are wind coefficient approximations for symmetrical ships given as

$$\begin{aligned} C_{w,x}(\gamma_w) &= c_{w,x} \cdot \cos(\gamma_w), \\ C_{w,y}(\gamma_w) &= c_{w,y} \cdot \sin(\gamma_w). \end{aligned} \quad (10.7)$$

Finally, using Equation (10.4), the wind power acting on the ferry is given by

$$\mathbf{P}_w = \mathbf{F}_w \cdot \mathbf{V}_w. \quad (10.8)$$

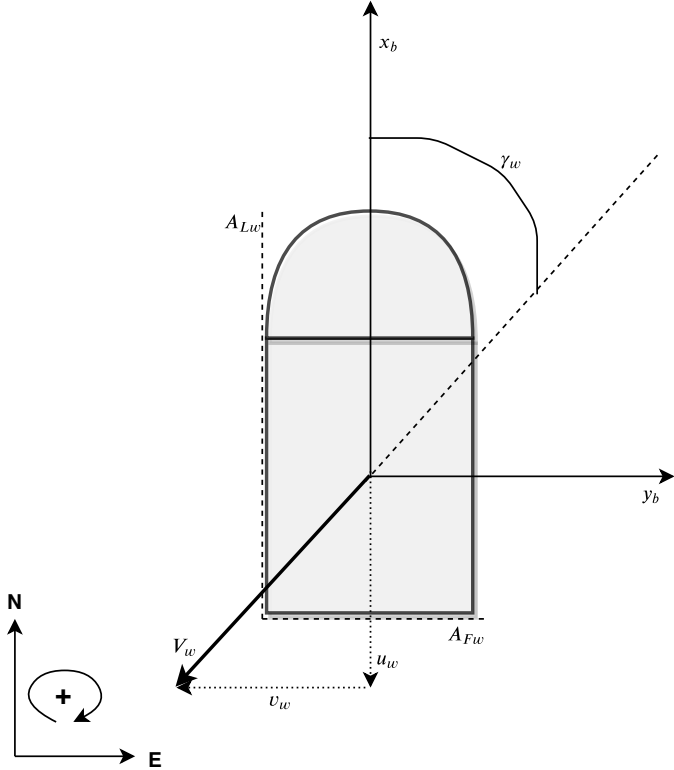


Figure 10.2: Wind force acting on ferry

### 10.2.1.2 Apparent wind power on ferry

As an example, a ferry is assumed to cross from the south harbour to the north harbour. The wind has a north-east direction, with a speed of 8 m/s and an angle of  $30^\circ$  relative to the bow.

Using the ferry specifications in table 6.3, the frontal projected wind area is calculated to

$$A_{Fw} = \text{Ferry breadth} \cdot \text{Ferry freeboard} = 16 \text{ m} \cdot 5 \text{ m} = 80 \text{ m}^2 \quad (10.9)$$

and the lateral projected wind area is

$$A_{Lw} = \text{Ferry length} \cdot \text{Ferry freeboard} = 84 \text{ m} \cdot 5 \text{ m} = 420 \text{ m}^2. \quad (10.10)$$

Using the experimental values  $c_{w,x} = 0.5$  and  $c_{w,y} = 0.7$  for the wind coefficient factors, the wind coefficient approximation components can be calculated as

$$\begin{aligned} C_{w,x}(\gamma_w) &= c_{w,x} \cdot \cos(\gamma_w) = 0.43, \\ C_{w,y}(\gamma_w) &= c_{w,y} \cdot \sin(\gamma_w) = 0.35. \end{aligned} \quad (10.11)$$

The wind power acting on the frontal projected area is

$$P_{Fw} = \frac{1}{2} \rho_a V_w^3 C_{w,x}(\gamma_w) A_{Fw} = 10,863 \text{ W}, \quad (10.12)$$

and the wind power acting on the lateral projected area is

$$P_{Lw} = \frac{1}{2} \rho_a V_w^3 C_{w,y}(\gamma_w) A_{Lw} = 46,099 \text{ W}. \quad (10.13)$$

Thus, the apparent wind power is given by

$$P_w = \sqrt{P_{Fw}^2 + P_{Lw}^2} = 47,362 \text{ W}. \quad (10.14)$$

With these results, the ferry should apply a power of 46.1 kW in the sway direction and 10.9 kW in the surge direction to maintain the desired speed and direction.

In Figure 10.3 the wind power under different wind directions in the surge com-

ponent is presented. As seen, the wind power is highest when the wind is coming directly in front of the ferry and decreases as the wind direction turns towards the side. When the wind direction is above  $90^\circ$ , the wind force contributes to the ferry motion and acts as a tailwind.

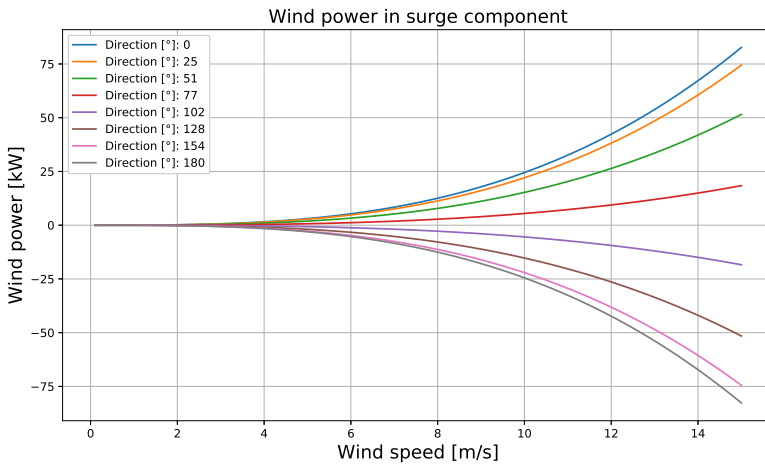


Figure 10.3: Wind power on ferry in surge direction

Figure 10.4 gives the wind power in the sway component with different wind directions. As seen, the wind power only works with negative effect and the ferry needs to use more power to maintain the same crossing line.

### 10.2.1.3 Wind data

Wind data is gathered from the Locationforecast API, developed by The Norwegian Meteorological Institute[69]. A Python script is used to pull the data from the API and to organize it in a database for further use in the simulations.

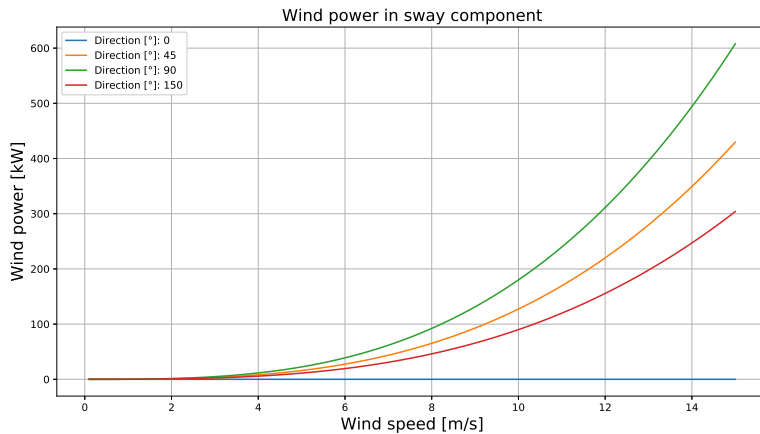


Figure 10.4: Wind power on ferry in sway direction

#### 10.2.1.4 Model implementation

When the charging station controller calculates a new charging profile for the ferry, it determines the average wind speed and direction for the next crossing. The average values are used to calculate the additional or less energy needed to be transferred to the ferry. This is further discussed in Section 13.3.

As the ferry is in transit, wind effect is applied to the model by using normal distributed values for the speed and direction. The forecasted wind speed is used as the mean value for the applied speed with a standard deviation of 2 m/s. The forecasted direction is used as the mean value for the applied direction with a standard deviation of 10°.

Only the wind power in surge direction is applied to the ferry system under the simulations in Part IV. This simplifies the prediction of wind power in the controller, and is also done for avoiding too much variation in wind effect on the ferry during transit. The applied wind effect is updated every 30 seconds during the crossing with new values for the speed and direction.

### 10.2.2 Ocean current modelling

Ocean currents are horizontal and vertical circulation systems of ocean waters produced by gravity, wind friction and water density variation in different parts of the ocean[68]. Similar to as the wind effect, a force from the current is acting on the ferry when it hits the construction. This force can be described by the pressure from the water per unit area, given as

$$\mathbf{F}_c = \mathbf{q}_c \cdot A. \quad (10.15)$$

Hence, the ocean current power can be calculated as

$$\mathbf{P}_c = \mathbf{F}_c \cdot \mathbf{V}_c, \quad (10.16)$$

where  $\mathbf{V}_c$  is the average current vector acting on the ferry.

#### 10.2.2.1 Ocean current forces on ferry

The modelled ocean current forces acting on the ferry is illustrated in Figure 10.5.  $V_c$  and  $\gamma_c$  denotes the current speed and the angle of attack relative to the bow, respectively.  $A_{Fc}$  represents the frontal projected current area of the ferry and  $A_{Lc}$  represents the lateral projected current area.  $u_c$  is the current acting on the frontal projected area and  $v_c$  is the current acting on the lateral projected area.

The dynamic pressure of the apparent ocean current is

$$q_c = \frac{1}{2} \rho_w V_c^2, \quad (10.17)$$

where  $\rho_w$  is the density of water defined here to be 997 kg/m<sup>3</sup>.

Given the calculation in Equation (10.15), the ocean current force vector can be formulated as

$$\mathbf{F}_c = \frac{1}{2} \rho_w V_c^2 \begin{bmatrix} C_{c,x}(\gamma_c) A_{Fc} \\ C_{c,y}(\gamma_c) A_{Lc} \end{bmatrix}, \quad (10.18)$$

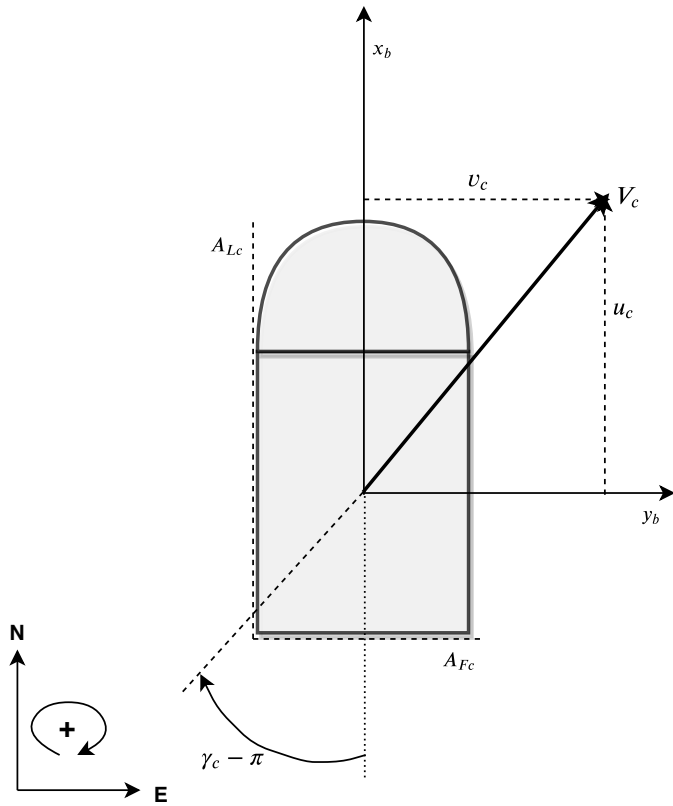


Figure 10.5: Current force acting on ferry

where  $C_{c,x}, C_{c,y}$  are current coefficient approximations given as

$$\begin{aligned} C_{c,x}(\gamma_c) &= c_{c,x} \cdot \cos(\gamma_c) \cdot |\cos(\gamma_c)|, \\ C_{c,y}(\gamma_c) &= c_{c,y} \cdot \sin(\gamma_c) \cdot \sin(\gamma_c). \end{aligned} \quad (10.19)$$

Values for the current coefficient approximations are shown in Figure 10.6 with the experimental values  $c_{c,x} = 0.45, c_{c,y} = 0.65$  for the coefficient factors. These values holds for a ferry crossing from south to north. When travelling the other way, the inverse values for  $C_{c,x}$  are used.

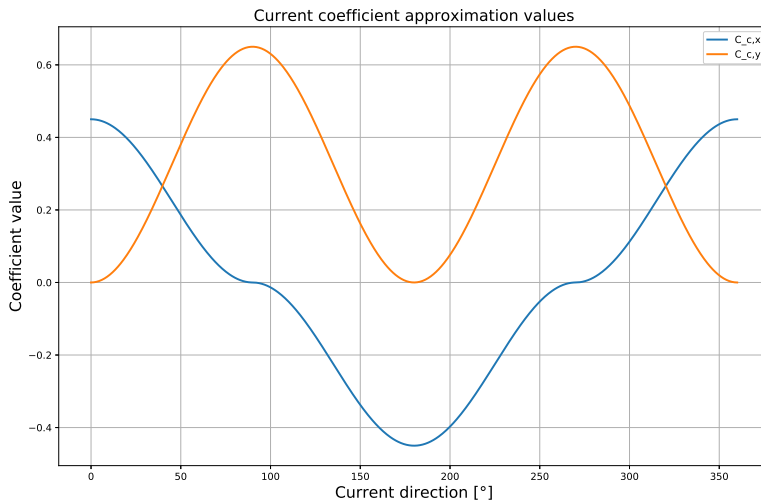


Figure 10.6: Current coefficient approximation values using  $c_{c,x} = 0.45, c_{c,y} = 0.65$  for ferry crossing in north direction.

Using Equation (10.16), the ocean current power acting on the ferry is given by

$$P_c = F_c \cdot V_c. \quad (10.20)$$

### 10.2.2.2 Apparent current power on ferry

As an example, assume a ferry crossing from the south harbour to north harbour. The ocean current is influencing the ferry movement with a speed of 0.6 m/s and an angle of 210° relative to the bow.

Using the ferry specifications in table 6.3, the frontal projected current area is calculated to

$$A_{Fc} = \text{Ferry breadth} \cdot \text{Ferry draft} = 16 \text{ m} \cdot 3.85 \text{ m} = 61.6 \text{ m}^2, \quad (10.21)$$

and the lateral projected current area is

$$A_{Lc} = \text{Ferry length} \cdot \text{Ferry draft} = 84 \text{ m} \cdot 3.85 \text{ m} = 323.4 \text{ m}^2. \quad (10.22)$$

The current coefficient approximation components can be calculated as

$$\begin{aligned} C_{c,x}(\gamma_c) &= 0.45 \cdot \cos(210^\circ) \cdot |\cos(210^\circ)| = -0.3375, \\ C_{c,y}(\gamma_c) &= 0.65 \cdot \sin(210^\circ) \cdot \sin(210^\circ) = 0.1625. \end{aligned} \quad (10.23)$$

The wind power acting on the frontal projected current area is

$$P_{Fc} = \frac{1}{2} \rho_a V_c^3 C_{c,x}(\gamma_c) A_{Fc} = -2,239 \text{ W}, \quad (10.24)$$

and the wind power acting on the lateral projected current area is

$$P_{Lc} = \frac{1}{2} \rho_a V_c^3 C_{c,y}(\gamma_c) A_{Lc} = 5,659 \text{ W}. \quad (10.25)$$

Thus, the apparent wind power is given by

$$P_c = \sqrt{P_{Fc}^2 + P_{Lc}^2} = 6,085 \text{ W}. \quad (10.26)$$

With these results, the ferry should decrease the power with 2.24 kW in the surge direction and increase with 5.66 kW in the sway direction to maintain the desired speed and direction.

### 10.2.2.3 Ocean current data

Ocean current data is gathered from the Oceanforecast API, developed by The Norwegian Meteorological Institute[70]. A Python script is used to pull the data from the API and to organize it in a database for further use in the simulations.

### 10.2.2.4 Model implementation

When the charging station controller calculates a new charging profile for the ferry, it determines the average ocean current and direction for the next crossing. The average values are used to calculate the additional or less energy needed to be transferred to the ferry.

As the ferry is in transit, ocean current is applied to the model by using normal distributed values for the current speed and direction. The forecasted current speed is used as the mean value for the applied speed with a standard deviation of 0.2 m/s. The forecasted direction is used as the mean value for the applied direction with a standard deviation of 10°.

Only the ocean current in surge direction is applied to the ferry system, based on the same reasons as given for the wind effect. The applied current is updated every 30 seconds during the crossing with new values for the speed and direction.



## **Part III**

# **Optimal Charge Planning**



# Chapter 11

## Problem Formulation

Optimal charge planning is, in the context of a hybrid ferry system, defined as the ability to predict future energy consumption and to optimally charge the batteries with respect to a set of objectives with corresponding priority. Optimal charging of the ferry- and shore batteries is further formulated in this chapter and prediction of future energy consumption is discussed in Chapter 13.

The problem formulation presented follows the same approach as in [54] by L. Serrao et. al. The energy management problem for hybrid electric vehicles outlined in this paper is used as inspiration for finding optimal charging controls for the ferry- and charging station batteries. In a mathematical form, the optimal control problem consists in finding the sequence of controls  $u(t)$  that leads to the minimization of the cost function  $J$ , defined in Equation (5.2).

The optimal control law is denoted as  $u^*(t)$ , and the corresponding state trajectory is denoted as  $x^*(t)$ . By definition, the optimal control is such that

$$J(x(t_0), u(t), x(t_f)) \geq J(x(t_0), u^*(t), x^*(t_f)), \quad \forall u(t) \neq u^*(t). \quad (11.1)$$

For the optimal control problem of charging a battery, the state variable  $x(t) \in \mathcal{R}$  is defined as the battery SoC, expressed as

$$x(t) = x(t_0) - \frac{1}{Q_{batt}} \cdot \int_{t_0}^t I(\tau) d\tau. \quad (11.2)$$

$u(t) \in \mathcal{R}^m$ , is the vector of control variables, and  $m$  represents how many control variables the problem depends on. A general definition of the control variables for the optimal control problem is

$$u(t) = \{u_{grid}(t), u_{cs}(t)\}, \quad (11.3)$$

where  $u_{grid}(t)$  is the controlled power from the grid to the ferry and  $u_{cs}$ , is the controlled power in and out of the charging station's battery. The degrees of freedom is 2 when optimizing the ferry charging, since both  $u_{grid}$  and  $u_{cs}$  are control variables. When optimizing the charging of the shore battery, the degree of freedom is 1, since  $u_{grid} := 0$ .

Finally, the power to the ferry is given by the combined power from the charging station's battery and the grid. Hence,

$$u_{ferry}(t) = u_{grid}(t) + u_{cs}(t) \quad (11.4)$$

## 11.1 Cost function

The objective for the optimal control problem is to minimize the total cost over a charging by considering the cost of electricity, battery power loss, battery aging and the grid penalty cost.

Since there are different considerations to take with regards to nightlay-, shore- and ferry charging, the cost functions are constructed individually for each of the three charging situations. However, the general terms that are common for all the three functions are further discussed below:

The general cost function is defined as

$$J = \int_0^{t_f} (\mu_1 \cdot J_{el} + \mu_2 \cdot J_{loss} + \mu_3 \cdot J_{aging} + \mu_4 \cdot J_{load}) dt, \quad (11.5)$$

where  $\mu = \{\mu_1, \mu_2, \mu_3, \mu_4\}$  is the vector defining the weighting factors. If the weighting is natural, the vector is defined as  $\mu_{natural} = \{1, 1, 1, 1\}$ . As seen, the cost function does not include a terminal cost, hence  $\phi(\cdot) = 0$ .

The term defining the cost of electricity,  $J_{el}$ , is given by

$$J_{el} = \xi(t, u(t)). \quad (11.6)$$

$\xi(\cdot)$  is the electricity cost function, discussed in Section 9.3, which depends on the time and the power drawn from the grid to either the ferry battery or the shore battery. The term includes both the market electricity price and the network tariff cost and has the unit [NOK/h].

To calculate the cost of battery power loss, the actual power loss during charging must first be found. This loss can be expressed as

$$P_{loss} = P_{loss, \%}(I_c) \cdot u(t), \quad (11.7)$$

where  $P_{loss, \%}$  is the approximation function for the power loss with regards to the applied C-rate, as discussed in Section 8.2. By multiplying this function with the applied battery power, the amount of power loss is found.

The term defining the cost of battery power loss,  $J_{loss}$ , is then given as

$$J_{loss} = \xi(t, P_{loss}). \quad (11.8)$$

Hence, the cost is found by using the same electricity cost function as used above, but instead account of the amount of power loss. The unit for the battery power loss term is [NOK/h].

The term defining the cost of battery aging,  $J_{aging}$ , is given as

$$J_{aging} = \frac{c_{batt}}{\Gamma} \cdot \sigma(u(t), \theta, x(t)) \cdot |I(x(t), u(t))| \quad (11.9)$$

where  $\sigma(\cdot)$  and  $\Gamma$  are the severity factor and the nominal battery life, respectively, as discussed in Section 8.3.  $c_{batt}$  is the price of one battery in NOK. With  $\Gamma$  having the unit [Ah],  $I$  having the unit [A] and  $\sigma(\cdot)$  being dimensionless, the unit for the battery aging term is [NOK/h].

As the last term, the grid penalty cost is calculated as

$$J_{load} = \begin{cases} \xi_{load}(t, u(t)), & \Leftrightarrow P_{net}(t) < 0 \cap u(t) \geq 1000 \text{ kW} \\ 0, & \Leftrightarrow P_{net}(t) \geq 0 \cup u(t) < 1000 \text{ kW}, \end{cases}$$

where  $\xi_{load}$  is the function giving the cost of utilizing the grid at a given time, as discussed in Section 9.1.1.

Combining all the terms and integrating over the entire charging period gives the total cost of charging the battery in NOK. As the penalty grid cost is event-based and the electricity price is step-wise, the general cost function is discontinuous. This means that the cost function is non-differentiable and thus non-convex. As the numerical method does not require the cost function to be differentiable, the discontinuity does not rise a problem here. However, the analytical method depends on differentiating the cost function, and therefore, simplifications must be made. This is discussed in Section 12.2, when solving the optimal control problem with Pontryagin's minimum principle.

The general cost function is further separated into three independent cost functions, which covers the three different charging situations in the hybrid ferry system.

### 11.1.1 Shore charging cost function

The shore charging cost function is used when the battery in the charging station is recharged after use. This is normally when the ferry disconnects from the charging station after docking for unloading and loading passengers.

The cost function is formulated as

$$J_{shore} = \int_0^{t_f} (\mu_1 \cdot J_{el,cs} + \mu_2 \cdot J_{loss,cs} + \mu_3 \cdot J_{aging,cs} + \mu_4 \cdot J_{load,cs}) dt \quad (11.11)$$

where  $J_{el,cs}$  is the cost of electricity for recharging the shore battery,  $J_{loss,cs}$  is the cost of the power loss in the shore battery and  $J_{aging,cs}$  is the cost of shore battery aging. The term considering the grid penalty cost,  $J_{load,cs}$ , is included but are rarely active, as the recharging power usually never exceeds 1000 kW. All terms related to the ferry are set to zero, i.e.  $u_{grid} := 0$ , since they do not influence the shore charging.

### 11.1.2 Ferry charging cost function

The ferry charging cost function is used when calculating the new charging profile for the ferry per shore docking. The function is formulated as

$$J_{ferry} = \int_0^{t_f} (\mu_1 \cdot J_{el,ferry} + \mu_2 \cdot J_{loss,ferry} + \mu_3 \cdot J_{aging,ferry} + \mu_4 \cdot J_{load,ferry}) dt, \quad (11.12)$$

where terms related to both charging the ferry battery and discharging the shore battery are included.  $J_{el,ferry}$  expresses the cost of electricity for charging the ferry battery and recharging the shore battery after the charging process of the ferry is finished. Hence,

$$J_{el,ferry} = \xi(t_1, u_{grid}) + \xi(t_2, u_{cs}), \quad (11.13)$$

where  $t_1$  defines the time throughout the ferry charging and  $t_2$  defines the forthcoming time sequence of the recharging of the shore battery. This is done to account for the variation in electricity price, which can influence the recharging of the shore battery. The optimization will therefore look at the profitability of drawing more power from the charging station with the expenses of battery power loss and aging.

The part related to the recharging electricity cost of the shore battery is, however, only an approximation of the real cost that the shore battery is subject to. This is caused by the time horizon for the ferry charging and the recharging of the shore battery being very different, and because the discharging and charging power of the shore battery is not the same. The inclusion can, on the other hand, be justified because it gives a better representation of the overall cost of charging the ferry.

In  $J_{loss,ferry}$  both the power loss in the ferry battery due to charging and the power loss in the shore battery due to both discharging and recharging are included. The term is calculated as

$$J_{loss,ferry} = \xi(t, P_{loss,ferry}) + 1.12 \cdot \xi(t, P_{loss,cs}), \quad (11.14)$$

where the factor 1.12 is selected as the relationship between discharging and charging time is normally 3 minutes to 26 minutes. The amount of power used for recharging the shore battery is therefore approximated to  $\frac{3}{26}$  of the power used when discharging. This is a simplification of the forthcoming power loss, and since an optimal charging profile is again calculated for this recharging, the cost of power loss may deviate from the actual.

The same holds for  $J_{batt}$ , which includes the action at the ferry battery and the shore battery, and is given as

$$J_{aging,ferry} = \frac{c_{batt,ferry}}{\Gamma} \cdot \sigma(u_{ferry}(t), \theta, x_{ferry}(t)) \cdot |I(x_{ferry}(t), u_{ferry}(t))| \\ + 1.12 \cdot \frac{c_{batt,cs}}{\Gamma} \cdot \sigma(u_{cs}(t), \theta, x_{cs}(t)) \cdot |I(x_{cs}(t), u_{cs}(t))|, \quad (11.15)$$

where  $c_{batt,ferry}$  and  $c_{batt,cs}$  are the costs of respectively the ferry- and charging station battery, given by the specifications in Tables 6.4 and 7.1. Both the cost of power loss and cost of battery aging will give a negative impact on utilizing the shore battery, and will then contribute to more power outtake from the grid.

The grid penalty cost term,  $J_{load}$ , is given by

$$J_{load,ferry} = \begin{cases} \xi_{load}(t, u_{grid}(t)), & \Leftrightarrow P_{net}(t) < 0 \cap u_{grid}(t) \geq 1000 \text{ kW} \\ 0, & \Leftrightarrow P_{net}(t) \geq 0 \cup u_{grid}(t) < 1000 \text{ kW}, \end{cases}$$

where the cost depends on the grid power under the conditions that are described in Section 9.1.1. It is further assumed that the recharging power of the shore battery never exceeds the penalty power level of 1000 kW, such that the recharging grid penalty cost is not needed to be included.

All the factors regarding the recharging of the shore battery are approximated, and therefore, the total cost for the ferry charging cost function may not represent the actual cost for charging the ferry battery. However, the overall system cost is better represented by including the factors.

### 11.1.3 Nightly charging cost function

The nightly charging cost function is used to calculate the optimal charging profile for the ferry battery at the end of the day. The cost function is formulated as

$$J_{nightlay} = \int_0^{t_f} (\mu_1 \cdot J_{el,ferry} + \mu_2 \cdot J_{loss,ferry} + \mu_3 \cdot J_{batt,ferry}) dt, \quad (11.17)$$

and is similar to the shore charging cost function discussed Section 11.1.1. However, the costs related to the ferry are instead considered, and  $u_{cs} := 0$ . As the capacity in the grid connected to the nightly station is limited at 1000 kW, the grid penalty cost is never present here.

## 11.2 Optimal control problem

The general optimal control problem for battery charging can be formulated based on the cost functions defined above and the constraints to which the optimization is subject to. The formulation follows the same structure as given in [24] by L. Serrao, where the optimization constraints are listed as:

- (a) system dynamics
- (b) initial state value
- (c) terminal state value
- (d) instantaneous state limitations
- (e) instantaneous control limitations

### (a) System dynamics

During the entire optimization horizon, the system evolves according to its dynamic equation

$$\dot{x}(t) = f(x(t), u(t)), \quad \forall t \in [t_0, t_f], \quad (11.18)$$

which represents the evolution of the battery SoC as a function of the battery power. Hence, by using Equation (8.4), the state variable is given as

$$\dot{x}(t) = -\frac{1}{Q_{nom}} \cdot \frac{V_{OC}(x(t)) - \sqrt{V_{OC}^2(x(t)) - 4R_{eq} \cdot u(t)}}{2 \cdot R_{eq}} = f(x(t), u(t)), \quad (11.19)$$

where the open circuit voltage depends on the battery SoC, and the effect of SoC on the internal resistance is assumed to be constant.

**(b) Initial state value**

The system state at the beginning of the optimization horizon must assume the initial value  $x_0$ . Hence,

$$x(t_0) = x_0. \quad (11.20)$$

**(c) Terminal state value**

The terminal value of the state must satisfy the equality constraint (hard constraint)

$$x(t_f) = x_f. \quad (11.21)$$

**(d) Instantaneous state limitations**

At each time  $t \in [t_0, t_f]$ , the battery state of charge,  $x(t)$ , must remain within lower and upper bounds:

$$x_{min} \leq x(t) \leq x_{max}, \quad (11.22)$$

such that

$$x(t) \in X(t), \quad (11.23)$$

where  $X \subset \mathcal{R}^m$  is the set of all the admissible state variables. For a more compact notation, the state constraints can also be written as

$$G(x(t), t) \leq 0, \quad (11.24)$$

where

$$G(x(t), t) = \begin{cases} x(t) - x_{max} \\ x_{min} - x(t). \end{cases}$$

For the optimal control problem of charging the ferry battery, it is assumed that the shore battery always remain within lower and upper bounds. Hence, when solving the optimal control problem for ferry charging, the only system variable is the ferry battery.

**(e) Instantaneous control limitations**

For the constraints on the control actions, both of the control variables,  $u_{grid}$  and  $u_{cs}$  are considered. At each time, the control variable must remain within lower and upper bounds:

$$u_{min} \leq u(t) \leq u_{max}, \quad (11.25)$$

such that

$$u(t) \in \mathcal{U}(t), \quad (11.26)$$

where  $\mathcal{U} \subset \mathcal{R}^m$  is the set of all the admissible control variables. For a more compact notation, the control variable constraints can also be written as

$$Q(u(t), t) \leq 0, \quad (11.27)$$

where

$$Q(u(t), t) = \begin{cases} u(t) - u_{max} \\ u_{min} - u(t). \end{cases}$$

At this point, the optimal control problem is completely defined, and can be formulated on the following mathematical form:

$$u^* = \arg \min_u : J \quad (11.28)$$

$$\text{subject to:} \quad (11.29)$$

$$\dot{x} = -\frac{1}{Q_{batt}} I(x, u) \quad (11.30)$$

$$x(t_0) = x_0 \quad (11.31)$$

$$x(t_f) = x_f \quad (11.32)$$

$$G(x(t), t) \leq 0, \quad \forall t \quad (11.33)$$

$$Q(u(t), t) \leq 0, \quad \forall t \quad (11.34)$$

$$x(t) \in \mathcal{X}, \quad \forall t \quad (11.35)$$

$$u(t) \in \mathcal{U}, \quad \forall t \quad (11.36)$$

Note that there is no saturation on the rate of change in state,  $\Delta x$ , and rate of change in control action,  $\Delta u$ . In a realistic charging process, the power would ramp up/down in amplitude instead of the instant ramp up/down modelled in this system. In the follow sections, two different methods to solve the optimal control problem are presented.



## Chapter 12

# Comparison of Optimization Methods

In this chapter, the dynamic programming principle and the Pontryagin's minimum principle are formulated with respect to the optimal control problem for ferry- and shore battery charging, given in Chapter 11. The two methods are then applied to two different charging scenarios, defined as follows:

### Nightlay charging scenario

This scenario takes place at the nightlay station between 02:00 and 06:00 the working day, where the task is to charge the ferry from 30 % to 60 % SoC. Since the charging period is over several hours, the price of electricity changes during the charging. As shown in Figure 12.1, the price is relatively constant from 02 to 05 and does a step up between 05 and 06. Hence, as a hypothesis, the optimal sequence of controls,  $u_{grid}^*$ , will try to avoid too much charging between 05 and 06 to minimize the cost of electricity.

The amount of passengers and the weather- and ocean conditions are not influencing the charging process. The optimal control problem consists solely in minimizing the cost of electricity, battery power loss and battery aging. The grid penalty cost is also neglected, since there is no undersupply of power during the charging period and

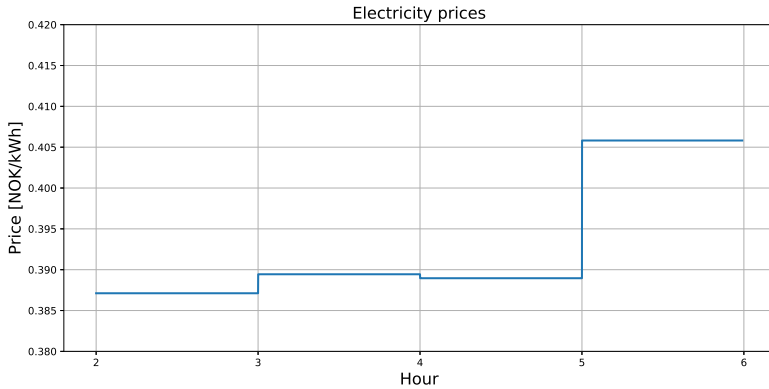


Figure 12.1: Electricity price variation during a working day from 02 to 06

because the grid power never exceeds 1000 kW. Profiles for the battery SoC, charging power and current during a typical nightlay charge using the standard method are shown in Figure 12.2. As seen, a constant current is applied to recharge the battery up to the desired SoC level. When applying the standard method to the battery charging, it is always assumed that the voltage is adjusted accordingly to obtain a constant current over the entire charging process.

### Normal charging scenario

In this scenario, the ferry is charged from 48 % to 60 % SoC within a charging time of 3 minutes. The start of the charging is set to 07:56:30 the working day, and therefore, the electricity price will not change during the charging period. Both the grid- and shore battery power are used to charge the ferry, and hence, the costs associated with recharging the shore battery should also be included in the analysis. The recharging of the shore battery starts 08:00 and has a duration of 26 minutes.

The profiles for the ferry SoC, battery power and current, together with the profiles for the shore battery dynamics and the grid power during the ferry charging are given in Figure 12.2. The profiles for the shore battery recharging are not included.

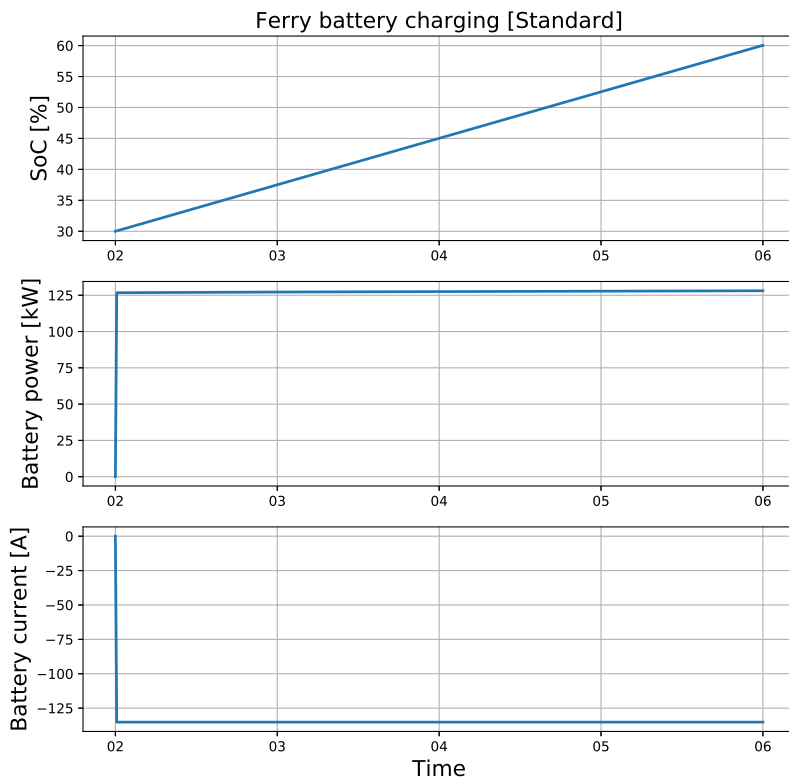


Figure 12.2: Nightly charging using standard method

As there is an under supply of power in the grid during the charging process, the grid penalty cost will be active and influence the charging. The optimal control problem will therefore try to find the optimal tradeoff between battery usage and grid utilization.

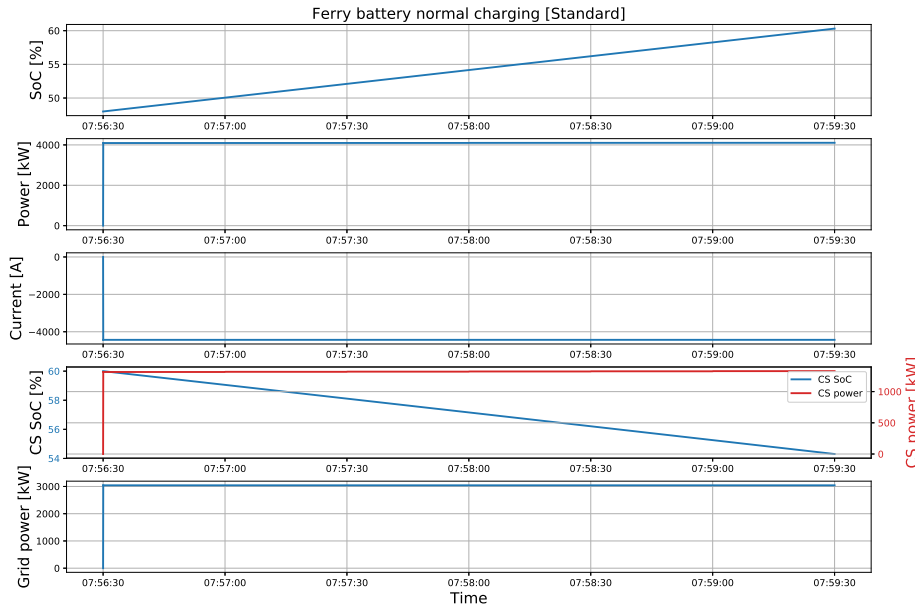


Figure 12.3: Normal charging using standard method

## 12.1 Dynamic programming

The dynamic programming (DP) principle can be described in formulas by:

### Principle of Optimality[57]

Let  $\pi^* = \{u_0^*, u_1^*, \dots, u_{N-1}^*\}$  be an optimal policy for the control problem. Consider the subproblem whereby we are at the state  $x_i$  at time  $i$  and wish to minimize the cost function,  $J_\pi(x_i)$ , from time  $i$  to time  $N$

$$J_\pi(x_i) = \phi(x_N) + \sum_{k=i}^{N-1} L_k(x_k, u_k), \quad (12.1)$$

where  $L_k$  is the instantaneous cost function and  $\phi$  is the terminal cost.

Then the truncated policy  $\{u_i^*, u_{i+1}^*, \dots, u_{N-1}^*\}$  is optimal for this subproblem.

For solving the optimal control problem, given by Equation (11.28) - Equation (11.36), with the dynamic programming principle, the problem formulation must be discretized. Discretization in time by a Forward Euler scheme gives the system equation on form

$$x_{k+1} = x_k - \frac{1}{Q_{nom}} \cdot \frac{V_{OC,k}(x_k) - \sqrt{V_{OC,k}^2(x_k) - 4R_{eq} \cdot u_k}}{2 \cdot R_{eq}} = f(x_k, u_k), \quad (12.2)$$

and the optimal control problem on the form

$$u^* = \arg \min_{\pi} : J \quad (12.3)$$

$$\text{subject to} \quad (12.4)$$

$$x_{k+1} = -\frac{1}{Q_{batt}} I(x_k, u_k) \quad (12.5)$$

$$x_{k=0} = x_0 \quad (12.6)$$

$$x_{k=N} = x_N \quad (12.7)$$

$$G(x_k, k) \leq 0, \quad \forall k \quad (12.8)$$

$$Q(u_k, k) \leq 0, \quad \forall k \quad (12.9)$$

$$x_k \in \mathcal{X}, \quad \forall k \quad (12.10)$$

$$u_k \in \mathcal{U}, \quad \forall k, \quad (12.11)$$

on the optimization horizon  $k = \{0, 1, 2, \dots, N\}$ , where  $N$  is the number of time steps in which the optimization horizon is subdivided. For the optimal control problem, the time step is set to 30 seconds, meaning a new control action is applied every 30 second. The general cost function, with the set of objectives discussed in Section 11.1, is formulated with regards to the DP method as

$$J_{\pi}(x_0) = \sum_{k=0}^{N-1} \mu_1 \cdot J_{el,k} + \mu_2 \cdot J_{loss,k} + \mu_3 \cdot J_{batt,k} + \mu_4 \cdot J_{load,k}, \quad (12.12)$$

where the cost function terms are discretized. As formulated in [24], the optimal cost function is the one that minimizes the total cost

$$J^*(x_0) = \arg \min_{\pi} J_{\pi}(x_0) \quad (12.13)$$

and the optimal policy  $\pi^* = \{u_0^*, u_1^*, \dots, u_{N-1}^*\}$  is such that

$$J_{\pi^*}(x_0) = J^*(x_0). \quad (12.14)$$

The method is implemented in Python by constructing a graph similar to the illustration in Figure 5.1. The algorithm starts by calculating the next SoC from the initial SoC by applying a set of admissible control actions to the battery. This procedure is followed for each node until the target SoC is reached. When the graph is fully constructed, the Dijkstra Shortest Path First-algorithm is used to find the optimal control actions with the lowest cost from the initial SoC to the target SoC. The sequence of control actions is then applied to the battery system. A description of the Dijkstra-algorithm is given in [55].

### 12.1.1 Optimal charging using dynamic programming

The principle is further applied to the charging scenarios presented in the chapter introduction and compared to the standard method of charging. The weighting factors in the cost function have a natural weighting for both the scenarios. Thus,  $\mu = \{1, 1, 1, 1\}$ .

#### Nightlay charging scenario

During the nightlay charging scenario, the factor with the highest influence is the cost of electricity. The charging profile should, however, keep the battery aging and power loss limited, and therefore not set a too high current when the electricity price is low. The optimized profiles for the battery SoC, charging power and current are given in Figure 12.4. As seen, the battery is charged with a higher current at the start, when the electricity price is low, compared to the end of the charging time. The current profile also increases the current amplitude for two periods under the charging. The first increase has a longer period than the second, because the electricity price is lower during this hour.

The results and costs associated with the optimal charging are given in Table 12.1. For comparison, the same charging is performed using the standard method, and the associated costs are added for comparison. As seen, the total cost of charging is slightly reduced by using the DP method, where the cost of electricity is the most, and only, profitable term.

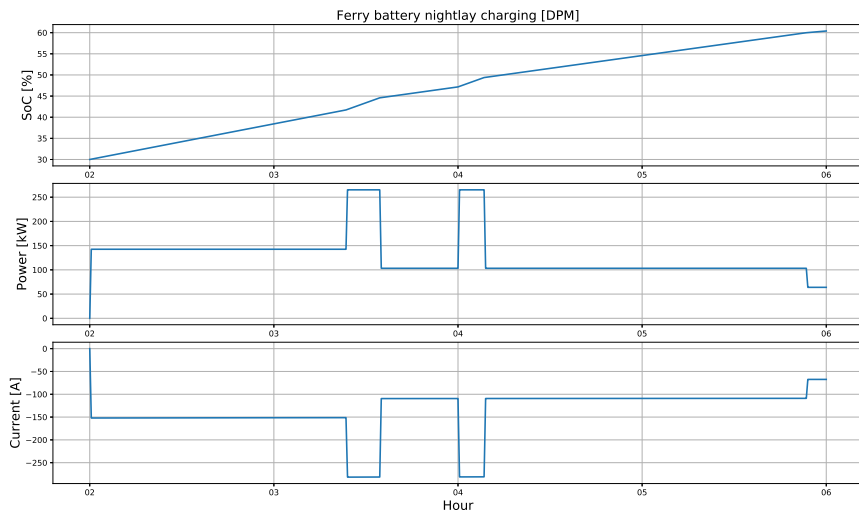


Figure 12.4: Nightly charging using the dynamic programming method

Table 12.1: Results and costs associated with nightly charging using DPM

Charging method	Final SoC [%]	Cost of electricity [NOK]	Cost of power loss [NOK]	Cost of battery aging [NOK]	Total charging cost [NOK]
DP method	60.40	265.31	4.40	60.15	329.86
Standard method	60.40	265.89	4.39	60.10	330.38

The relative shy reduction in cost can be appointed to two factors: The resolution of the SoC and the number of control actions are limited to avoid too high computation time, which give less optimal values for the charging profile. The second factor is the variation in electricity price, which is relatively low over the simulation period.

### Normal charging scenario

As discussed in the chapter introduction, the normal charging scenario is divided into two parts, where the first part considers charging of the ferry battery, and the second part considers recharging of the shore battery. The profiles for the ferry SoC, power and current and shore battery SoC and power, together with the grid power, using optimal charging are shown in Figure 12.5. The profiles for the shore battery recharging are not included.

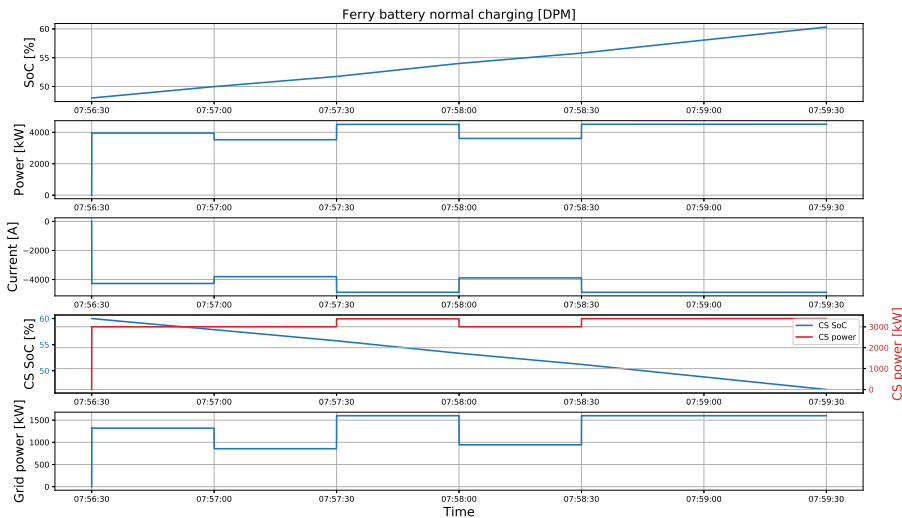


Figure 12.5: Normal charging with DPM

As seen in the figure, the charging station battery is almost fully utilized to make the grid power as small as possible. Hence, the optimization calculates a higher saving from reducing the grid penalty cost than the cost of using the shore battery.

The costs associated with charging the ferry battery and recharging the shore battery are listed in Table 12.2. The costs related to the battery power loss and aging are higher for the ferry charging situation due to higher battery utilization, and the electricity cost is higher for the shore recharging situation. The penalty grid cost is limited during the ferry charging process and not present at the recharging process.

Table 12.2: Results and costs associated with normal charging using DPM method

Battery	Start SoC [%]	Final SoC [%]	Cost of electricity [NOK]	Cost of power loss [NOK]	Cost of battery aging [NOK]	Grid penalty cost [NOK]	Total charging cost [NOK]
Ferry	48.00	60.32	37.09	11.56	58.40	9.60	116.65
Shore	46.41	59.46	87.06	1.67	18.46	0	107.19

The results from using the DP method and the standard method are compared in Table 12.3. The total charging cost is reduced by NOK 9.83,- using the DP method, which is ensured by the decrease in grid penalty cost. All other costs are higher, but the optimization correctly calculates more profit by reducing the grid power when charging the ferry.

Table 12.3: Results and costs comparison between DPM and standard method under normal charging

Charging method	Controlled Ah	Cost of electricity [NOK]	Cost of power loss [NOK]	Cost of battery aging [NOK]	Grid penalty cost [NOK]	Total charging cost [NOK]
DP method	541.32	124.16	13.23	76.87	9.60	223.84
Standard method	352.36	120.44	8.01	49.84	55.39	233.67

## 12.2 Pontryagin's minimum principle

The Pontryagin's minimum principle (PMP) is selected as the second optimization method for solving the optimal control problem for battery charging. As the method is analytical, the system equation and problem formulation is again back on continuous form as outlined in Chapter 11. The following formulation follows the same structure as presented in [54] by L. Serrao et. al:

The Hamiltonian for the general control problem is defined as

$$H(x(t), u(t), \lambda(t)) = -\lambda(t) \cdot f(x(t), u(t)) + \mu_1 \cdot J_{el}(t) + \mu_2 \cdot J_{loss}(t) + \mu_3 \cdot J_{batt}(t) + \mu_4 \cdot J_{load}(t), \quad (12.15)$$

where  $f(x(t), u(t))$  is given by Equation (11.19), and the control action  $u(t)$  is obtained at each instant as the value that minimizes the Hamiltonian function. Hence,

$$u^*(t) = \underset{u}{\operatorname{arg\,min}} : H(x(t), u(t), \lambda(t)). \quad (12.16)$$

The co-state variable,  $\lambda(t)$ , appearing in the Hamiltonian function is calculated from the dynamic equation given in Equation (5.7). Thus,

$$\begin{aligned} \dot{\lambda}(t) &= -\frac{\partial H(x(t), u(t), t, \lambda(t))}{\partial x} \\ &= \lambda(t) \frac{\partial}{\partial x} \left( -\frac{1}{Q_{nom}} I(x(t), u(t)) \right) \\ &\quad - \mu_1 \frac{\partial}{\partial x} \left( \xi(t) \cdot u(t) \right) \\ &\quad - \mu_2 \cdot R_{eq} \frac{\partial}{\partial x} \left( \xi(t) \cdot |I(x(t), u(t))|^2 \right) \\ &\quad - \mu_3 \cdot \frac{c_{batt}}{\Gamma} \frac{\partial}{\partial x} \left( \sigma(u(t), \theta, x(t)) \cdot |I(x(t), u(t))| \right) \\ &\quad - \mu_4 \cdot \frac{\partial}{\partial x} \left( \xi_{load}(t, u(t)) \right). \end{aligned} \quad (12.17)$$

By assuming that the effect of SoC on the open-circuit voltage,  $V_{OC}$ , is negligible, the SoC will not be a function of the current, and the co-state dynamic, given in Equation (12.17), can be simplified to

$$\dot{\lambda}(t) = -\mu_3 \cdot \frac{c_{batt}}{\Gamma} \cdot |I(u(t))| \frac{\partial \sigma(u(t), \theta, x(t))}{\partial x}. \quad (12.18)$$

This can be justified since the operational area of the SoC will always be in the range 20-65 %, where the curve is relatively flat, as seen in Figure 8.3a. The variation of the severity factor with respect to the SoC is calculated as

$$\begin{aligned} \frac{\partial \sigma(\cdot)}{\partial x} &= \frac{\partial}{\partial x} \frac{\Gamma}{\gamma(u(t), \theta, x(t))} = \Gamma \cdot \frac{\partial}{\partial x} \left[ \gamma(u(t), \theta, x(t)) \right]^{-1} \\ &= \Gamma \cdot \left[ \frac{\alpha \cdot \exp\left(-\frac{-E_a + \eta \cdot I_c}{R_g \cdot (273.15 + \theta)}\right) \cdot 20^{-\frac{1}{z}} \cdot \left(\frac{\exp\left(-\frac{-E_a + \eta \cdot I_c}{R_g \cdot (273.15 + \theta)}\right)}{\alpha \cdot x + \beta}\right)^{-\frac{1}{z} - 1}}{z \cdot (\alpha \cdot x + \beta)^2} \right]. \end{aligned} \quad (12.19)$$

With this simplification, the optimization problem can be regarded as continuous within the operational regions for the state variable and the control actions. Equation (12.18), together with Equation (11.19), represents a dynamic system of two differential equations with two variables,  $x(t)$  and  $\lambda(t)$ . As the initial and final value of the state  $x$  is known, these can be used as the two boundary conditions needed for solving the state equation[54].

This two-point boundary value problem can be solved numerically by using an iterative procedure as the state boundary condition is defined at the final time. The procedure is known as the shooting method and consists of replacing the two-point boundary value problem with a conventional initial-condition problem, starting with an initial guess for  $\lambda_{t_0}$ . The solution of the problem is then obtained by integrating Equation (12.18) and Equation (11.19), and replacing at each time instant the value of  $u$  that minimizes the Hamiltonian function given in Equation (12.15). If the final value of the state does not match the desired terminal condition  $x^*(t_f) = x_f \pm 0.2\%$ , the value of  $\lambda_{t_0}$  is adjusted iteratively until the terminal condition on the state is met[54].

### 12.2.1 Optimal charging using minimum principle

The principle is further applied to the charging scenarios described in the chapter introduction. As for the DP method, the weighting factors have a natural weighting for both the scenarios.

#### Nightlay charging scenario

The charging profiles for the nightlay charging scenario using PMP are presented in Figure 12.6. As seen, the optimization calculates that the cost of electricity is lowest at the start of the charging period and high between 05 and 06. The battery is therefore recharged before 05 to minimize the electricity cost.

As discussed in Section 12.2, an initial guess for  $\lambda_0$  is applied to the algorithm at start, and the sensitivity for this initial value, with respect to the optimal nightlay charging problem, is shown in Figure 12.7. When trying to find the optimal value for  $\lambda_0$  a binary search method is used. This method starts by setting a lower and an upper boundary value, say 1000 and 1050, and then uses the mean value, 1025, as the new  $\lambda_0$ . If the difference between the final SoC and the target SoC is above 0, the last calculated  $\lambda_0$  is used as the new lower boundary value, and if the difference is below 0,  $\lambda_0$  is the new upper boundary value. This is iteratively proceeded until the optimal value for  $\lambda_0$  is found.

The results using PMP for optimal charging are given in Table 12.4, and compared to the standard method. As seen, the total charging cost is reduced by NOK 2,-, and the electricity cost is reduced by NOK 2.63,-. The costs related to battery power loss and aging slightly increase, as the optimal way of charging with respect to these factors are to apply a constant current.

Table 12.4: Results and costs associated with nightlay charging using PMP method

Charging method	Final SoC [%]	Cost of electricity [NOK]	Cost of power loss [NOK]	Cost of battery aging [NOK]	Total charging cost [NOK]
PMP method	60.06	260.38	4.48	59.84	324.70
Standard method	60.06	263.01	4.33	59.36	326.71

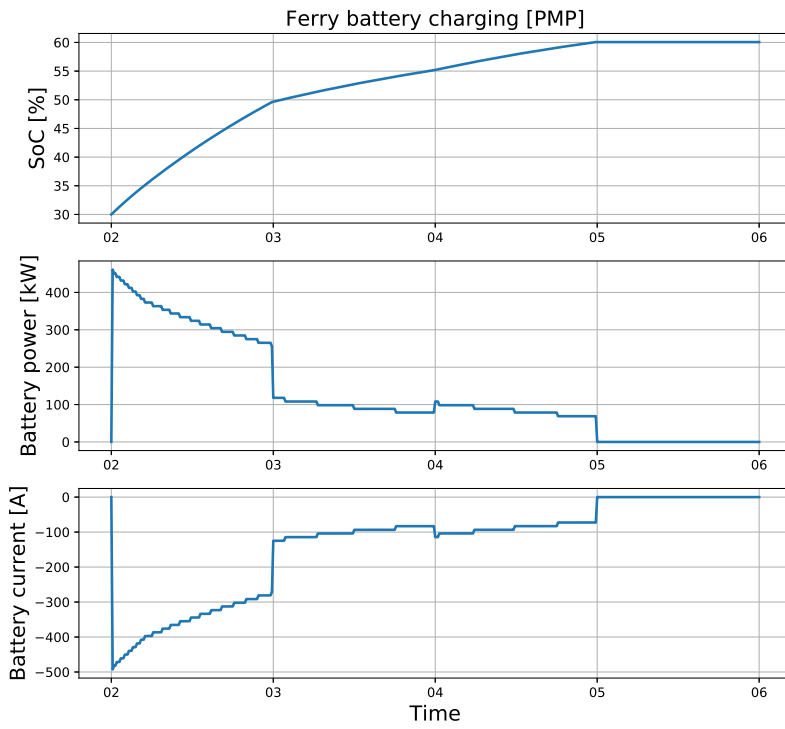


Figure 12.6: Nightlay charging with PMP charging method

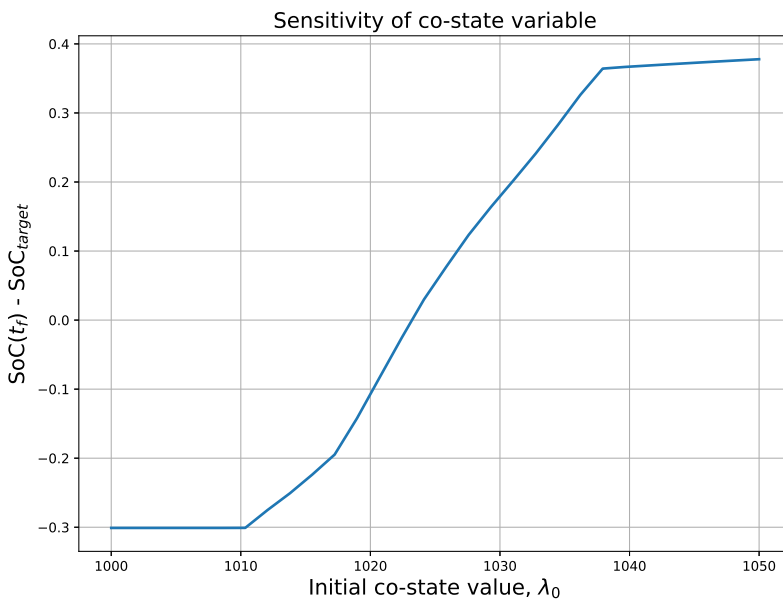


Figure 12.7: Effect of initial co-state value on target SoC.

### Normal charging scenario

Applying the principle on the normal charging scenario gives the profiles for ferry charging as shown in Figure 12.8. The method calculates a constant power for both the grid- and shore battery power. The grid power is set to 1003.86 kW, just above the grid penalty power level, and the battery power is set to the rated power of 3432 kW.

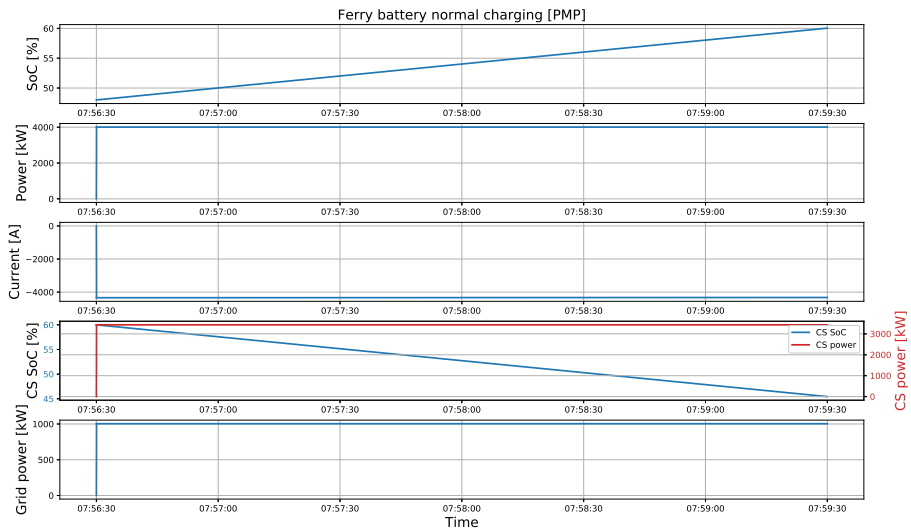


Figure 12.8: Normal charging with PMP charging method

For the recharging of the shore battery, shown in Figure 12.9, the grid power starts at 446 kW and decreases throughout the charging process down to 343.2 kW at the end. As the battery power loss and aging are the only factors influencing the cost function during this recharging, the method calculates a lower cost when the SoC is low, and a higher cost as the SoC increases, due to the formulation of the battery aging cost. This causes the decrease in power as seen in the figure.

However, by applying a constant power, with the mean value between 343.2 kW and 446 kW, the same contribution to the cost of battery power loss and aging would be achieved. Hence, charging with a constant current is optimal when the charging is only influenced by the cost of battery power loss and aging.

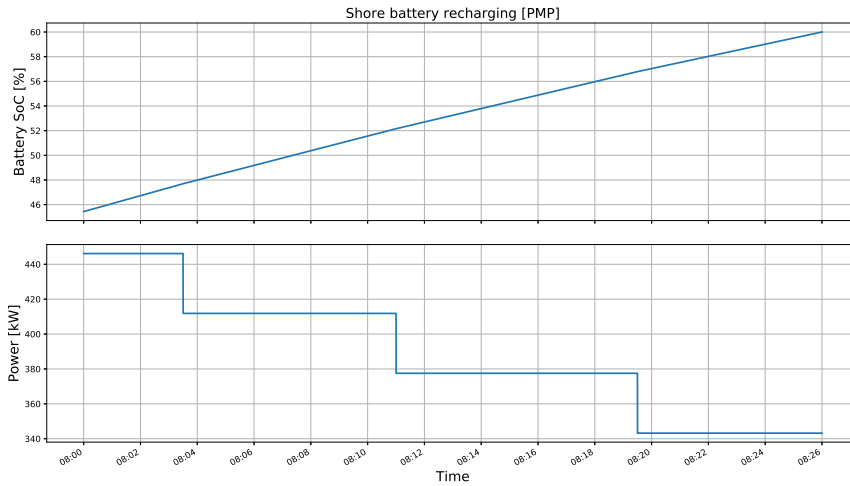


Figure 12.9: Shore battery recharging using PMP

The associated costs for charging the ferry battery and recharging the shore battery, using PMP, are given in Table 12.5. As seen, the total charging cost related to the recharging is higher than the ferry charging cost. This is opposite of what happened in the DP method charging, and is caused by even more shore battery utilization during the ferry charging.

Table 12.5: Results and costs associated with normal charging using PMP method

Battery	Start SoC [%]	Final SoC [%]	Cost of electricity [NOK]	Cost of power loss [NOK]	Cost of battery aging [NOK]	Grid penalty cost [NOK]	Total charging cost [NOK]
Ferry	48.00	60.03	28.23	11.95	59.51	0.11	99.80
Shore	45.44	60.00	97.11	1.90	20.67	0	119.69

In Table 12.6, the charging results are compared to the standard method. The optimal method reduces the total charging cost by NOK 19.2,- by minimizing the grid power outtake above the penalty power level. All the other costs are higher due to more battery utilization.

Table 12.6: Results and costs comparison between PMP and standard method under normal charging

Charging method	Controlled Ah	Cost of electricity [NOK]	Cost of power loss [NOK]	Cost of battery aging [NOK]	Grid penalty cost [NOK]	Total charging cost [NOK]
PMP method	566.19	125.35	13.85	80.19	0.11	219.49
Standard method	360.27	124.29	8.12	50.84	55.39	238.64

### 12.3 Numerical versus analytical method

Comparing the performance of the two optimization methods, the analytical method is clearly better than the numerical for the optimal control problem. In both the charging scenarios the Pontryagin's minimum principle gives better results, with less computation time. One reason for this is that limited resolution for the dynamic programming problem is used to reduce the computation time and memory usage.

The dynamic programming principle has a specific high computation time when calculating the optimal power split between the shore battery and the grid power, since two control variables are used. With unlimited computation time and memory, the DP method should, however, give the most optimal solution to the control problem.

When considering the analytical method, the assumptions made for simplifying the co-state variable should be taken into account. If the simplification of the system equations is excessive, the model may not be representative of the real system and the resulting optimal control may actually be sub-optimal[24]. However, based on the results from the charging scenarios and the computation time, Pontryagin's minimum principle is the preferred method used for further simulations.

## Chapter 13

# Prediction of Future Energy Consumption

The second step in optimal charge planning is energy planning and prediction of future energy consumption. By introducing this, the capacity objective for the charging changes from being to substitute the consumed energy during the last crossing, to substitute the consumed energy for the forthcoming crossing. The ability to accurately predict this future energy consumption is vital to ensure safe, reliable and optimal operation.

### 13.1 Planning by power losses

Since energy is dissipated at all stages during a charging, the first step for achieving safe, reliable and optimal operation should be to include the power losses in a charging process.

Since power loss in the battery is dependent on the C-rate, the battery power loss is included when calculating the optimal charging profile. In the shore charging scenario and the nightlay charging scenario, the power loss is compensated for by every control action applied to the battery. In the ferry charging scenario, the power loss in both the

shore battery and ferry battery are compensated for by the calculated control actions.

The power loss in the ferry battery during the crossing is more complex to predict because of varying propulsion power and external factors. The loss is however compensated for by adding a constant factor to the transferred energy. As the average power over a normal crossing under nominal conditions is 1036 kW, the average power loss in the battery due to discharge is calculated to be 2.7%. However, with discrepancies from the nominal conditions, this makes the compensation not 100% accurate.

As the efficiency in the other system components are static, meaning that they do not change with respect to the charging current, the controller compensates for the loss by adding an additional factor to the transferred energy. Planning by power losses is taken into account in both the scenarios presented in Part IV.

## 13.2 Planning by the route schedule

A good way to start the planning of energy transfer to the ferry is by using the route schedule to predict the forthcoming nominal energy consumption. As the nominal ferry consumption changes with the transit time, and the transit time changes with the route schedule, the controller can use this information to determine an approximate value for the consumption. Table 6.1 is implemented in the controller, and gives the energy consumption under reference conditions.

As the consumption is significantly lower when the transit time is 12 minutes compared to 11 minutes, the effect by reducing the charging power on battery power loss and aging is high. This is further studied in the simulations in Part IV.

## 13.3 Planning by external factors

The external factors described in Chapter 10 are further used to predict ferry energy consumption during transit. The factors are predicted by the charging controller when the ferry connects to the charging station, and are considered when the target SoC for the forthcoming charging is set.

### 13.3.1 Passenger planning

The statistical data for the amount of passenger car units (PCU), given in Figure 10.1, is used by the controller to either increase or decrease the energy transferred to the ferry. The PCU value predicted by the south charging station controller against the actual value applied to the ferry in simulations is given in Figure 13.1.

As seen, the actual PCU value changes more rapidly than the predicted value. This is because the amount of passengers changes when leaving both the south- and north charging station, and because the predicted value is only updated on hourly basis. Hence, between 12 and 18, as is the time period shown in the figure, the predicted value changes 6 times.

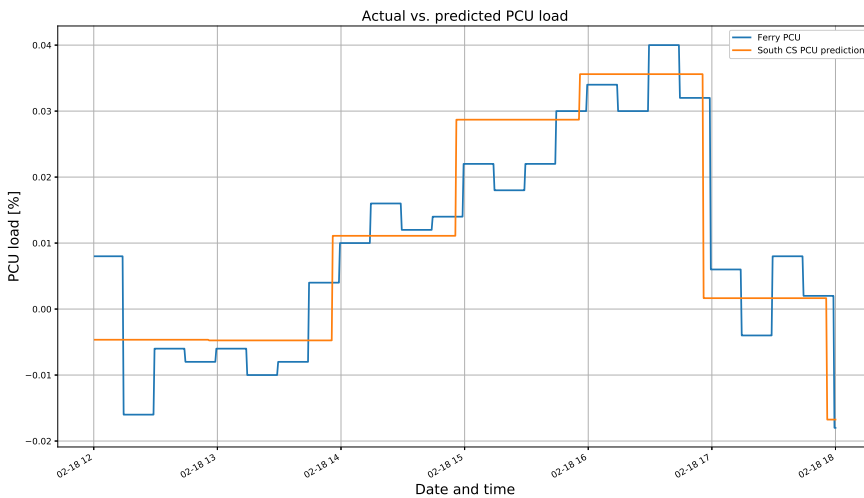


Figure 13.1: PCU prediction by the south charging station controller

Since the controller calculates the amount of passengers when the ferry connects to the charging station, and the actual value is applied when the ferry disconnects, the predicted value always lies before the actual, as shown in the figure. The ferry charging time is, however, compensated for, such that if the ferry connects at 12:56 and leaves at 13:00, the value for the new hour is used.

The prediction works fairly well, and follows the main characteristic for the actual amount of passengers. But since the actual value is impossible to accurately predict, there will be some discrepancies.

### 13.3.2 Wind and ocean current planning

Weather- and ocean conditions impacts the ferry energy consumption by making the operator use more or less propulsion power to keep the ferry stable, on route and with the required transit speed. The charging station controllers are predicting the wind- and ocean current effect on the ferry during transit. This is done by using information about the weather- and ocean conditions from the Norwegian Meteorological Institute, and by using the modelling approach presented in Section 10.2.

The controller is gathering the data by running two APIs: Oceanforecast[70] and Locationforecast[69]. The weather- and ocean data used for the simulations in Part IV are given in Appendices D and E, respectively.

The prediction of wind effect on the ferry by the south- and north charging station controller is presented in Figure 13.2. The figure shows the prediction of wind in the period between 12 and 18 the working day, where the wind first appears calm, before increasing in speed. The wind has an northern direction during the period, as seen by the sign of the effect for the two controllers. When the ferry is at the south harbour, the controller calculates positive positive contribution for the wind effect as the ferry experiences a headwind on the next crossing. At the north station, the controller calculates a tailwind.

Since the controller only uses the predicted weather information and because the actual wind conditions are hard to pre-determine, there will be discrepancies. As seen by the wind power curve in Figure 10.3, the increase in power is exponential with the increase in wind speed, and therefore, the actual values will sometimes be much higher than the predicted.

The prediction of ocean current power by the south- and north charging station controller is shown in Figure 13.3. The principle here is exactly the same as when predicting the wind power effect, but the influence from the ocean current on the ferry is much lower.

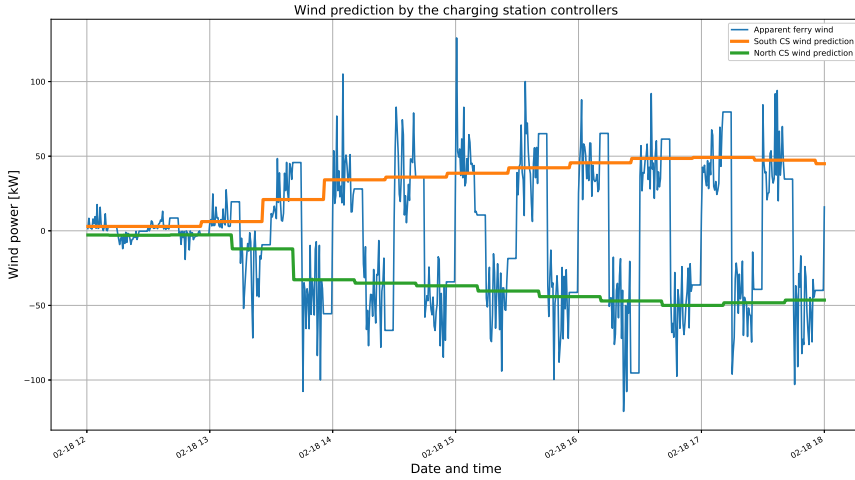


Figure 13.2: Wind prediction by the charging station controllers

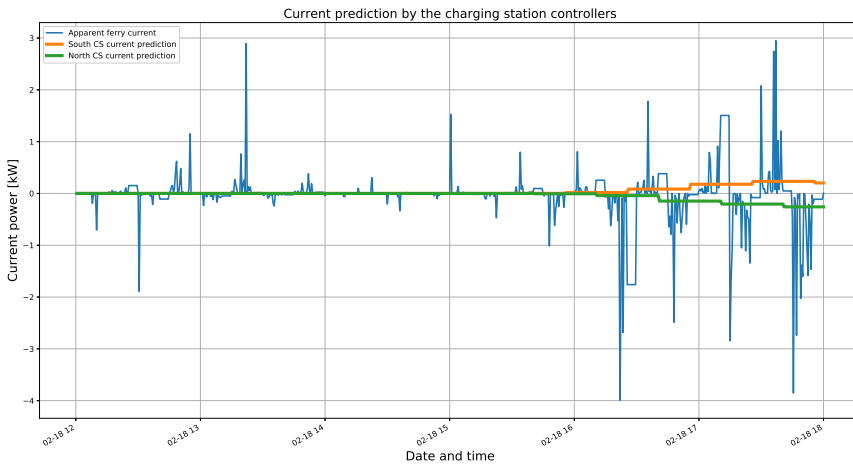


Figure 13.3: Ocean current prediction by the charging station controllers

A fair discussion is how vital accurately prediction of the ocean current conditions is, based on its effect on the ferry. The simulated operational area is very little influenced by large ocean currents, and maybe this prediction is more important when planning the charge on vessels that operates on more open waters. On the other hand, the prediction of wind- and current effects works fairly well and is important when trying to find the overall energy consumption

Planning by external factors is taken into account in the scenario presented in Chapter 14.

### 13.4 Planning by cost of electricity

By including the electricity price variation for the entire day, and not just the price variation within one charging period, better scheduling of energy accordingly to the price can be achieved. When planning by cost of electricity, simple logic is implemented to the charging controllers to schedule the transferred energy with regards to the price dynamic that present day.

The objective of the new logic is to reduce the energy transferred to the battery during times with high electricity price and increase the amount of energy in times with low electricity price. The logic uses the daily average price under operational hours and the current price to calculate a factor which is either used to increase or decrease the amount of energy transferred.

The prices during the hours when the ferry is in nightlay are not included in the logic. This is because the ferry is always recharged back to a nominal SoC during the nightlay, and therefore, the energy planning by cost of electricity is not useful in this situation. The electricity prices under operational hours for the working day and the weekend are shown in Tables 13.1 and 13.2, respectively, with its corresponding average values.

Table 13.1: Electricity prices during working day operational hours

Op. hours	5	6	7	8	9	10	11	12	13	14	15	16	17	18	19	20	21	22	23	Mean
Prices [NOK/kWh]	0.406	0.426	0.463	0.474	0.446	0.433	0.423	0.419	0.414	0.406	0.404	0.407	0.414	0.426	0.437	0.434	0.425	0.414	0.399	0.425

Table 13.2: Electricity prices during weekend operational hours

Op. hours	0	1	6	7	8	9	10	11	12	13	14	15	16	17	18	19	20	21	22	23	Mean
Prices [NOK/kWh]	0.383	0.365	0.373	0.382	0.390	0.399	0.396	0.393	0.385	0.382	0.378	0.379	0.378	0.386	0.405	0.414	0.416	0.409	0.399	0.383	0.390

The electricity planning factor is calculated as

$$E_{el}(t) = -\frac{\xi_{el}(t) - \xi_{avg}}{\xi_{avg}} \cdot \alpha_{el}, \quad (13.1)$$

where  $\xi_{el}(t)$  is the electricity market price at given time of the current day, and  $\xi_{avg}$  is the mean price of the current day.  $\alpha_{el}$  is the scale factor determining the impact of the planning factor and is here set to 0.857 for the working day and 1.475 for the weekend. The outcome of this is that 10 % less energy will be transferred to the battery at the time with the highest price, and 5 % more energy will be transferred when the price is at its lowest for the working day. For the weekend, 10 % less energy will be transferred when the price is highest and 9.5 % more energy when the price is lowest.

The difference in scheduled energy at the time with the highest and lowest price over the working day is caused by the price distribution throughout the operational hours. As seen by the electricity price data in Figure 4.2, there are more hours with a relatively low price than there are hours with a high price, making the difference between the highest price and the average to be 0.049 NOK/kWh, and the difference between the lowest price and the average to be 0.026 NOK/kWh.

Planning by cost of electricity is taken into account in the scenario presented in Chapter 15.



## **Part IV**

# **Simulation**



# Chapter 14

## Scenario I: Energy Planning

### 14.1 Scenario description

In this scenario, the hybrid ferry system is simulated over one working day and one weekend day. The simulation starts at the time the ferry leaves the nightlay station Friday morning and ends when the route schedule for Sunday morning starts. Over this period, the ferry has had 124 crossings between north and south harbour and 4 crossings between south harbour and nightlay station. The simulation includes two nightlay charging scenarios, where the ferry battery is recharged back up to 60 % SoC.

The key goal in this simulation is to reduce the associated charging costs by using energy planning and optimal charging of batteries. Energy planning includes the prediction of future energy consumption and the compensation of power loss in the components to calculate a new target SoC for the battery. The objective for the optimal charging is to minimize the cost of electricity, battery power loss, battery aging and the grid penalty cost, and the optimization is applied to every charging process.

The hybrid ferry system should in addition be operated inside system constraints, and always be able to follow the route schedule with sufficient capacity in the batteries. The operation is all-electric, meaning that the diesel generators are not active and used as an energy source. When optimizing, the cost functions have natural weighting. All system specifications are set accordingly to the modelled hybrid ferry system presented in Part II, if not stated else.

### 14.1.1 Operational profile

The operational profiles for the working day and the weekend are given in Figures 14.1 and 14.2, respectively. The operation is continuous between the two days, but they are plotted independently for clarity.

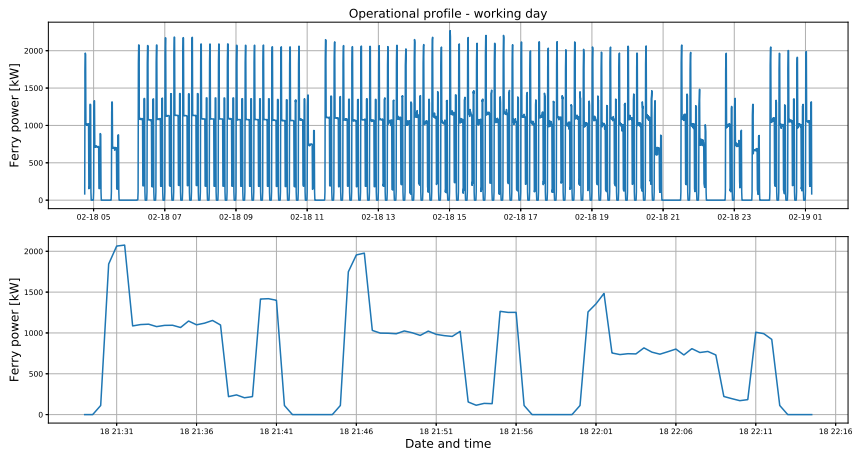


Figure 14.1: Working day operational profile

The working day operational profile has the busiest route schedule, with the most crossings. This means that the ferry charging time is normally shorter and the system experiences more events with high utilization of the batteries. The working day operational profile is described in more detail in Section 6.1.1. As the frequency of the crossings are relatively high and profile data can be hard to read, the figures include in addition a zoomed extract over some of the crossings to easier see the ferry dynamic under transit.

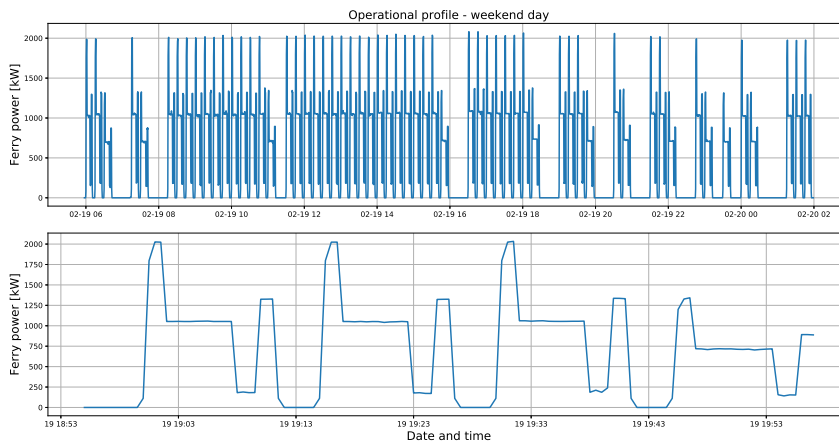


Figure 14.2: Weekend day operational profile

The ferry has several more pauses during the weekend operation, as seen by the profile in Figure 14.2. This means that the ferry can take longer time for charging, and thus, achieve less stress on the battery and reduce the power losses. The charging station battery will in this scenario be less utilized, since the grid supply can, in the longer pauses, deliver the power necessary to charge the ferry alone. The weekend day operational profile is described in more detail in Section 6.1.2.

### 14.1.2 External factors

The amount of passengers, wind conditions and ocean current conditions change randomly, but within bounds of the predicted and statistical values, over the simulation period. The impact on the ferry of these external factors throughout the working day and weekend are given in Figures 14.3 and 14.4, respectively.

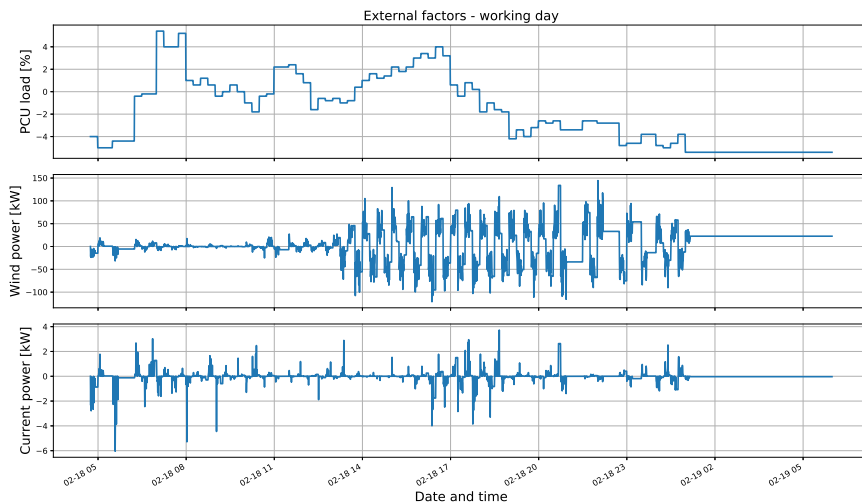


Figure 14.3: External factors during working day

As discussed in Section 10.1, the amount of passengers is quantified in PCUs, where the PCU load gives the effect on the ferry. When the PCU load is 0, the number of PCUs onboard the ferry is 25 and the energy consumption is at nominal value. A positive value for the PCU load indicates more energy consumption due to more passengers than the nominal value, and a negative value indicates less energy consumption due to a lower passenger amount. The curve for the PCU load is similar to the electricity price curve for the working day, but the tops are shifted some after.

The wind power acting on the ferry changes significantly over the working day. From being relatively calm conditions in the morning, the wind takes up in speed throughout the afternoon and evening. The wind has mostly a northern direction,

and when the ferry crosses from the north harbour to the south, the wind power is negative, since the ferry experiences a tailwind from the north. This changes on the way back to the north station, as the ferry experiences a headwind.

The ocean current power is more random and changes rapidly over the working day. There is an increase of current speed concentrated between 17 and 19, but overall the influence of ocean current is little compared to the total power of the ferry system. The current has a northern direction as average over the working day.

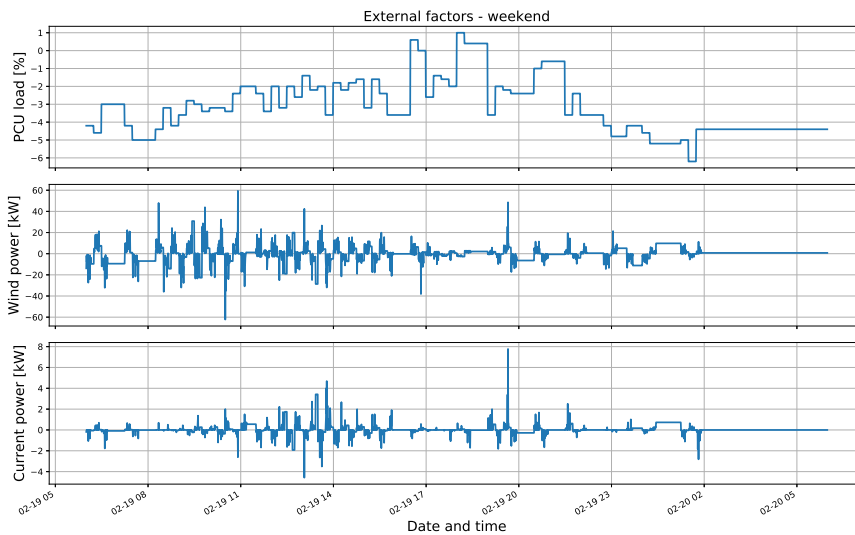


Figure 14.4: External factors during weekend day

The PCU load is notable lower over the weekend. This means that the ferry uses overall less energy, with an exception at 17, where the PCU load is at nominal value.

The apparent wind power on the ferry is largest in the morning and afternoon over the weekend, with a northern direction. This changes throughout the evening, when the wind turns to a western direction, which does not impact the ferry as much in surge motion.

The current changes towards a south direction around 13 and turns back to a northern direction around 19. However, the current speed is marginal and does not have significant impact on the ferry energy consumption.

When the ferry is in nightlay and at the charging stations, the external factors does not impact the energy consumption. As the external factor values are not updated until the ferry disconnects from the charging station, the values are held constant during the docked periods, as seen in the figures. Only a reduced hotel load of 80.3 kW is needed to be delivered extra to the ferry under nightlay charging.

The external factor values applied to the ferry are the same for all the performed simulations, which is done to easier compare the different charging methods. This is ensured by a pre-defined seeding sequence, such that the random function calculates the same random value at each time step for all simulations.

## 14.2 Scenario simulation

### 14.2.1 Standard method charging

For comparison, the results over the same simulation period using the standard method of charging are presented. The standard method replaces the same amount of energy consumed during the last trip and applies a constant current to the battery to reach the determined capacity level.

The SoC dynamics in the ferry battery and both the charging station batteries are shown in Figure 14.5. As seen, the ferry battery is recharged back to 60 % SoC before every crossing, which is achieved by the combined power from the grid and the shore battery. When the ferry is in transit, the controller calculates the charging time for the shore battery, and then sets the lowest constant current to reach 60 % SoC by the time the ferry again connects to the station. This is done to get the lowest stress on the battery and to limit the power loss.

When there is a longer period of no activity at the charging station batteries, the controller has calculated that the grid power is sufficient for delivering the energy needed for the ferry. Hence, the shore batteries are not used excessively.

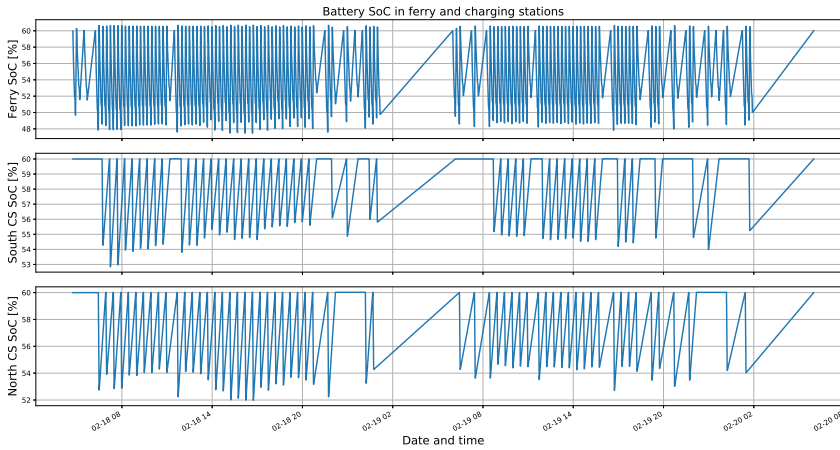


Figure 14.5: Battery SoC dynamic in ferry and charging stations

The standard method does not predict future PCU load, wind conditions and ocean current conditions when calculating the charging profile. Electricity price, grid penalty cost and battery degradation factors are also not accounted for. The results from the simulation are given in Table 14.1.

Table 14.1: Results and costs associated with standard method charging

Charging method	Controlled Ah	Cost of electricity [NOK]	Cost of power loss [NOK]	Cost of battery aging [NOK]	Grid penalty cost [NOK]	Total charging cost [NOK]
Standard method	42707.65	15799.41	788.25	5934.93	853.30	23375.89

The value for the controlled Ah-throughput illustrates how much the three batteries in the system are utilized. The value is accumulated for every Ah in or out of the batteries with an exception for the ferry battery when discharging. The battery power in the ferry during transit is not a controlled variable in this system, and hence, the amount of Ah out of the ferry battery is not accounted for.

The cost of electricity is the total sum of drawing electricity from the three grid supplies in the system. All the power flowing from the grid supplies into the system

are included, but not the energy already stored in the batteries. The cost of electricity combines the varying electricity market price and the network tariff cost, as described in Section 9.3.

The costs of battery power loss and aging are related to the controllable Ah-throughput. This means that power loss and aging in the ferry battery during transit are not accounted for. However, when discussing battery state of health later in this section, the ferry battery degradation under transit is included.

The grid penalty cost is the cost of utilizing the grid when there is an undersupply of power in the electricity system. The hybrid ferry system is only affected by this in two periods over the working day, between 06 - 11 and 18 - 21. Note that the grid penalty cost is a separate cost and not included in the cost of electricity.

Combining the four factors outlined above, the total charging cost over the simulation period is given. The standard method, with the results, are further used as a reference for analyzing the performance of the next charging method.

## 14.2.2 Optimal charge planning method

Instead of replacing the already consumed energy, as in the case for standard charging, the optimal charge planning method targets to replace the forthcoming consumed energy. The method relies on satisfactory prediction of future external factors as discussed in Chapter 13, and assumes that the charging system can dynamically change the rate of current to follow the optimal charging profile formulated in Chapter 11.

### 14.2.2.1 Ferry data

The battery power- and SoC profiles for the working day and the weekend are given in Figures 14.6 and 14.7, respectively. As seen, the battery SoC level is slowly decreasing throughout both the working day and the weekend. The SoC is reduced down to 20.0% over the working day, for then to be recharged back to 60% during the nightlay charging. Over the weekend, the SoC is reduced down to 22.9%, before being recharged up to 60%. The average decrease in capacity between 06:15 - 00:44 the first day is 7.6 Ah (0.42%) per crossing, and between 08:15 - 01:30 the second day, the average

decrease in capacity is 8.2 Ah (0.46%) per crossing.

One reason for the negative slope is that the optimal charging profile is calculating the lowest possible power output from the battery to minimize the costs of power loss and aging in the shore battery. As there are higher losses associated with the transfer of energy from the shore battery to the ferry compared with the grid, an already low calculated power from the shore battery will result in less energy being transferred to the ferry system. The compensation for power losses in the system is also not 100% accurate, as discussed in Section 13.1.

Another reason for the negative slope is that the predicted energy consumption deviates from the actual. This amplifies the decrease when the predicted energy is lower than the actual consumed energy. The error between the predicted and actual wind load gives the most contribution, and slightly changes the slope between 14 - 21 the working day, when the wind is most active.

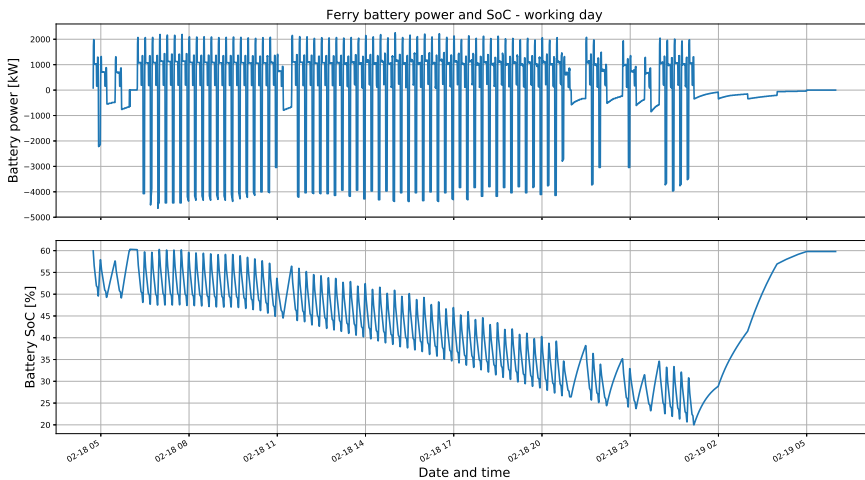


Figure 14.6: Ferry characteristics during working day

The same effects as seen during the working day also holds for the weekend. The nightlay charging is used to recharge the ferry battery up to 60 % SoC, and as seen in the figures, the shape of the SoC is similar for the two nightlay charging situations. This

is because the electricity price has the same variation for the two charging situations and the optimal charging is minimizing the cost of electricity. From the data, given in Figure 9.4, the weekend electricity price is lowest between 03 - 04, and thus, the charging profile is calculating to deliver the most energy between this period. As the electricity price is highest between 05 - 06, the profile plans to be finished with the charging before this time.

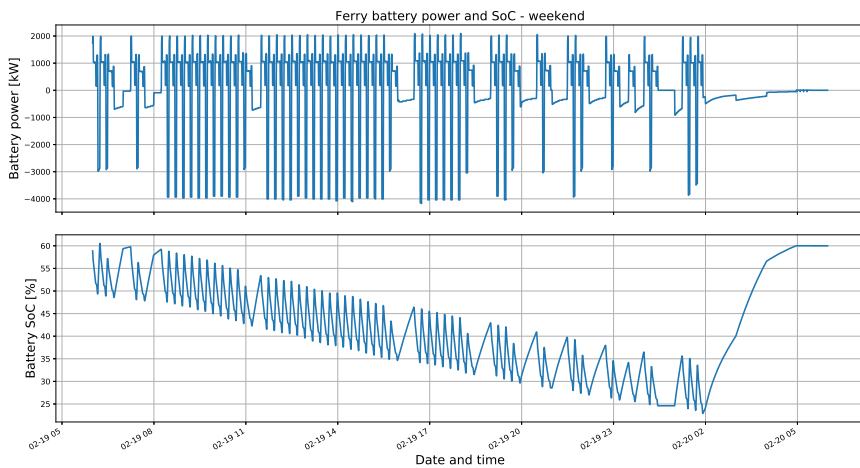


Figure 14.7: Ferry characteristics during weekend day

#### 14.2.2.2 Charging station data

The battery usage in the charging stations are highly influenced by the energy planning and charging method used. The dynamics for the battery power and SoC in the south- and north charging station over the simulation period are given in Figures 14.8 and 14.9, respectively.

When charging the ferry, an optimal power split between the grid power and shore battery power is calculated. This usually consist in setting the grid power to maximum to minimize the charging station's battery power loss, aging and recharging costs. A factor trying to counteract the use of grid power is the grid penalty cost, which is

active for two periods during the working day, between 06 - 11 and 18 - 21.

As seen in the profiles for the battery power and SoC, the characteristic changes significantly between 06 - 11 the working day. The controller here calculates the savings for lowering the grid power as higher than the cost of utilizing the shore battery. Hence, more power is transferred from the shore battery to the ferry, which gives the decrease in SoC as seen for the two shore batteries.

Between 18 - 21 the controller calculates the combined costs of electricity, power loss and aging due to recharging the shore battery as higher than the savings of lowering the grid power under ferry charging. The grid power is therefore set to maximum during this period by the controller.

Over the period where the ferry experiences higher wind power, the battery utilization at the two charging stations changes accordingly. The south station controller predicts a higher energy consumption for the next crossing and hence, sets the battery power higher. At the north charging station, the controller calculates less energy consumption and then sets the battery power lower.

Except from the period between 06 - 11, the two shore batteries are overall less utilized when using optimal charge planning compared to the standard method. When the controller predicts a low energy consumption for the ferry, the grid capacity is usually sufficient to charge the battery to the target SoC. This is seen in Figure 14.8, at the south charging station before the crossing at 22:00 and 23:00 both days, where the next transit time is 12 minutes and the ferry only receives power from the grid.

Since the time margin for recharging the charging station battery is longer than for ferry charging, the optimal charging profile also accounts for variation in electricity price during the recharging. This is seen in the figures by the power steps for the negative charging power in the shore batteries. A good example of this is the recharging of the battery at the south charging station between 08:45 - 09:11, where the controller calculates the savings of delaying the recharging to 09, when the price is lower, as higher than the grid penalty cost of charging at 1036 kW from 09:00 to 09:11. This is the only event where the recharging power of the shore battery exceeds the penalty power level of 1000 kW and it has marginal effect on the total grid penalty cost.

The battery state of health dynamic and the accumulated cost of electricity for

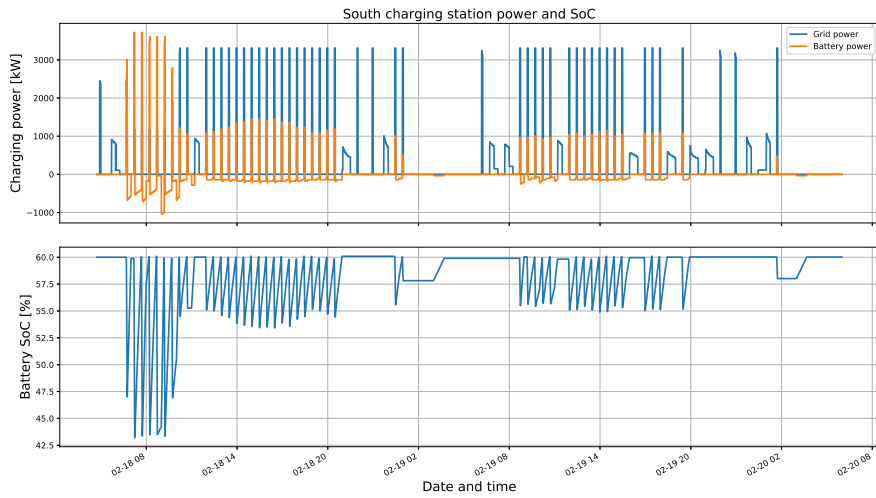


Figure 14.8: South charging station characteristics

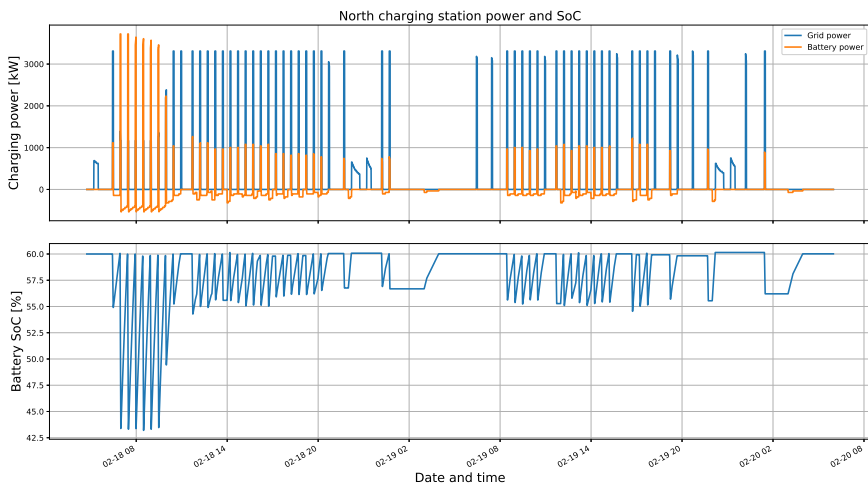


Figure 14.9: North charging station characteristics

each charging station are presented in Figure 14.10. The figure gives a good indication of the battery utilization at each charging station. Over the period between 14 - 20 on the working day, the battery usage at the south station is clearly higher compared to the north station, as the battery SoH decreases and the accumulated electricity price increases. The main reason for this is that the south station controller predicts a higher energy consumption for the next crossing as the ferry experiences tailwind. The south charging station has in addition four more charging events than the north, because of the crossings due to nightlay charging.

Throughout the weekend, the deviation between the two stations increases, as there are several more pauses with longer charging time at the south charging station. Hence, the electricity cost of providing hotel power becomes bigger. At the end of the simulation period, the respective decrease in SoH at the south station battery and the north station battery are 0.014% and 0.013%.

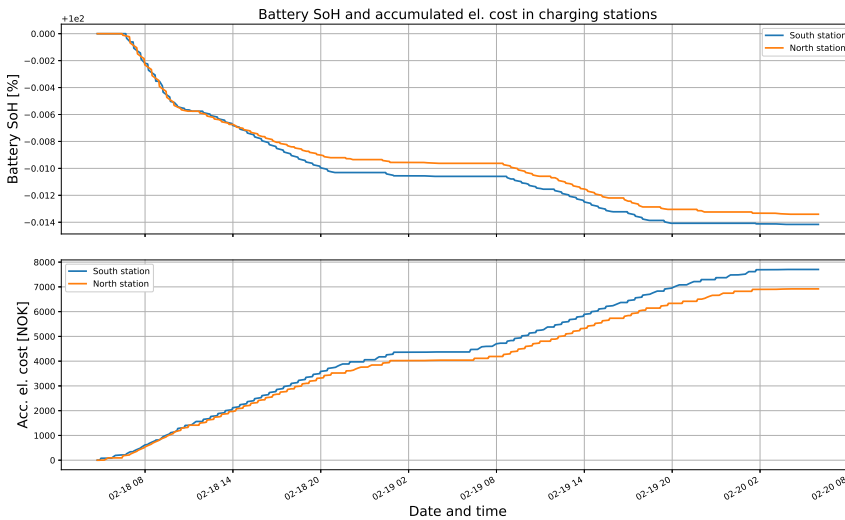


Figure 14.10: Charging station dynamics of battery SoH and accumulated el. cost

### 14.3 Scenario results and discussion

The results and costs associated with the system using the optimal charge planning method over the simulation period are given in Table 14.2, with a comparison to the standard method results in Table 14.1. The most significant saving factors are related to the battery aging- and grid penalty cost. The savings in battery aging cost can be assigned to two factors: the energy planning, which ensures less battery utilization by predicting the future energy consumption, and the decrease in SoC, which causes an overall reduction in C-rate for the ferry battery. The savings in grid penalty cost are caused by the optimization of ferry- and shore battery charging.

Table 14.2: Results and costs associated with optimal charge planning

Charging method	Controlled Ah	Cost of electricity [NOK]	Cost of power loss [NOK]	Cost of battery aging [NOK]	Grid penalty cost [NOK]	Total charging cost [NOK]
Optimal method	41971.33	15705.17	759.35	5534.77	281.45	22280.75
Change (standard)	736.32	-94.24	-28.90	-400.15	-571.85	-1095.14
% change (standard)	-1.7	-0.60	-3.7	-6.7	-67	-4.7

To further look at the numbers behind the results, the systems costs are divided into working day and weekend and presented in Table 14.3. The biggest factor contributing to the overall savings the working day is the reduction in grid penalty cost. Since higher battery utilization is caused by the benefit of lowering the grid penalty cost, the cost of electricity, battery power loss and aging are higher during the working day.

The related savings are completely different for the weekend day. There is a big benefit of predicting the future energy consumption for the associated costs of power loss and aging. Since there are longer pauses for the ferry over the weekend, the controller can also achieve more from the electricity cost optimization. Hence, all the other system costs are reduced over the weekend using the optimal method.

Table 14.3: Comparison of system costs

Charging method	Day	Cost of electricity [NOK]	Cost of power loss [NOK]	Cost of battery aging [NOK]	Grid penalty cost [NOK]	Total cost [NOK]
Standard	Working day	8918.00	469.18	3389.35	853.30	13629.82
	Weekend	6881.41	319.07	2545.58	0	9746.07
<b>Optimal</b>	Working day	8928.14	496.47	3452.24	281.45	13158.30
	Weekend	6777.03	262.88	2082.53	0	9122.45
% change	Working day	0.11	5.8	1.9	-67	-3.5
	Weekend	-1.5	-17.6	-18.2	0	-6.4

The degradation in each battery are given in Table 14.4 and compared against the standard method. For the north charging station battery and the ferry battery, the degradation is reduced by using the optimal method. Due to higher predicted energy consumption in the south charging station controller, the battery degradation is here higher compared to the standard method. However, since the ferry battery is the largest and with the highest contribution on overall cost, large savings are made by the reduction in utilization for the ferry battery, as seen in the tables above.

Table 14.4: Comparison of battery degradation in Scenario I

Method	South CS [%]	North CS [%]	Ferry [%]
Standard	0.012	0.016	0.071
Optimal	0.014	0.013	0.066

Since there are more working days throughout a year than there are weekend days, an estimate for the annual savings for the system costs are presented in Table 14.5. The estimate is based on a year with 251 working days, 104 weekend days and 10 public holidays. The public holiday operation are further merged with the weekend day operation. As should be noted, there can be large variations in electricity prices and weather conditions throughout a year, and these factors are not included in the estimates for the annual savings.

Table 14.5: Annual savings

Day	Cost of electricity [NOK]	Cost of power loss [NOK]	Cost of battery aging [NOK]	Grid penalty cost [NOK]	Total charging cost [NOK]
Working days	2,544.78	6,851.43	15,785.39	-143,534.35	-118,352.75
Weekend days	-11,899.32	-6,405.66	-52,787.69	0	-71,092.68
Total	-9,354.54	445.77	-37,002.31	-143,534.35	-189,445.43

The savings in grid penalty cost has the biggest influence on annual basis, and covers approximately 76 % of the overall system savings. The second most important factor is the reduction in battery aging cost, where the savings during the weekend days are covering the loss over the working days. The same is also seen in the cost of electricity. This does not hold for the cost of battery power loss, which is increased on an annual basis by using the optimal method.

The cost of electricity has a direct impact on the cash flow for the ferry operator, and is easy measured when accounting independent of the type of operation. The cost of power loss should be as low as possible, since the cost is not on basis of something useful. In addition, the amount of energy that is dissipated is needed to be repurchased by the ferry operator to be utilized.

The battery aging cost is a cost that represents the loss of value in the battery system, and it is profitable for both the ferry operator and battery system integrator to reduce this cost. The ferry operator can reduce the cost by decreasing the stress on the battery during operation, and the system integrator can implement smarter charging methods for increasing the battery lifetime and thus, making the battery system more attractive for the ferry operator.

As the grid penalty cost is not present in today's electricity system, it is difficult to make a statement on the actual savings related to this cost. However, the simulation shows that for the grid distributor to obtain a reduction in grid power outtake, the cost level needs to be high. This is based on the second period of undersupply in the grid, where the controller calculates the cost of utilizing the shore battery as higher than the savings for reducing the grid power.

Hence, the grid penalty cost should be in the same magnitude as the cost associated with recharging the shore battery to have any influence. Another approach the grid distributor can take to reduce the grid load during times with undersupply is to reward the end user for drawing less power. This reward should also be in the same magnitude as the cost associated with the shore recharging to have any effect. The optimization framework presented here can further be used to analyze the sensitivity of the grid penalty cost up against a financially sustainable ferry operation.



## Chapter 15

# Scenario II: Energy Planning by Cost of Electricity

### 15.1 Scenario description

In this scenario, simple logic to schedule the transfer of energy with regards to electricity price are implemented to the charging controllers. The logic is based on the electricity planning factor, further described in Section 13.4, and is taken into use when calculating the charging of the ferry- and shore batteries. The scenario is included to show how top level planning of energy can improve savings in the system costs.

The grid penalty cost is not included in this scenario. Hence,  $J_{load} := 0$  in all the optimal control cost functions. This is done to see how the optimal charge planning method works on the current situation for the hybrid ferry system, where no such penalty cost is included.

As the electricity planning factor is used when charging the shore batteries, this adds an extra element to the charging compared to Scenario I, where the goal was only to recharge the shore batteries back to the nominal SoC of 60 %. Here, the shore batteries operates on a SoC of 54% when the ferry is in operation, such that during times with low electricity price, the shore batteries can be charged up to 60%. The simulation

is else similar to Scenario I, with the same external factors impacting the ferry with equal magnitude, and with prediction of future factors and optimal charging turned on in the controllers. When optimizing, the cost functions have natural weighting for the cost terms. All system specifications are set accordingly to the modelled hybrid ferry system presented in Part II, if not stated else.

## 15.2 Scenario simulation

### 15.2.1 Standard- and optimal method charging from Scenario I

The results using the standard method are included for analyzing the performance of the new optimal method. In addition, the optimal method used in Scenario I (SI), without the influence of grid penalty cost, is included for comparison. Thus, the difference between the optimal method presented in this scenario and the optimal method used in SI is the contribution from the electricity planning factor. The system costs associated with the two charging methods in SI are presented in Table 15.1.

For the standard method, the system costs are similar compared to SI, but with a decrease in total cost because of no grid penalty cost. The hybrid ferry operation is simulated again with the optimal method from SI, but without the influence of a grid penalty cost. Hence, the associated system costs are changed compared to the optimal method in SI.

Table 15.1: Results and costs associated with the standard- and optimal charging method from SI

Charging method	Controlled Ah	Cost of electricity [NOK]	Cost of power loss [NOK]	Cost of battery aging [NOK]	Total charging cost [NOK]
Standard method	42707.65	15799.41	788.25	5934.93	22522.59
Optimal method (SI)	39534.16	15632.23	705.08	5280.50	21617.81

The battery SoC dynamic for the ferry- and charging station batteries using the optimal method from SI are given in Figure 15.1. As seen, the shore batteries are no longer deep cycled between 7 - 11 the working day, since the grid penalty cost is not present. For the rest of the working day and the weekend, the profiles follows the same characteristics as presented in SI.

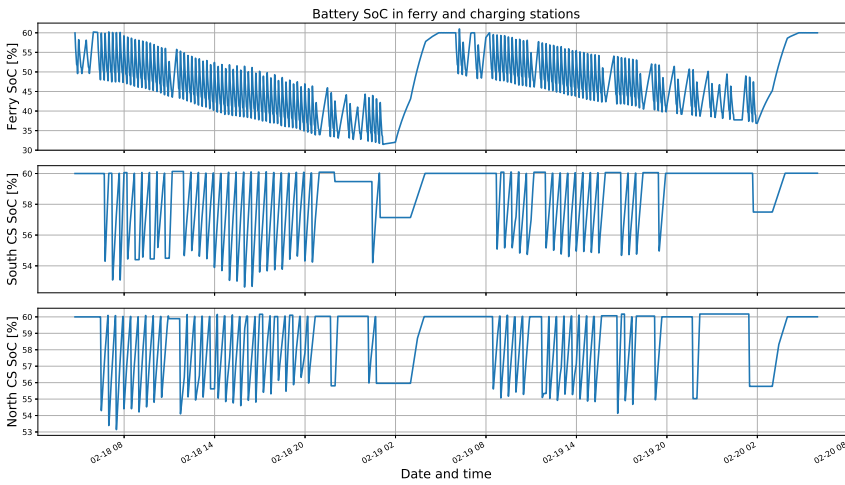


Figure 15.1: Battery SoC dynamic in ferry and charging stations using optimal method from SI

### 15.2.2 Ferry data

The dynamics for the ferry battery power and SoC are given for the working day and weekend in Figures 15.2 and 15.3. Since the factors impacting the ferry are the same as in SI, the dynamic follows the same characteristics.

The battery SoC level reduction during the working day morning is, however, more steep. This is because of the high electricity price, making the controller output less energy to the ferry. As the electricity price decreases during the afternoon, the controller calculates a higher amount of energy transferred to the ferry, which lifts the battery SoC level. The SoC level changes accordingly to the electricity price dynamic throughout the evening and night, where it first decreases for then to increase again. At the end of the day, the battery SoC is reduced to 26.4% before being recharged back to 60%.

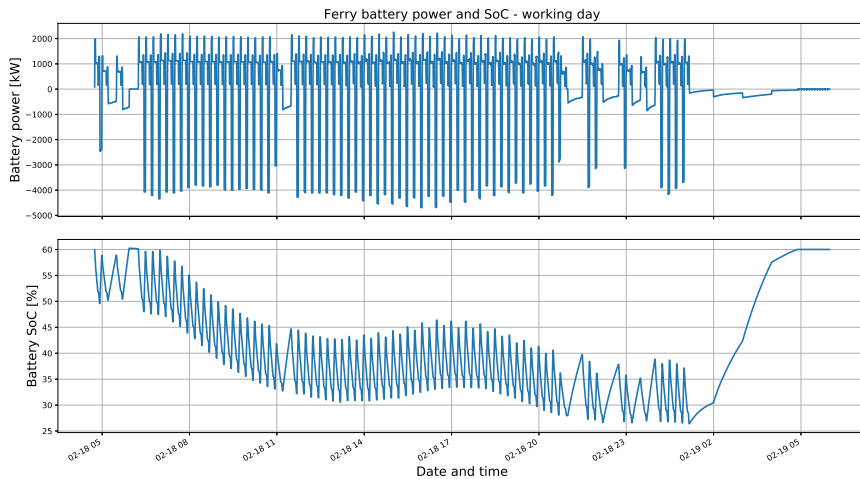


Figure 15.2: Ferry dynamics during working day in scenario II

The same characteristic is present during the weekend, where the battery SoC follows the electricity price dynamic. Since there are less crossings and because they are more evenly distributed between times with high and low electricity price, the battery SoC level is only reduced to 34.5% at the end of the day. For fair comparison with the standard- and optimal method in SI, the battery is again recharged up to 60%.

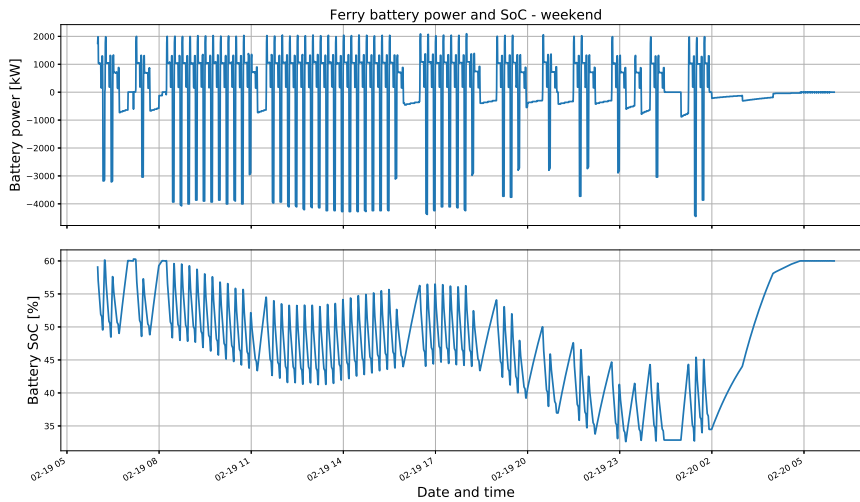


Figure 15.3: Ferry characteristics during weekend day in scenario II

### 15.2.3 Charging station data

With the electricity planning factor being implemented in the recharging of the shore batteries, and because the grid penalty cost is not included, the battery dynamic at the charging stations changes significantly compared to SI. The shore batteries are here set to operate around a SoC of 54% when the ferry is not in nightlay. The controller then sets a SoC lower than 54% when the price is high and a SoC higher when the price is low. The grid- and battery power profiles, together with the SoC, for the south- and north charging station are given in Figures 15.4 and 15.5, respectively.

The two periods, between 7 - 9 and 18 - 20, where the electricity price is highest

during the working day are found by the drops in SoC level for the shore batteries. As the price gets lower, the SoC level increases, and before the first nightlay charging, the SoC level in the south station battery has retained a SoC of 52.6%, while the SoC in the north station battery is 51.4%.

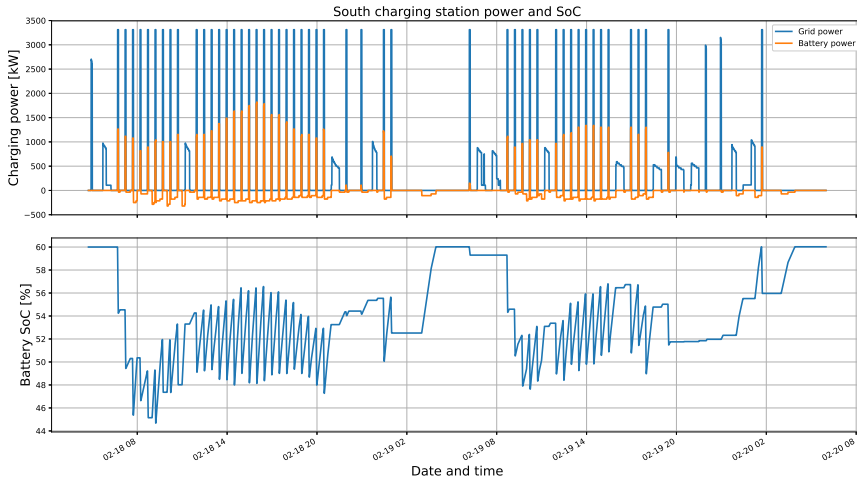


Figure 15.4: South charging station characteristics in scenario II

Following the first nightlay charge, the SoC level again decreases to avoid high charging during the weekend morning. The curve over the weekend follows the same characteristic as the curve during the working day, but the curve tops are shifted two hours later on the day, as similar to the electricity price.

The battery state of health dynamic and the accumulated cost of electricity for each charging station are presented in Figure 15.6. The curves have the same characteristics as in Scenario I, but as the batteries are less utilized, the degradation is reduced.

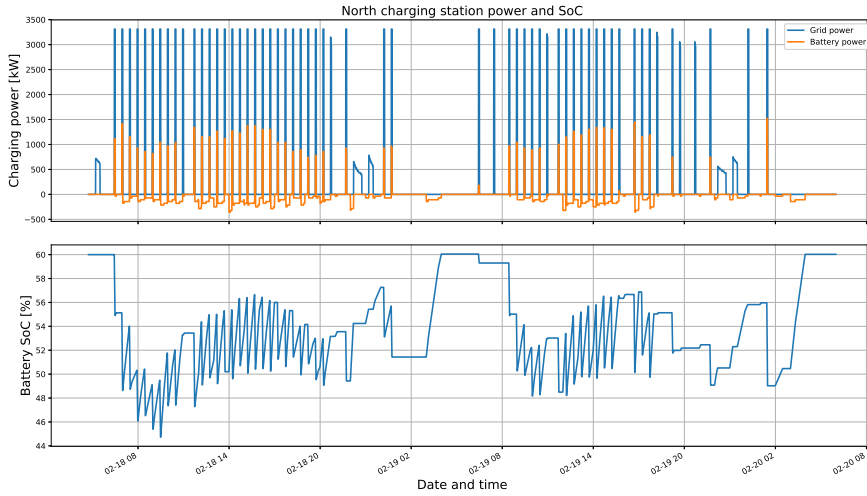


Figure 15.5: North charging station characteristics in scenario II

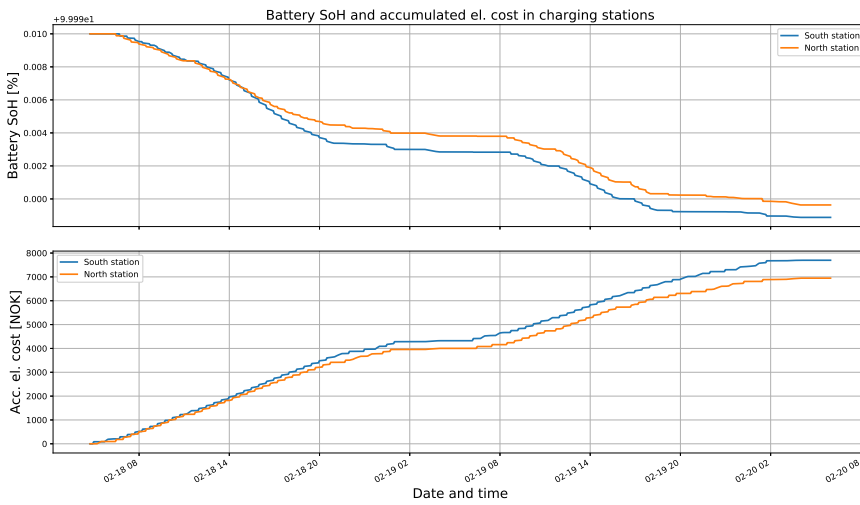


Figure 15.6: Charging station dynamics of battery SoH and accumulated el. cost in scenario II

### 15.3 Scenario results and discussion

The results from using optimal charge planning, together with an electricity planning factor, are presented in Table 15.2, with a comparison to the standard method and optimal method used in SI. All the associated system costs are reduced using energy planning by cost of electricity, where the reduction in battery aging cost is most significant. As in SI, the savings related to the battery power loss and aging can be assigned to the energy planning.

Table 15.2: Results and costs associated with optimal charge planning in scenario II

Charging method	Controlled Ah	Cost of electricity [NOK]	Cost of power loss [NOK]	Cost of battery aging [NOK]	Total charging cost [NOK]
Optimal method (SII)	39529.15	15580.76	699.94	5142.96	21423.67
Change (Standard)	-2442.18	-218.65	-88.31	-791.97	-1098.92
% change (Standard)	-7.4	-1.4	-11.2	-13.3	-4.9
Change (Optimal SI)	-5.00	-51.46	-5.14	-137.54	-194.14
% change (Optimal SI)	-0.01	-0.33	-0.73	-2.6	-0.90

Comparing the two optimal methods proposed, the savings for adding an electricity planning factor is NOK 194,- over the simulation period. Around 71% of this saving can be assigned to the reduction in battery aging cost, and around 27% to the reduction in electricity cost. The reduction in battery aging cost is an indirect effect of the route schedule, since the crossings are more frequent during the times with higher electricity price. This causes the controller to calculate a lower energy transfer in these periods, and thus, reduces the battery utilization.

The system costs are further divided into type of day and presented in Table 15.3. As seen, the electricity cost related savings are higher over the working day than the weekend, which is caused by larger variations in electricity price. Hence, implementation of an electricity planning factor is more profitable with regards to electricity cost

with higher variations in electricity price.

Due to more crossings with longer transit time, the prediction of future energy consumption gives more profit on the cost of battery power loss and aging during the weekend, when comparing with the standard method. This is caused by less energy being calculated to be transferred, which reduces the current rate and battery stress. However, as the system costs related to the working day are larger than for the weekend, the overall performance of the optimal method is equal for both days compared against the standard method.

Comparing the two optimal methods against each other, the new method using an electricity planning factor performs better both days, with a higher profitability over the working day than the weekend. Over the weekend, the battery power loss is slightly higher using the new optimal method, but the battery aging is, to a small degree, reduced. One possible explanation for this is that the battery utilization is some Ah higher with the new method, but the batteries operates on a higher SoC using the optimal method in SI, such that the battery aging is accelerated a bit more.

Table 15.3: Comparison of system costs in Scenario II

Charging method	Day	Cost of electricity [NOK]	Cost of power loss [NOK]	Cost of battery aging [NOK]	Total cost [NOK]
Standard	Working day	8918.00	469.18	3389.35	12776.52
	Weekend	6881.41	319.07	2545.58	9746.07
Optimal (SI)	Working day	8834.29	431.18	3078.44	12343.91
	Weekend	6797.94	273.89	2202.06	9273.90
<b>Optimal (SII)</b>	Working day	8791.07	423.51	2942.02	12156.60
	Weekend	6789.69	276.43	2200.94	9267.07
% change (STD)	Working day	-1.4	-9.7	-13.2	-4.9
	Weekend	-1.3	-13.4	-13.5	-4.9
% change (OPT SI)	Working day	-0.49	-1.8	-4.4	-1.5
	Weekend	-0.12	0.93	-0.05	-0.07

A more detailed look at the electricity cost at the three charging stations with a split between working day and weekend is given in Table 15.4. As seen, the north charging station benefits from predicting the forthcoming energy consumption, and especially during the weekend. The ferry has 9 departures from the north station with a crossing time of 12 minutes over the weekend route schedule. By predicting this, less power from both the grid supply and the shore battery are transferred to the ferry, which in turn reduces the cost of electricity.

As the ferry on average experiences more wind from a northern direction, the energy consumption is calculated to be less at the north charging station. As the opposite is true for the south charging station, there is also an increase in electricity cost here. The ferry has only 2 departures with a crossing time of 12 minutes during the weekend route from the south station, and thus, the ferry must be charged more from this side. However, the charging time is often longer at the south side, so the charging can be planned after the variation in electricity price.

Since the battery SoC in the ferry is reduced to a lower value before the nightlay charging using the new optimal method, more energy is needed to be delivered during nightlay, which increases the charging cost at the nightlay station. However, the overall contribution from energy planning and from the optimization of charging makes the savings at the north station so high that it covers the increase in cost at the other stations.

Table 15.4: Electricity cost comparison in Scenario II

Day	Charging station	Standard method [NOK]	Optimal method (SI) [NOK]	Optimal method (SII) [NOK]	% change (STD / OPT SI)
Working day	South	4208.42	4370.91	4323.26	2.7 / -1.1
	North	4437.84	4039.62	4002.02	-9.8 / -0.9
	Nightlay	271.74	423.75	465.79	71.4 / 9.9
Weekend	South	3236.35	3402.14	3374.33	4.3 / -0.8
	North	3302.54	2945.04	2944.80	-10.8 / -0.008
	Nightlay	241.34	349.56	369.37	53 / 5.7
Total		15799.41	15632.23	15580.76	-1.4 / -0.33

A large part of the overall savings can be assigned to the reduction in battery degradation. Table 15.5 shows the reduction in battery SoH using the new optimal method compared to the standard method and optimal method in SI. As seen, the decrease in battery aging are highest at the north charging station and the ferry battery, which is caused by the factors already discussed above.

Table 15.5: Comparison of battery degradation in Scenario II

Method	South CS [%]	North CS [%]	Ferry [%]
Standard	0.012	0.017	0.072
Optimal (SI)	0.012	0.011	0.068
Optimal (SII)	0.011	0.010	0.067

An estimate for the annual savings of system costs are given in Table 15.6. As seen, the new optimal method using energy planning by cost of electricity reduces all the system costs, independent of the type of day. The savings due to lower battery aging has the highest influence on annual basis, and covers approximately 72 % of the overall savings. The second most important factor is the reduction in electricity cost, which covers 20 % of the annual savings.

Table 15.6: Annual savings using energy planning by cost of electricity

Day	Cost of electricity [NOK]	Cost of power loss [NOK]	Cost of battery aging [NOK]	Total charging cost [NOK]
Working days	-31,859.43	-11,463.17	-112,279.83	-155,602.43
Weekend days	-10,456.08	-4,860.96	-39,288.96	-54,606.00
Total	-42,315.51	-16,324.13	-151,568.79	-210,208.43

As the battery aging cost represents a loss of value in the battery system, the savings can be used to estimate how long it takes for the optimal method to earn in the cost of the batteries in the system. With a total battery cost of NOK 24,024,000,- for the three batteries, the years it takes for the optimal method to save as much as the battery cost is 15.9 years. If a normal battery life is expected to be 10 years, the optimal method would have saved 63.0% of the total battery cost by this time.

The logic behind the electricity planning factor works fairly well since the electricity price do not vary too much between an hour to the next. If, however, the price would change from a very high price to a very low, this logic would set a high SoC and the following  $\Delta\text{SoC}$  would be high. This scenario could be less profitable with regards to battery power loss and aging.

With more aggressive planning and slightly higher variation in electricity price, the electricity planning factor could give larger savings. By, for instance, dropping the recharging of the ferry- and shore batteries during times with high electricity price could give a larger margin on the electricity cost savings. However, the aggressive planning should be measured up against the increase in costs of battery power loss and aging, and should therefore be a point for further study.

Adding a top layer logic on the electricity price variation, and looking at the whole day instead of just the next crossing when determining the charging power, seems likely to give larger savings on the electricity price.

## **Part V**

# **Conclusions & Future Work**



# Chapter 16

## Conclusions

### Summary

This thesis has presented a method for optimal charge planning in hybrid ferry systems. The method gives *an* optimal solution to the battery charging problem as the optimization is based on a set of objectives which may not include all the factors influencing the battery charging. In the first part, background theory on ferry systems and operation, battery energy storage, the electricity system and optimization methods were presented. This gave the foundation for appropriate modelling of the hybrid ferry system and the external factors impacting the ferry operation in part 2.

A proposal on optimal charge planning was given in part 3, with a separate section on the optimal control problem for ferry- and shore battery charging and on the energy planning. The objective for the optimal control problem was defined to minimize the cost of electricity, battery power loss, battery aging and grid penalty cost. The problem was then solved using a numerical- and analytical optimization method. Energy planning was then formulated as the prediction of future energy consumption by considering the power loss, route schedule and external factors. An example of energy planning by cost of electricity was also proposed.

A hybrid ferry system using optimal charge planning for battery charging was then simulated over a working day and a weekend in part 4. Two scenarios were

presented, where the first scenario was under the influence of a grid penalty cost and used ordinary energy planning for calculating the energy transfer to the ferry. In the second scenario, the system was not influenced by a grid penalty cost and used energy planning by cost of electricity to set the energy transfer to both the ferry- and shore batteries. Both scenarios were compared up against a simulation of the system using the current standard method of charging.

## Results

Based on performance and computation time for solving the optimal control problem, the analytical method was concluded to be the best alternative for further implementation in the charging station controller. Simulations showed that the proposed method for optimal charging of ferry- and shore batteries reduced the overall cost associated with charging compared to the standard constant current method. However, under no influence of a grid penalty cost and variation in electricity price, the constant current method is seen as the most optimal way to charge the battery to minimize the battery power loss and aging.

Using the proposed method for optimal charge planning in a modelled hybrid ferry system, under the influence of a grid penalty cost, is shown to give large savings related to the imposed penalty cost from the grid distributor. As the penalty cost is needed to be high for giving the tender an incentive to reduce the grid power outtake, an optimal calculation of the distribution between grid- and shore battery power is seen to be vital in reducing the system costs.

The results from using optimal charge planning together with an electricity planning factor is seen to highly reduce the associated charging costs in a modelled system under no influence of a grid penalty. The savings during a working day is approximately three times the savings during a weekend day, which is caused by larger variations in electricity price and higher potential in the prediction of future energy consumption due to more frequent operation. For a ferry experiencing almost similar external factors and variation in electricity price over year, the potential savings using the optimal charge planning method instead of the standard method is estimated to be above NOK 200,000,- in the modelled system.

## **Recommendations**

A list of recommendations based on the outcome of this thesis is given below:

- An optimization method for charging the hybrid ferry system batteries should be implemented if the system is under influence of other factors than the internal battery power loss and battery aging factors.
- A constant current charging method should be used when the system is only influenced by the internal battery power loss and battery aging factors.
- To reduce overall battery power loss and aging, prediction of future energy consumption should be implemented if accurate prediction can be achieved.
- An electricity planning factor could be used to improve the system performance when there are considerably variations in electricity price.



## Chapter 17

# Future Work

Today, there is a rapid development in the field of hybrid ferry systems. New information and communications technology (ICT) solutions are being implemented in the ferry for more efficient, optimal and secure operation. With the use of machine learning and big data algorithms, opportunities for better operation that are not yet thought of can be found.

In the scope of this thesis, there are several possibilities for more optimal operation. Some of the future work that can be based on the thesis results are further elaborated below:

### **Charge planning improvement**

For more accurate prediction of future energy consumption, logging of real operational data should be considered. By logging data for the energy consumption and matching this up against the corresponding amount of passengers, weather and ocean conditions, better estimates of the impact of the external factors can be obtained. For example, sensors to measure the wind speed and direction can easily be installed on the ferry and be used for continuous optimization of the operation by combining the obtained wind data and the ferry data to find more accurate values for the wind coefficients.

Top layer energy optimization should be a point for further work, where the amount of energy transferred to the ferry is optimized based on future values for the route schedule, electricity price variation, amount of passengers and weather conditions. The optimization should have a longer time horizon than what is formulated in this thesis, where the amount of energy is only estimated by the factors for the next crossing.

The prediction of future energy consumption could be even more useful in ferries with autonomous operation, as it could contribute to more predictable use of the propellers and reduce some uncertainty in the operation.

For implementation of the optimization in a real working charge management system, constraints on the rate of change for the state variable and control actions should be considered. This would give a more accurate representation of the transient dynamics in the battery and prevent system component damages.

### **Modelling improvement**

As the dynamic behavior of the battery and the optimization depends on the empirical battery model used, more accurate results could be achieved by fitting the modelled aging parameter values to the measured aging values for the battery type in the hybrid ferry system. The optimization could then be calculated with less deviation between the modelled dynamics and the actual battery dynamics, and give better results.

### **Other potential savings**

By having energy storage with high capacity, the hybrid ferry system is in a position to transfer some of this energy back to the grid. Helping the grid distributor in load leveling and selling electricity on the grid for income are potential benefits from this. An optimal control problem could then be formulated with the objective to calculate the optimal tradeoff between earnings of transferring energy back to the grid and the cost of battery utilization.

All the possibilities for better operation of hybrid ferry systems are not stated in this thesis. With willingness to further look at the undiscovered possibilities and to realize the potential benefits, an even more sustainable ferry operation could be within reach.

# Appendix



# Appendix A

## Application File Structure

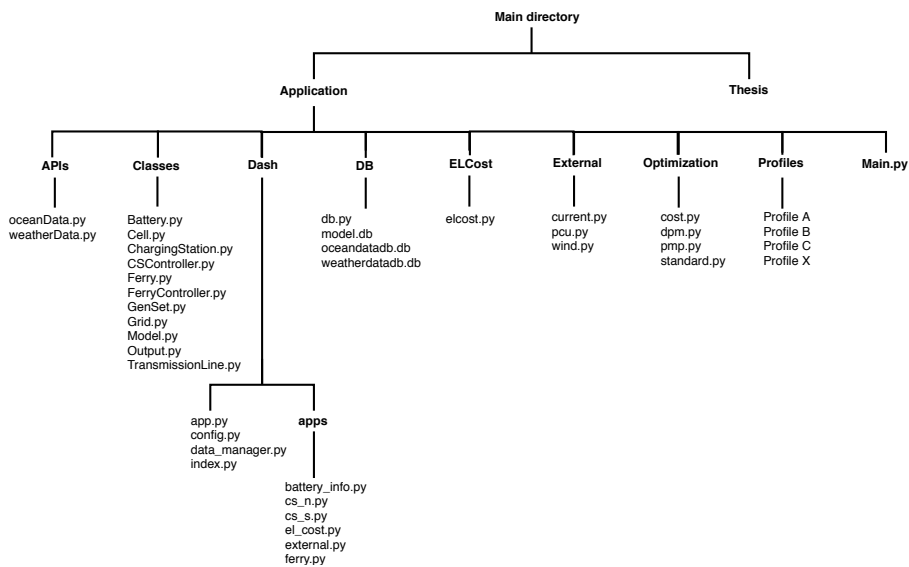


Figure A.1: Application file structure



## **Appendix B**

# **LiFePO<sub>4</sub> Cell Datasheet**

## + Nanophosphate® High Power Lithium Ion Cell ANR26650*m1-B*



A123's high-performance Nanophosphate® lithium iron phosphate ( $\text{LiFePO}_4$ ) battery technology delivers high power and energy density combined with excellent safety performance and extensive life cycling in a lighter weight, more compact package. Our cells have low capacity loss and impedance growth over time as well as high usable energy over a wide state of charge (SOC) range, allowing our systems to meet end-of-life power and energy requirements with minimal pack oversizing.



### APPLICATIONS

#### COMMERCIAL SOLUTIONS

Advanced lead acid replacement batteries for:

- + Datacenter UPS
- + Telecom backup
- + IT backup
- + Autonomously guided vehicles (AGVs)
- + Industrial robotics and material handling equipment
- + Medical devices

#### GOVERNMENT SOLUTIONS

- + Military vehicles
- + Military power grids
- + Soldier power
- + Directed energy

#### GRID SOLUTIONS

Versatile, flexible and proven storage solutions for the grid:

- + Frequency regulation
- + Renewables integration
- + Reserve capacity
- + Transmission and distribution

#### TRANSPORTATION SOLUTIONS

Hybrid, plug-in hybrid and electric vehicle battery systems for:

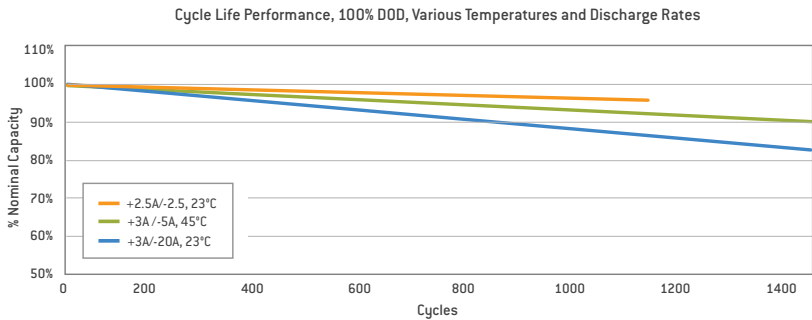
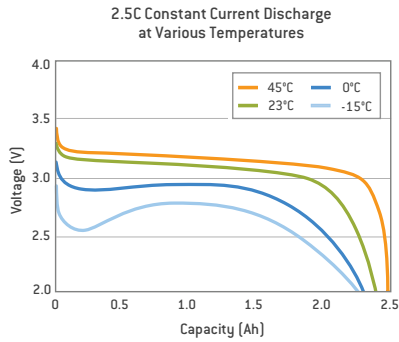
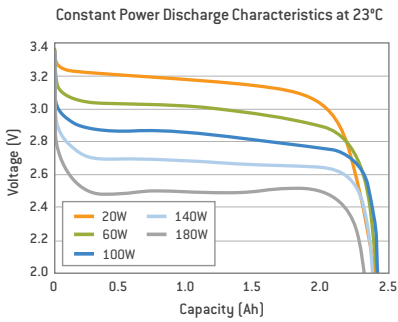
- + Commercial vehicles
- + Off-highway vehicles
- + Passenger vehicles

### ANR26650*m1-B* TECHNICAL DATA

Cell Dimensions	ø26 x 65 mm
Cell Weight	76g
Cell Capacity (nominal/minimum) [0.5C Rate]	2.5/2.4 Ah
Voltage (nominal)	3.3V
Internal Impedance (1kHz AC typical)	6mΩ
Power*	2600 W/kg
Recommended Standard Charge Method	2.5A to 3.6V CCCV, 60 min
Recommended Fast Charge Method to 80% SOC	10A to 3.6V CC, 12 min
Maximum Continuous Discharge	50A
Maximum Pulse Discharge (10 seconds)	120A
Cycle Life at 20A Discharge, 100% DOD	>1,000 cycles
Operating Temperature	-30°C to 55°C
Storage Temperature	-40°C to 60°C

\* ~2600W as measured by A123 modified HPPC Method @ 23°C, 50% SOC, 10 second discharge

**+ Nanophosphate® High Power Lithium Ion Cell**  
**ANR26650M1-B**



This document represents typical data. Performance may vary depending on use conditions and application.  
 A123 Systems makes no warranty explicit or implied with this data sheet. Contents subject to change without notice.

**CORPORATE HEADQUARTERS**

A123 Systems, Inc.  
 200 West Street  
 Waltham, MA 02451

[www.a123systems.com](http://www.a123systems.com)



©2012 A123 Systems, Inc. All rights reserved.  
 MD100113-02



## **Appendix C**

# **Ferry Route Schedule**

31 Aukra–Hollingsholmen												
	F14 Aukra				F14 Hollingsholmen				F14 Aukra			
	Måndag - fredag				Laurdag				Söndag			
00:00	00:25:00	00:25	04:35:00	00:00	00:15:00	00:15	00:15:00	09:00:00	00:15:00	00:15	01:00:00	
-	-	-	-	00:30	00:15:00	00:45	05:30:00	01:15	00:15:00	01:30	04:45:00	
05:00	00:30:00	05:30	00:45:00	-	-	-	-	-	-	-	-	
06:15	00:15:00	06:30	00:15:00	06:15	00:15:00	06:30	00:45:00	06:15	00:15:00	06:30	00:45:00	
06:45	00:15:00	07:00	00:15:00	-	-	-	-	-	-	-	-	
07:15	00:15:00	07:30	00:15:00	07:15	00:15:00	07:30	00:45:00	07:15	00:15:00	07:30	00:45:00	
07:45	00:15:00	08:00	00:15:00	-	-	-	-	-	-	-	-	
08:15	00:15:00	08:30	00:15:00	08:15	00:15:00	08:30	00:15:00	08:15	00:15:00	08:30	00:15:00	
08:45	00:15:00	09:00	00:15:00	08:45	00:15:00	09:00	00:15:00	08:45	00:15:00	09:00	00:45:00	
09:15	00:15:00	09:30	00:15:00	09:15	00:15:00	09:30	00:15:00	-	-	-	-	
09:45	00:15:00	10:00	00:15:00	09:45	00:15:00	10:00	00:15:00	09:45	00:15:00	10:00	00:15:00	
10:15	00:15:00	10:30	00:15:00	10:15	00:15:00	10:30	00:15:00	10:15	00:15:00	10:30	01:00:00	
10:45	00:15:00	11:00	00:30:00	10:45	00:15:00	11:00	00:30:00	-	-	-	-	
11:30	00:15:00	11:45	00:15:00	11:30	00:15:00	11:45	00:15:00	11:30	00:15:00	11:45	00:15:00	
12:00	00:15:00	12:15	00:15:00	12:00	00:15:00	12:15	00:15:00	12:00	00:15:00	12:15	00:15:00	
12:30	00:15:00	12:45	00:15:00	12:30	00:15:00	12:45	00:15:00	12:30	00:15:00	12:45	00:15:00	
13:00	00:15:00	13:15	00:15:00	13:00	00:15:00	13:15	00:15:00	13:00	00:15:00	13:15	00:15:00	
13:30	00:15:00	13:45	00:15:00	13:30	00:15:00	13:45	00:15:00	13:30	00:15:00	13:45	00:45:00	
14:00	00:15:00	14:15	00:15:00	14:00	00:15:00	14:15	00:15:00	-	-	-	-	
14:30	00:15:00	14:45	00:15:00	14:30	00:15:00	14:45	00:15:00	14:30	00:15:00	14:45	00:45:00	
15:00	00:15:00	15:15	00:15:00	15:00	00:15:00	15:15	00:15:00	-	-	-	-	
15:30	00:15:00	15:45	00:15:00	15:30	00:15:00	15:45	00:45:00	15:30	00:15:00	15:45	00:15:00	
16:00	00:15:00	16:15	00:15:00	-	-	-	-	16:00	00:15:00	16:15	00:15:00	
16:30	00:15:00	16:45	00:15:00	16:30	00:15:00	16:45	00:15:00	16:30	00:15:00	16:45	00:15:00	
17:00	00:15:00	17:15	00:15:00	17:00	00:15:00	17:15	00:15:00	17:00	00:15:00	17:15	00:15:00	
17:30	00:15:00	17:45	00:15:00	17:30	00:15:00	17:45	00:15:00	17:30	00:15:00	17:45	00:15:00	
18:00	00:15:00	18:15	00:15:00	18:00	00:15:00	18:15	00:45:00	18:00	00:15:00	18:15	00:15:00	
18:30	00:15:00	18:45	00:15:00	-	-	-	-	18:30	00:15:00	18:45	00:15:00	
19:00	00:15:00	19:15	00:15:00	19:00	00:15:00	19:15	00:15:00	19:00	00:15:00	19:15	00:15:00	
19:30	00:15:00	19:45	00:15:00	19:30	00:15:00	19:45	00:45:00	19:30	00:15:00	19:45	00:15:00	
20:00	00:15:00	20:15	00:15:00	-	-	-	-	20:00	00:15:00	20:15	00:15:00	
20:30	00:15:00	20:45	00:45:00	20:30	00:15:00	20:45	00:45:00	20:30	00:15:00	20:45	00:45:00	
21:30	00:15:00	21:45	00:15:00	21:30	00:15:00	21:45	00:15:00	21:30	00:15:00	21:45	00:15:00	
22:00	00:45:00	22:45	00:15:00	22:00	00:45:00	22:45	00:15:00	22:00	00:45:00	22:45	00:15:00	
23:00	00:30:00	23:30	00:30:00	23:00	00:30:00	23:30	00:30:00	23:00	00:30:00	23:30	00:30:00	

Note:

Yellow/orange marking denotes 12-minute trips. All other are 11-minute trips.

Figure C.1: Ferry route schedule used in modelling

## **Appendix D**

# **Weather Data**

<b>Wind conditions</b>					
Hollingsholmen - Aukra					
<b>Time and date</b>	<b>Wind speed [m/s]</b>	<b>Wind direction [°]</b>	<b>Time and date</b>	<b>Wind speed [m/s]</b>	<b>Wind direction [°]</b>
03.05.2019 17:00	7.20	21.00	04.05.2019 18:00	8.80	305.40
03.05.2019 18:00	6.10	6.60	04.05.2019 19:00	8.40	299.50
03.05.2019 19:00	4.80	29.20	04.05.2019 20:00	8.70	292.40
03.05.2019 20:00	3.70	22.90	04.05.2019 21:00	9.40	287.40
03.05.2019 21:00	1.90	344.00	04.05.2019 22:00	9.60	283.80
03.05.2019 22:00	1.50	45.40	04.05.2019 23:00	9.40	280.50
03.05.2019 23:00	6.70	347.40	05.05.2019 00:00	10.60	267.10
04.05.2019 00:00	5.00	335.10	05.05.2019 01:00	10.60	272.90
04.05.2019 01:00	5.90	302.60	05.05.2019 02:00	7.20	292.40
04.05.2019 02:00	11.20	345.10	05.05.2019 03:00	7.00	289.50
04.05.2019 03:00	11.50	352.00	05.05.2019 04:00	8.50	270.00
04.05.2019 04:00	12.20	353.40	05.05.2019 05:00	9.50	272.30
04.05.2019 05:00	12.70	355.80	05.05.2019 06:00	7.70	257.60
04.05.2019 06:00	12.40	353.40	05.05.2019 07:00	6.10	245.60
04.05.2019 07:00	11.90	349.20	05.05.2019 08:00	6.80	305.40
04.05.2019 08:00	11.80	346.40	05.05.2019 09:00	5.70	282.90
04.05.2019 09:00	12.20	346.60	05.05.2019 10:00	6.00	283.70
04.05.2019 10:00	12.60	345.60	05.05.2019 11:00	5.90	294.40
04.05.2019 11:00	11.90	343.70	05.05.2019 12:00	5.40	324.40
04.05.2019 12:00	11.10	340.00	05.05.2019 13:00	4.30	2.10
04.05.2019 13:00	10.40	336.10	05.05.2019 14:00	3.10	21.10
04.05.2019 14:00	9.80	331.20	05.05.2019 15:00	5.60	21.20
04.05.2019 15:00	9.50	322.40	05.05.2019 16:00	6.30	22.60
04.05.2019 16:00	9.30	315.30	05.05.2019 17:00	6.00	31.00
04.05.2019 17:00	9.30	310.40	05.05.2019 18:00	5.40	37.90

## **Appendix E**

# **Ocean Current Data**

<b>Ocean current conditions</b> Hollingsholmen - Aukra					
Time and date	Current speed [m/s]	Current direction [°]	Time and date	Current speed [m/s]	Current direction [°]
14.05.2019 08:00	0.23	337.70	15.05.2019 09:00	0.17	323.80
14.05.2019 09:00	0.22	340.50	15.05.2019 10:00	0.15	329.10
14.05.2019 10:00	0.16	339.40	15.05.2019 11:00	0.08	322.00
14.05.2019 11:00	0.11	335.40	15.05.2019 12:00	0.05	247.70
14.05.2019 12:00	0.06	333.20	15.05.2019 13:00	0.08	214.80
14.05.2019 13:00	0.04	316.30	15.05.2019 14:00	0.09	193.90
14.05.2019 14:00	0.03	317.10	15.05.2019 15:00	0.14	186.50
14.05.2019 15:00	0.00	263.30	15.05.2019 16:00	0.22	177.90
14.05.2019 16:00	0.04	208.50	15.05.2019 17:00	0.22	169.40
14.05.2019 17:00	0.05	236.00	15.05.2019 18:00	0.15	156.00
14.05.2019 18:00	0.09	263.80	15.05.2019 19:00	0.08	138.60
14.05.2019 19:00	0.15	291.20	15.05.2019 20:00	0.06	211.00
14.05.2019 20:00	0.25	326.50	15.05.2019 21:00	0.16	283.70
14.05.2019 21:00	0.27	347.90	15.05.2019 22:00	0.22	329.10
14.05.2019 22:00	0.18	347.70	15.05.2019 23:00	0.19	335.70
14.05.2019 23:00	0.07	2.60	16.05.2019 00:00	0.12	343.60
15.05.2019 00:00	0.01	348.30	16.05.2019 01:00	0.07	343.20
15.05.2019 01:00	0.04	224.90	16.05.2019 02:00	0.02	264.00
15.05.2019 02:00	0.10	212.00	16.05.2019 03:00	0.07	217.00
15.05.2019 03:00	0.15	205.00	16.05.2019 04:00	0.10	210.40
15.05.2019 04:00	0.14	176.00	16.05.2019 05:00	0.07	185.60
15.05.2019 05:00	0.15	144.90	16.05.2019 06:00	0.09	82.90
15.05.2019 06:00	0.14	129.20	16.05.2019 07:00	0.11	73.10
15.05.2019 07:00	0.09	139.60	16.05.2019 08:00	0.03	20.20
15.05.2019 08:00	0.08	227.10	16.05.2019 09:00	0.21	311.60





# References

- [1] Dash, “dash-salesforce-crm,” 2019, last accessed 2019-05-24. [Online]. Available: <https://github.com/plotly/dash-salesforce-crm>
- [2] O. Moen, “Erfaringer så langt med drift og lading av «batteri-fartøy»,” apr 2018. [Online]. Available: <https://www.nek.no/wp-content/uploads/2018/05/9-14-00{ }Landstromsforum-Siemens-120418{ }Odd{ }Moen.pdf>
- [3] J. A. Suul, “Introduction to marine power systems and control of power electronic converters,” 2018, lecture at NTNU autumn 2018.
- [4] O. R. Valmot, “Slik fungerer batteriet som endret verden,” nov 2013. [Online]. Available: <https://www.tu.no/artikler/slik-fungerer-batteriet-som-endret-verden/233862>
- [5] A. Barré, B. Deguilhem, S. Grolleau, M. Gérard, F. Suard, and D. Riu, “A review on lithium-ion battery ageing mechanisms and estimations for automotive applications,” *Journal of Power Sources*, vol. 241, pp. 680–689, nov 2013. [Online]. Available: <https://www.sciencedirect.com/science/article/pii/S0378775313008185>
- [6] BKK, “Slik fungerer stromnettet,” last accessed 2019-03-11. [Online]. Available: <https://www.bkk.no/nett/slik-fungerer-stromnettet>
- [7] Nord Pool AS, “Day-ahead prices,” last accessed 2019-05-06. [Online]. Available: <https://www.nordpoolgroup.com/Market-data1/Dayahead/Area-Prices/ALL1/Hourly/?view=table>

- [8] Emoscopes, “Wikimedia Commons - Ship length measurements,” last accessed 2019-05-08. [Online]. Available: [https://commons.wikimedia.org/wiki/File:Ship{}\\_length{}\\_measurements.svg](https://commons.wikimedia.org/wiki/File:Ship{}_length{}_measurements.svg)
- [9] Prime Minister Erna Solberg, “From political ambitions to zero emissions,” 2019. [Online]. Available: <https://www.regjeringen.no/en/aktuelt/from-political-ambitions-to-zero-emissions/id2626995/>
- [10] R. K. Pachauri, M. R. Allen, V. R. Barros, J. Broome, W. Cramer, R. Christ, J. A. Church, L. Clarke, Q. Dahe, P. Dasgupta, N. K. Dubash, O. Edenhofer, I. Elgizouli, C. B. Field, P. Forster, P. Friedlingstein, J. Fuglestad, L. Gomez-Echeverri, S. Hallegatte, G. Hegerl, M. Howden, K. Jiang, B. J. Cisneroz, V. Kattsov, H. Lee, K. J. Mach, J. Marotzke, M. D. Mastrandrea, L. Meyer, J. Minx, Y. Mulugetta, K. O’Brien, M. Oppenheimer, J. J. Pereira, R. Pichs-Madruga, G.-K. Plattner, H.-O. Pörtner, S. B. Power, B. Preston, N. H. Ravindranath, A. Reisinger, K. Riahi, M. Rusticucci, R. Scholes, K. Seyboth, Y. Sokona, R. Stavins, T. F. Stocker, P. Tschakert, D. van Vuuren, and J.-P. van Ypserle, *Climate Change 2014: Synthesis Report. Contribution of Working Groups I, II and III to the Fifth Assessment Report of the Intergovernmental Panel on Climate Change*, R. K. Pachauri and L. Meyer, Eds. Geneva, Switzerland: IPCC, 2014. [Online]. Available: [https://www.ipcc.ch/site/assets/uploads/2018/02/SYR{}\\_AR5{}\\_FINAL{}\\_full.pdf](https://www.ipcc.ch/site/assets/uploads/2018/02/SYR{}_AR5{}_FINAL{}_full.pdf)
- [11] R. Sims and R. Schaeffer, “Transport Climate Change 2014: Mitigation of Climate Change. Contribution of Working Group III to the Fifth Assessment Report of the Intergovernmental Panel on Climate Change ed O Edenhofer et al,” *Cambridge and New York: Cambridge University Press.*, 2014. [Online]. Available: [https://www.ipcc.ch/site/assets/uploads/2018/02/ipcc{}\\_wg3{}\\_ar5{}\\_chapter8.pdf](https://www.ipcc.ch/site/assets/uploads/2018/02/ipcc{}_wg3{}_ar5{}_chapter8.pdf)
- [12] Miljødirektoratet, “Klimagassutslipp fra transport | Miljøstatus,” 2018, last accessed 2019-05-13. [Online]. Available: <https://www.miljostatus.no/tema/klima/norske-klimagassutslipp/utslipp-av-klimagasser-fra-transport/>
- [13] K. og miljødepartementet, “Slik skal Norge nå klimamålene for 2030,”

- jun 2017. [Online]. Available: <https://www.regjeringen.no/no/aktuelt/slik-skal-norge-na-klimamalene-for-2030/id2557549/>
- [14] NVE, “Nasjonal varedeklarasjon 2017,” 2017, last accessed 2019-05-13. [Online]. Available: <https://www.nve.no/reguleringsmyndigheten-for-energi-rme-marked-og-monopol/varedeklarasjon/nasjonal-varedeklarasjon-2017/>
- [15] Energifakta Norge, “Electricity production,” last accessed 2019-03-12. [Online]. Available: <https://energifaktanorge.no/en/norsk-energiforsyning/kraftproduksjon/>
- [16] D. Jolly, “Norway Is a Model for Encouraging Electric Car Sales - The New York Times,” 2015, last accessed 2019-05-13. [Online]. Available: <https://www.nytimes.com/2015/10/17/business/international/norway-is-global-model-for-encouraging-sales-of-electric-cars.html?r=0>
- [17] N. elbilforening, “Antall elbiler og ladestasjoner i Norge,” 2018, last accessed 2019-05-13. [Online]. Available: <https://elbil.no/elbilstatistikk/>
- [18] Samferdselsdepartementet, “En grønnere transporthverdag,” apr 2017. [Online]. Available: <https://www.regjeringen.no/no/aktuelt/en-gronnere-transporthverdag/id2548633/>
- [19] Norwegian Ministry of Climate and Environment, “Norway’s Seventh National Communication Under the Framework Convention on Climate Change,” Tech. Rep., 2018. [Online]. Available: [http://unfccc.int/files/national\\_reports/annex\\_i\\_natcom/submitted\\_natcom/application/pdf/529371\\_norway-nc7-br3-1-nc7-br3-final.pdf](http://unfccc.int/files/national_reports/annex_i_natcom/submitted_natcom/application/pdf/529371_norway-nc7-br3-1-nc7-br3-final.pdf)
- [20] Maritime Battery Forum and S. Henningsgård, “Life cycle analysis of batteries in maritime sector,” 2016. [Online]. Available: [https://www.nho.no/siteassets/nhos-filer-og-bilder/filer-og-dokumenter/nox-fondet/dette-er-nox-fondet/presentasjoner-og-rapporter/life-cycle-analysis-for-batteries-in-maritime-sector\\_final\\_v0.1.pdf](https://www.nho.no/siteassets/nhos-filer-og-bilder/filer-og-dokumenter/nox-fondet/dette-er-nox-fondet/presentasjoner-og-rapporter/life-cycle-analysis-for-batteries-in-maritime-sector_final_v0.1.pdf)

- [21] L. Tang, G. Rizzoni, and S. Onori, "Energy Management Strategy for HEVs Including Battery Life Optimization," *IEEE Transactions on Transportation Electrification*, vol. 1, no. 3, pp. 211–222, oct 2015. [Online]. Available: <http://ieeexplore.ieee.org/document/7217846/>
- [22] L. Serrao, S. Onori, and G. Rizzoni, "ECMS as a realization of Pontryagin's minimum principle for HEV control," in *2009 American Control Conference*. IEEE, 2009, pp. 3964–3969. [Online]. Available: <http://ieeexplore.ieee.org/document/5160628/>
- [23] A. Hoke, A. Brissette, D. Maksimovic, A. Pratt, and K. Smith, "Electric vehicle charge optimization including effects of lithium-ion battery degradation," in *2011 IEEE Vehicle Power and Propulsion Conference*. IEEE, sep 2011, pp. 1–8. [Online]. Available: <http://ieeexplore.ieee.org/document/6043046/>
- [24] L. Serrao, "A comparative analysis of energy management strategies for hybrid electric vehicles," 2009. [Online]. Available: [http://rave.ohiolink.edu/etdc/view?acc\\_{\\_}num=osu1243934217](http://rave.ohiolink.edu/etdc/view?acc_{_}num=osu1243934217)
- [25] M. Broussely, P. Biensan, F. Bonhomme, P. Blanchard, S. Herreyre, K. Nechev, and R. Staniewicz, "Main aging mechanisms in Li ion batteries," *Journal of Power Sources*, vol. 146, no. 1-2, pp. 90–96, aug 2005. [Online]. Available: <https://www.sciencedirect.com/science/article/pii/S0378775305005082>
- [26] V. Marano, S. Onori, Y. Guezennec, G. Rizzoni, and N. Madella, "Lithium-ion batteries life estimation for plug-in hybrid electric vehicles," in *2009 IEEE Vehicle Power and Propulsion Conference*. IEEE, sep 2009, pp. 536–543. [Online]. Available: <http://ieeexplore.ieee.org/document/5289803/>
- [27] J. Wang, P. Liu, J. Hicks-Garner, E. Sherman, S. Soukiazian, M. Verbrugge, H. Tataria, J. Musser, and P. Finamore, "Cycle-life model for graphite-LiFePO4 cells," *Journal of Power Sources*, vol. 196, no. 8, pp. 3942–3948, apr 2011. [Online]. Available: <https://www.sciencedirect.com/science/article/pii/S0378775310021269>

- [28] G. Suri and S. Onori, "A control-oriented cycle-life model for hybrid electric vehicle lithium-ion batteries," *Energy*, vol. 96, pp. 644–653, feb 2016. [Online]. Available: <https://www.sciencedirect.com/science/article/pii/S0360544215016382>
- [29] Plotly, "Dash by Plotly," 2019, last accessed 2019-05-07. [Online]. Available: <https://plot.ly/products/dash/>
- [30] DNV GL, "Elektrifisering av bilferger i Norge – kartlegging av investeringsbehov i strømmettet," 2015. [Online]. Available: <https://www.energinorge.no/contentassets/0ae3a2b651ae4e83a0487ad493c3270c/elektrifisering-av-bilferger-i-norge.pdf>
- [31] E. Skjong, R. Volden, E. Rødskar, M. Molinas, T. A. Johansen, and J. Cunningham, "Past, Present, and Future Challenges of the Marine Vessel's Electrical Power System," *IEEE Transactions on Transportation Electrification*, vol. 2, no. 4, pp. 522–537, 2016.
- [32] M. V. Finnekås, "Identification of Key Parameters and Potential Solutions for Smarter Charging of Battery Ferries," 2018.
- [33] F. Martini, "Siemens - Setting a Course for Carbon-Free Shipping," 2014, last accessed 2019-04-15. [Online]. Available: <http://www.siemens.com.tw/release/pof.asp?p=13>
- [34] Ships of CalMac, "Hallaig: History," nov 2013. [Online]. Available: <http://www.shipsofcalmac.co.uk/h{ }hallaig.asp>
- [35] V. Staudt, R. Bartelt, and C. Heising, "Fault Scenarios in DC Ship Grids: The advantages and disadvantages of modular multilevel converters." *IEEE Electrification Magazine*, vol. 3, no. 2, pp. 40–48, 2015. [Online]. Available: <https://ieeexplore.ieee.org/abstract/document/7116691>
- [36] Wärtsilä, "Wireless charging," Tech. Rep., 2018. [Online]. Available: <https://www.wartsila.com/docs/default-source/product-files/ps/wireless-charging-leaflet-2018.pdf>

- [37] ABB, “ABB powering largest emission-free electric ferries,” last accessed 2019-04-16. [Online]. Available: <https://new.abb.com/marine/references/hh-ferries>
- [38] L. Lu, X. Han, J. Li, J. Hua, and M. Ouyang, “A review on the key issues for lithium-ion battery management in electric vehicles,” *Journal of Power Sources*, vol. 226, pp. 272–288, mar 2013. [Online]. Available: <https://www.sciencedirect.com/science/article/pii/S0378775312016163>
- [39] S. Bashash, S. J. Moura, J. C. Forman, and H. K. Fathy, “Plug-in hybrid electric vehicle charge pattern optimization for energy cost and battery longevity,” *Journal of Power Sources*, vol. 196, no. 1, pp. 541–549, 2011. [Online]. Available: <https://www.sciencedirect.com/science/article/pii/S0378775310011390>
- [40] B. Lawson, “Battery Performance Characteristics,” last accessed 2019-05-24. [Online]. Available: <https://www.mpoweruk.com/performance.htm>
- [41] M. Rouse, “What is battery life? - Definition from WhatIs.com,” 2013, last accessed 2019-04-23. [Online]. Available: <https://whatis.techtarget.com/definition/battery-life>
- [42] M. Patel, *Shipboard electrical power systems*. CRC Press, 2012.
- [43] J. Vetter, P. Novák, M. Wagner, C. Veit, K.-C. Möller, J. Besenhard, M. Winter, M. Wohlfahrt-Mehrens, C. Vogler, and A. Hammouche, “Ageing mechanisms in lithium-ion batteries,” *Journal of Power Sources*, vol. 147, no. 1-2, pp. 269–281, sep 2005. [Online]. Available: <https://www.sciencedirect.com/science/article/pii/S0378775305000832>
- [44] E. Wikner and Others, “Lithium ion Battery Aging: Battery Lifetime Testing and Physics-based Modeling for Electric Vehicle Applications,” Ph.D. dissertation, Department of Electrical Engineering, Chalmers University of Technology, 2017.
- [45] Norwegian Ministry of Petroleum and Energy, “ENERGY AND WATER RESOURCES IN NORWAY,” Tech. Rep., 2015. [Online]. Available: [https://www.regjeringen.no/contentassets/fd89d9e2c39a4ac2b9c9a95bf156089a/facts}\\_{2015}\\_{energy}\\_{and}\\_{water}\\_{web}.pdf](https://www.regjeringen.no/contentassets/fd89d9e2c39a4ac2b9c9a95bf156089a/facts}_{2015}_{energy}_{and}_{water}_{web}.pdf)

- [46] NVE, “Network Regulation,” last accessed 2019-03-11. [Online]. Available: <https://www.nve.no/energy-market-and-regulation/network-regulation/?ref=mainmenu>
- [47] Energifakta Norge, “The electricity grid,” last accessed 2019-03-12. [Online]. Available: <https://energifaktanorge.no/en/norsk-energiforsyning/kraftnett/>
- [48] Energi Norge, “Hvorfor betaler vi nettleie og hvorfor øker den?” Tech. Rep., 2018. [Online]. Available: <https://www.energinorge.no/contentassets/ecb78680d7484879b1385d1f61aa766f/nettleien---mars-2018.pdf>
- [49] Skagerak Energi, “Grid rental,” last accessed 2019-03-11. [Online]. Available: <http://www.skageraknaturgass.no/eway/default.aspx?pid=323{&}trg=MainRight{ }11665{&}MainArea{ }11660=11665:0:{&}MainRight{ }11665=11667:0:10,4354>
- [50] NVE, “Network tariffs,” 2017, last accessed 2019-03-14. [Online]. Available: <https://www.nve.no/energy-market-and-regulation/network-regulation/network-tariffs/?ref=mainmenu>
- [51] —, “Forslag til endring i forskrift om kontroll av nettvirksomhet,” 2017. [Online]. Available: <http://publikasjoner.nve.no/hoeringsdokument/2017/hoeringsdokument2017{ }05.pdf>
- [52] H. Sæle, “SINTEF - Smart meters,” last accessed 2019-03-11. [Online]. Available: <https://www.sintef.no/en/advanced-metering-and-control-systems/>
- [53] J. Nocedal and S. Wright, *Numerical Optimization*. Springer Science & Business Media, 2006.
- [54] L. Serrao, S. Onori, and G. Rizzoni, “A Comparative Analysis of Energy Management Strategies for Hybrid Electric Vehicles,” 2011. [Online]. Available: <http://dynamicsystems.asmedigitalcollection.asme.org/article.aspx?articleid=1414021>
- [55] T. H. Cormen, *Introduction to algorithms*. MIT Press, 2009.

- [56] F. L. Lewis, D. L. Vrabie, and V. L. Syrmos, *OPTIMAL CONTROL Third Edition*, 2012. [Online]. Available: <https://onlinelibrary.wiley.com/doi/book/10.1002/9781118122631>
- [57] D. P. Bertsekas, *Dynamic Programming and Optimal Control*, 3rd ed., 2005.
- [58] H. J. Sussmann and J. C. Willems, “300 years of optimal control: from the brachy- tochrone to the maximum principle,” *IEEE Control Systems Magazine*, vol. 17, no. 3, pp. 32–44, 1997.
- [59] Fjord1, “Aukra - Hollingsholmen,” last accessed 2019-05-25. [On- line]. Available: <https://www.fjord1.no/Ruteoversikt/Moere-og-Romsdal/Aukra-Hollingsholmen>
- [60] Sjøfartsdirektoratet, “Fartøyet llut eira,” 2019, last accessed 2019-06-02. [Online]. Available: <https://www.sdir.no/skipssok/#/shipdetails/23962/1>
- [61] A. Fotouhi, D. J. Auger, K. Propp, S. Longo, and M. Wild, “A review on electric vehicle battery modelling: From Lithium-ion toward Lithium–Sulphur,” *Renewable and Sustainable Energy Reviews*, vol. 56, pp. 1008–1021, apr 2016. [Online]. Available: <https://www.sciencedirect.com/science/article/pii/S1364032115013921>
- [62] A. Shafiei, A. Momeni, and S. S. Williamson, “Battery modeling approaches and management techniques for Plug-in Hybrid Electric Vehicles,” in *2011 IEEE Vehicle Power and Propulsion Conference*. IEEE, sep 2011, pp. 1–5. [Online]. Available: <http://ieeexplore.ieee.org/document/6043191/>
- [63] A123 Systems, “Nanophosphate High Power Lithium Ion Cell ANR26650M1-B,” *Data Sheet*, pp. 2–3, 2012. [Online]. Available: [https://a123batteries.com/product/\\_images/uploaded/\\_images/26650.pdf](https://a123batteries.com/product/_images/uploaded/_images/26650.pdf)
- [64] L. Serrao, S. Onori, A. Sciarretta, Y. Guezennec, and G. Rizzoni, “Optimal energy management of hybrid electric vehicles including battery aging,” in *Proceedings of the 2011 American Control Conference*. IEEE, jun 2011, pp. 2125–2130. [Online]. Available: <http://ieeexplore.ieee.org/document/5991576/>

- [65] Statnett SF, “Last ned grunndata,” last accessed 2019-05-26. [Online]. Available: <https://www.statnett.no/for-aktorer-i-kraftbransjen/tall-og-data-fra-kraftsystemet/last-ned-grunndata/>
- [66] Skagerak Nett, “Priser næringskunder,” last accessed 2019-05-06. [Online]. Available: <https://www.skageraknett.no/priser-naringskunder/category1586.html>
- [67] S. vegvesen, “Ferjedatabanken - Forsiden,” last accessed 2019-04-29. [Online]. Available: <http://fdb.triona.no/>
- [68] T. I. Fossen, *Handbook of marine craft hydrodynamics and motion control*, first edit ed. John Wiley & Sons, 2011.
- [69] M. institutt, “Locationforecast,” last accessed 2019-05-03. [Online]. Available: <https://api.met.no/weatherapi/locationforecast/1.9/documentation>
- [70] —, “Oceanforecast,” last accessed 2019-05-03. [Online]. Available: <https://api.met.no/weatherapi/oceanforecast/0.9/documentation>